Washington University in St. Louis
Washington University Open Scholarship

All Theses and Dissertations (ETDs)

January 2010

Determing the Properties of Dense Matter: Superconductivity, Bulk Viscosity, and Light Reflection in Compact Stars

Gerald Good
Washington University in St. Louis

Follow this and additional works at: https://openscholarship.wustl.edu/etd

WASHINGTON UNIVERSITY

Department of Physics

Dissertation Examination Committee:
Mark Alford, Chair
Claude Bernard
Ramanath Cowsik
Willem Dickhoff
Renato Feres
Lee Sobotka

DETERMINING THE PROPERTIES OF DENSE MATTER:

SUPERCONDUCTIVITY, BULK VISCOSITY, AND LIGHT REFLECTION IN

COMPACT STARS

by

Gerald J. Good

A dissertation presented to the
Graduate School of Arts and Sciences
of Washington University in
partial fulfillment of the
requirements for the degree
of Doctor of Philosophy

May 2010

Saint Louis, Missouri

Abstract

In this dissertation, we investigate the properties of matter, denser than nuclei, that exists inside compact stars. First, we examine a mixed superfluid/superconductor system, which likely occurs in neutron star cores. We derive an effective theory of Cooper pair quasiparticles from a microscopic theory of nucleons, and calculate the coupling strengths between quasiparticles. We then calculate the structure of magnetic flux tubes, taking into consideration interactions between neutron and proton Cooper pairs. We find that interactions between the condensates can lead to interesting phenomena and new phases at the border between type-I and type-II behavior. Next, we examine the response of nuclear matter to vibrational modes by calculating the bulk viscosity from purely leptonic processes. We find that for hot neutron stars, the bulk viscosity due to leptons is very small compared to the bulk viscosity due to nucleons, but for cold neutron stars, the leptonic component is dominant. Finally, we derive the reflection and transmission properties of light at boundaries between phases of matter that have two independent $U(1)$ generators, which may exist at the surface of "strange stars" or at boundaries between different phases of matter in a neutron star.

Acknowledgements

First, I would like to thank my parents, friends and coworkers that have supported me during this long process. Specifically, I would like to thank Ryan Claus and Sean Hanley for listening to my obtuse descriptions of flux tubes and solutions of systems of coupled ODEs, which probably bored them to tears. Thanks also to Dan Northem for constantly asking "when are you going to be done with your thesis?" and reading a draft.

I would also like to thank those in the physics community that I interacted with during this research. Thanks to Sanjay Reddy at Los Alamos National Laboratory for collaborating with Prof. Alford and I on our paper about quasiparticle interactions, and for suggesting the topic of leptonic bulk viscosity. Thanks also to Krishna Rajagopal, Tanmoy Bhattacharya, Max Metlitski, Gautam Rupak, Ariel Zhitnitsky, Egor Babaev, Greg Comer, Igor Luk'yanchuk, Fidel Schaposnik, Martin Speight, Marcelo Gleiser, Joel Thorarinson, Peter Shternin, and Dima Yakovlev for helpful comments on the publications that this thesis is based on.

I also want to thank the many excellent professors and postdocs that I have learned from over the past 15 years or so: Peter Rolnick, Ian Lindevald, Mohammad

Contents

List of Figures

List of Tables

Chapter 1

Introduction

1.1 Theoretical Phases of Matter at High Density

Determining the phase diagram of very hot or very dense matter is a challenging theoretical problem on the forefront of today's nuclear and particle physics research. The primary challenge is a lack of experimental data about how matter in these regimes behaves. At high temperature and low density ($T \gtrsim 150$ MeV, $\mu_{baryon} \lesssim 500$ MeV), it is predicted that matter consists of a Quark-Gluon Plasma (QGP), while at low temperature and high density ($T \lesssim 50$ MeV, $\mu_{baryon} \gtrsim 1000$ MeV) , theory predicts a number of different phases consisting of color-superconducting quark matter (Fig 1.1 [1]).

Recently, the Relativistic Heavy Ion Collider at Brookhaven has begun exploring the high temperature, low density regime of the phase diagram, but it is unlikely that a terrestrial experiment will be able to explore the low temperature, high density
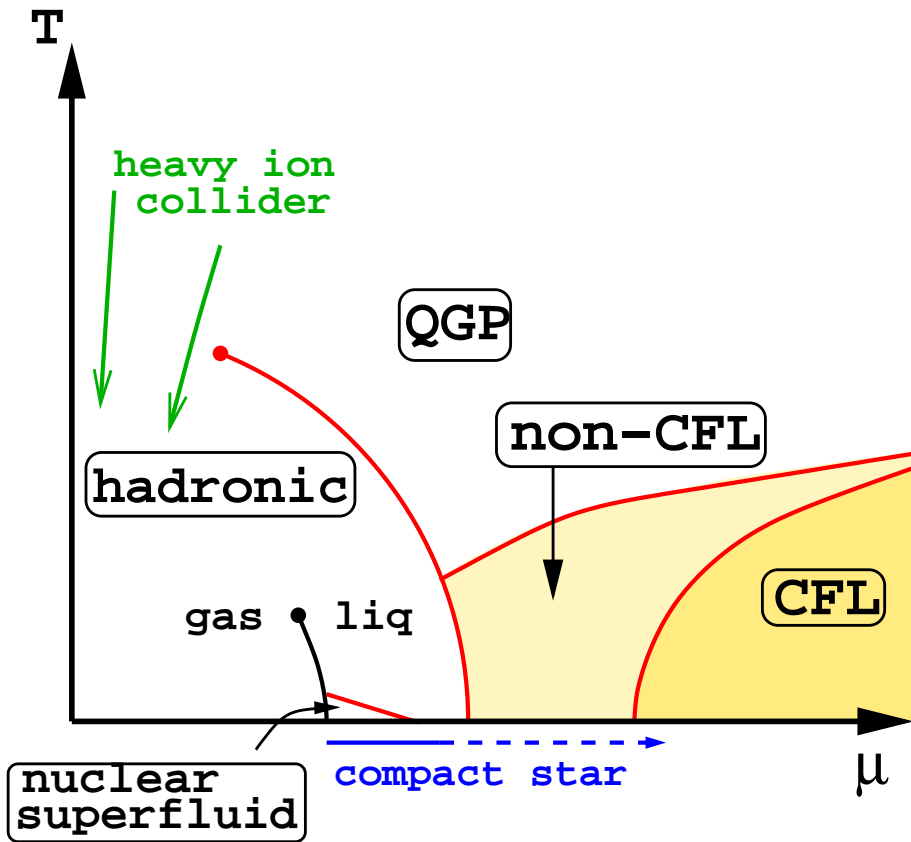
Figure 1.1:   Notional phase diagram for nuclear and quark matter at high density and temperature [1].

regime. To collect data that can verify the theoretical predictions in this regime, we must turn to our friends the astronomers and astrophysicists. Based on measurements of mass and radii, the predicted quark matter phases may exist inside compact stars. Pulsars and X-ray bursters are compact objects that are likely neutron stars, but some could possibly be "strange stars" that are purely composed of quark matter [2].

1.2   Internal structure of neutron stars

The nuclear matter in the neutron star core ranges from a few times the normal
nuclear density, $\rho_0 = 0.15$ nucleons/fm^3, to an order of magnitude higher [2]. This
dense matter is also very cold compared to the nuclear temperature scale; the typical
temperature of a neutron star is less than about 10^8 K [2]. (In comparison, the quark-
gluon plasma created at RHIC has a temperature on the order of 10^{12} K.) . Therefore,
it is likely that quark matter can exist inside of neutron stars. Neutron stars likely
have an "onion" structure, where the phase of matter depends on the depth from the
star's surface. The crust layers are thought to be a crystalline arrangement of nuclei
and electrons. As the depth increases, the density becomes larger than the "drip
density", where neutrons begin to drip out of nuclei, so nuclei and a nucleon fluid
coexist. Increasing the depth further, the nuclei dissolve into pure nucleon fluid. In
the neutron star core, the nucleons may become deconfined, resulting in quark matter
(Fig 1.2).

However, there is no way to directly observe these properties. Pulsars have been
identified as rotating neutron stars; the observable properties are the spin rate (pulsar
frequency), spin-down rate due to energy losses, glitches (sudden changes in spin-down
rate), and thermal emission from neutrinos and photons. More generally, neutron
stars that accrete matter from a binary partner may be the source of X-ray bursts.
To make a connection between neutron star observations and dense matter theories,
star models must be constructed based on a theory of the constituent matter, and

quark–hybrid
star

traditional neutron star

hyperon
star

neutron star with
pion condensate

N+e
N+e+n

n,p,e, μ

superconducting protons

n superfluid

n,p,e, μ

$\Sigma,\Lambda,\Xi,\Delta$

H

u,d,s
2SC
CFL

π^-

crust

Fe

10^6 g/cm^3

10^{11} g/cm^3

10^{14} g/cm^3

strange
quark
matter
(u,d,s quarks)

CFL

2SC

CFL

K^-

Hydrogen/He
atmosphere

strange star

nucleon star

R ~ 10 km
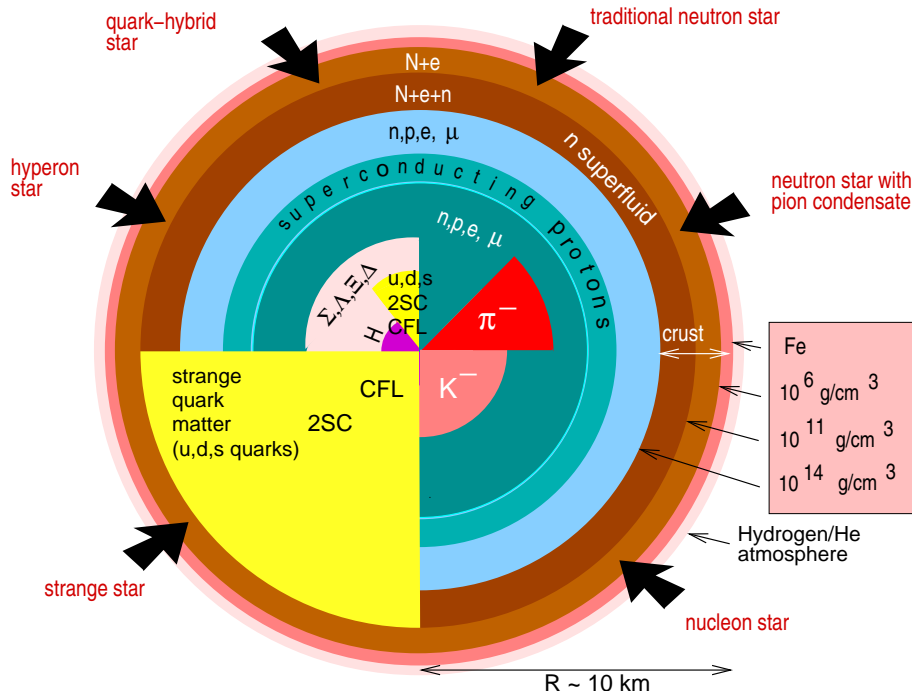
Figure 1.2: Illustration of a number of possible models for the internal structure of a neutron star [3].

the model results compared to neutron star properties.

One of the interesting predictions about the neutron star core is that the neutrons should form a superfluid and the protons should form a superconductor. Since the strong nuclear force has a long-range attractive part, the Bardeen-Cooper-Schreiffer (BCS) mechanism induces pairing between nucleons [4]. The neutron superfluid rotates by forming a triangular array of vortices, called an Abrikosov lattice. This model of a neutron superfluid has been invoked to explain the phenomena of neutron star glitches [2]. Over time, the neutron star's rotation frequency decreases as it loses energy. Occasionally, the rotation frequency of the star will increase suddenly, then return to its normal trend of decreasing again - this sudden increase in frequency is

called a glitch. In order for the rotation frequency of the star to decrease, vortices need to move toward the outside of the star, but this causes stress on the neutron star crust, because the ends of the vortices are pinned to the crust. It is thought that a glitch occurs when the buildup of stress cause a massive realignment of the crust ("starquake") so that the vortices can move outward [2].

Based on the predicted properties of the neutron star core matter, the proton superconductivity should be of type II [5]. In a type II superconductor, magnetic flux is allowed to penetrate the superconductor in quantized *flux tubes*. These flux tubes also form an Abrikosov lattice. It has also been shown that neutron vortices become pinned to proton flux tubes, because the neutrons drag protons around with them ("entrainment") and magnetize the vortices [6].

1.3 Isospin asymmetry and Cooper pair interactions

Recently, it has been suggested that nuclear matter in neutron stars might be a type-I superconductor. The astrophysical evidence is that certain neutron stars have long precession periods, and it has been suggested that this means the proton superconductivity cannot be type-II [7], although that inference has been contested [8, 9]. A theoretical argument for type-I superconductivity in neutron star cores was then presented by Buckley et. al. in Ref. [10]. These authors assumed that the effective potential for the Cooper pair fields has a $U(2)$ symmetry under rotation of proton

and neutron Cooper pairs into each other. Specifically, the effective potential for the Cooper pair fields was assumed to take the form

$$V(|\Delta_{pp}|^2, |\Delta_{nn}|^2) \approx U(|\Delta_{pp}|^2 + |\Delta_{nn}|^2)$$

$$= -\mu_c(|\Delta_{pp}|^2 + |\Delta_{nn}|^2) + a(|\Delta_{pp}|^2 + |\Delta_{nn}|^2)^2 + \cdots$$

(1.1)

The assumption that the potential is approximately a function of $|\Delta_{pp}|^2 + |\Delta_{nn}|^2$ leads to $|\Delta_{pp}|^2|\Delta_{nn}|^2$ cross terms, which provide a strong repulsive interaction between the neutron and proton Cooper pair condensates. It is argued in Ref. [10] that this leads to a long-range attraction between proton flux tubes, i.e. type-I superconductivity.

The assumed $U(2)$ symmetry was justified by invoking the isospin symmetry of the underlying nuclear interaction. The authors of Ref. [10] admit that isospin is severely broken by the constraint of electrical neutrality, which, combined with beta-equilibration, greatly suppresses the proton Fermi momentum relative to the neutron Fermi momentum, but they claim that this does not affect the interaction between the *p-p* and *n-n* Cooper pairs. This seems implausible, since it is well known in the theory of superconductivity that the coefficients of the terms in the Landau-Ginzburg effective theory, including the quartic coupling a, depend strongly on the Fermi momenta of the underlying fermions [11]. For example, for a one component Fermi gas, just below the BCS critical point, the effective Landau-Ginzburg potential is

$$V(|\Delta|^2) = -\mu|\Delta|^2 + a|\Delta|^4 + \cdots$$

(1.2)

where $\mu \approx N_F(T_c - T)/T_c$, and N_F is the density of states at the Fermi surface, so

for non-relativistic fermions $N_F \propto m p_F$ where m is the mass and p_F is the Fermi momentum. The minimum of the potential occurs at $\Delta_0 = \sqrt{\mu/(2a)}$, so the quartic coefficient is $a = \mu/(2\Delta_0^2)$. The binding energy of the condensate is then $V(\Delta_0) = -\frac{1}{2}N_F\Delta_0^2$, a well-known result in the superconductivity literature [12]. We see that μ, a, and $V(\Delta_0)$ are all very sensitive to the Fermi momenta of the underlying fermions. Clearly for protons and neutrons in a neutron star, which have very different Fermi momenta but similar pairing condensates Δ, this will not give an effective potential of the form (1.1).

In chapter 2 (based on [13]), we back up our reasoning with a concrete calculation. Starting from a four-fermion interaction model (known as the NJL model) of protons and neutrons with $U(2)$ symmetry, an effective Lagrangian for pair quasiparticles is derived. The NJL couplings are treated as variables, and are determined using gap equations and the predicted values of the neutron and proton gaps. The couplings between the pair quasiparticles are then determined at both $T = 0$ and at finite temperature. It was found that the coupling between neutron pairs and a proton pairs was smaller than the coupling between two neutron pairs or the coupling between two proton pairs by about two orders of magnitude. This finding seems to rule out the assumption of a $U(2)$ symmetry for the effective theory of Cooper pairs.

1.4 Flux tubes and the type-I/type-II transition in a superconductor coupled to a superfluid

In chapter 3 (based on [14]) we investigate a system that has both a charged conden-
sate, leading to superconductivity, and a neutral condensate, leading to superfluidity.
We focus on the magnetic flux tubes that are associated with the superconducting
condensate, and study how they are modified by the presence of the superfluid, as-
suming that the two condensates can interact with each other via density and gradient
("entrainment") interactions. Nuclear matter is an example of this type of system,
which at sufficiently high density undergoes Cooper pairing of both neutrons and
protons. We will present our calculations in this context, referring to the charged
condensate as the "proton condensate" and the neutral one as the "neutron conden-
sate", and choosing values appropriate to nuclear matter for our parameters when
presenting numerical results.

We study the type I versus type II nature of a (proton) superconductor coupled
to a (neutron) superfluid, using an effective theory for the protons and neutrons
that contains four-fermion interaction terms which lead to s-wave pairing. We do not
include higher-angular-momentum pairing, although that would be needed for a more
realistic analysis of high-density nuclear matter. Our analysis extends that of Ref. [10]
in the following ways: (a) Our model, like that of Ref. [10], contains a coupling a_{np}
between the magnitudes of the neutron and proton condensates, and self-couplings
a_{nn} and a_{pp}, but we survey the whole range of values of a_{np}, from zero to of order a_{pp};

(b) we also include "entrainment" interactions between the gradients of the proton and neutron condensates; (c) we use a simpler and more direct method to study the type-I/type-II phase boundary, using the energetics of flux tube coalescence/fission: we calculate the energy of flux tubes with a wide range of magnetic fluxes, from one quantum to several hundred quanta, and find which one has the lowest energy per unit flux. As we will see, this has the additional benefit of allowing us to find exotic stable multi-quantum flux tubes, such as have been found in systems of two coupled superconductors [15]. However, as we discuss below, our analysis is not sensitive to minima in the interaction energy at finite separation between flux tubes.

Our analysis is entirely at zero temperature. This is a good approximation for neutron star matter near nuclear saturation density, where the critical temperatures for the superfluid and superconductor are of order MeV [16, 17, 18]. The temperature of a compact star drops below this value within minutes of its formation in a supernova, and is at or below the keV range after the first 1000 years [19]. When we discuss type-I versus type-II behavior we are referring to the response of the system to a magnetic field at the lower critical value, at $T = 0$.

As far as we know, there has been no previous work on how a flux tube in a superconductor is affected by a gradient coupling to a co-existing superfluid. However, there has been work on possible knot solitons [20], vortices in the $SO(5)$ model of high-temperature superconductivity [21], and on the complementary situation, a superfluid vortex with gradient coupling to a co-existing superconductor. There the coupling leads to the "entrainment" or Andreev-Bashkin effect [22] whereby the pro-

ton condensate is dragged along with the neutron condensate, producing a non-zero proton current around the vortex, dressing it with some magnetic flux [23]. It is interesting to note that this flux is not a multiple of the flux quantum for proton flux tubes. This is possible because of the difference between the energetics of a neutron vortex and a proton flux tube. The flux tube has energy density localized to the vicinity of its core. Far from the core the energy density must vanish, which means the proton field must change in phase by a multiple of 2π, and the the vector potential must cancel the resultant gradient, leading to a quantized magnetic flux. A neutron vortex, by contrast, has gradient energy that is not localized to the vicinity of the vortex, and the total energy per unit length diverges in the infinite volume limit. The vector potential is therefore not constrained to cancel any gradient in the proton field, and takes on a value that minimizes the overall energy, with no quantization condition on the resulting magnetic flux.

Returning to the situation that we study, a proton flux tube in a neutron super-fluid background, we do not expect a similar behavior. This is because the proton flux tube's energy density is localized around its core, giving it (unlike the neutron vortex) a finite energy per unit length. If the neutron condensate were entrained, and developed non-zero circulation around the flux tube, it would acquire a non-localized energy density, leading to an infinite energy per unit length for the flux tube, which is clearly energetically disfavored. We will see in chapter 3 that the effect of gradient couplings on the proton superconductor is more subtle: it leads to metastable regions near the type-I/type-II boundary.

1.5 Leptonic contribution to the bulk viscosity of nuclear matter

The bulk viscosity of nuclear matter plays an important role in the damping of oscillations in neutron stars. One well-known example is r-modes, which, if the interior of the star is a perfect (dissipationless) fluid, become unstable with respect to the emission of gravitational waves [24, 25, 26]. This emission acts as a brake on the rotation of the star. However, r-mode spindown will not occur if the r-mode is sufficiently strongly damped, for example by shear or bulk viscosity of the matter in the interior of the star. It is therefore important to calculate of the bulk viscosity of the various candidate phases in a neutron star. Several calculations exist in the literature, for nuclear [27, 28, 29, 30, 31, 32] and hyperonic [33, 34, 35] as well as for unpaired quark matter [36, 37, 38] and various color-superconducting phases [39, 40, 41, 42, 43, 44].

In chapter 4 (based on [45]) we will study β-equilibrated nuclear matter. We will assume that the density is high enough that the negative-charge chemical potential μ_l is greater than the mass of the muon, so the matter consists of neutrons, protons, electrons and muons. Such matter is expected to exist in the core of the star. In previous calculations of bulk viscosity of $npe\mu$ nuclear matter the focus has been on the contribution from interconversion of neutrons and protons via weak interactions. But nuclear matter at neutron-star densities is expected to show Cooper pairing of protons (superconductivity) or neutrons (superfluidity) [16, 17, 46] either of which will suppress interconversion by a factor of order $\exp(-\Delta/T)$, where Δ is the energy gap at

the Fermi surface. This opens up the possibility that, in superfluid or superconducting phases, the dominant contribution to the bulk viscosity might come from purely leptonic processes. The relevant process is conversion of electrons to muons (and vice versa) via either the direct Urca process or the modified Urca process. The direct Urca leptonic conversion process is forbidden by energy and momentum conservation: in converting an electron near its Fermi surface to a muon near its Fermi surface, the change in free energy is very small (of order T), so the emitted neutrinos carry momentum and energy of this order. But the change of momentum of the charged lepton is large, at least $\mu_l - \sqrt{\mu_l^2 - m_\mu^2}$, and the low-energy neutrino cannot carry this much momentum. However, the modified Urca process can occur; for example, two electrons with energy slightly above the Fermi energy can scatter to an electron and a muon with energies near the Fermi energy, or an electron and muon can scatter to two muons. The strongest interaction between leptons is electromagnetism, so this process proceeds via exchange of a photon, whose propagator should include the effects of screening by the nuclear medium. As the temperature decreases, the process will become suppressed as the Fermi distributions assume their zero-temperature step function profiles, but at finite temperature the modified Urca process will result in a non-zero contribution to the bulk viscosity.

We calculate the leptonic bulk viscosity arising from the processes $e + \ell \rightleftharpoons \mu + \ell + \nu + \bar{\nu}$, where $\ell = e$ or μ. We conclude that, if the protons and neutrons are both ungapped, i.e if there is neither superfluidity nor superconductivity, then the bulk viscosity from these purely leptonic processes is several orders of magnitude smaller

than that from the nucleonic processes. However, once the temperature drops below the critical value for Cooper pairing of the protons or neutrons, the nucleonic bulk viscosity at frequencies $\gtrsim 10\,\mathrm{Hz}$ is strongly suppressed, and leptonic processes become the dominant source of bulk viscosity at those frequencies.

In chapter 4, we lay out the process for calculating the bulk viscosity of a two-component leptonic system under application of a periodic volume and pressure perturbation. A crucial component of this calculation is the conversion rate between electrons and muons, which is discussed in great detail. We show the numerical results of our calculations and how they compare to the bulk viscosity resulting from modified Urca equilibration of the nucleon population.

1.6 Strange stars: an example interface between phases of a U(1)×U(1) gauge theory

It is possible that 3-flavor strange quark matter is absolutely stable, resulting in "strange stars" where the entire star may consist of quark matter instead of nucleonic matter [2]. In the vaccum outside the star, hadrons are confined, and inside the star, quarks are deconfined. In chapter 5 (based on [47]), the reflection and transmission properties of light at the boundary between these two phases is investigated, as well as the properties at boundaries between other possible phases.

We study boundaries between phases in which different linear combinations of gauge generators are free. Mixing of gauge generators is familiar from the standard

model of particle physics, and the possibility of creating neighboring domains in which different linear combinations of gauge generators are free is now receiving serious attention. To set the stage for this work we first briefly review a concrete example.

In the standard model, the propagating $U(1)$ gauge boson (the photon) is associated with a particular Abelian $U(1)_Q$ subgroup of the full standard model gauge group. This subgroup emerged unbroken from the electroweak Higgs symmetry breaking $SU(2) \otimes U(1)_Y \to U(1)_Q$ at the TeV scale, and is generated by some linear combination of the "W_3" generator of the $SU(2)$ weak interaction and the "Y" generator of the $U(1)$ hypercharge interaction.

We now know that in quark matter the gauge group for the propagating $U(1)$ gauge boson will be rotated into a different direction by a further layer of symmetry breaking at the MeV scale. At sufficiently high density, quark matter will develop a condensate of quark Cooper pairs that plays the role of a Higgs field [48, 49]. (For reviews of this phenomenon of "color superconductivity" see Ref. [50]). In the real world, quark matter is expected to contain the three lightest flavors, and in this case the condensate forms a "color-flavor-locked" (CFL) phase [51], in which a linear combination of the photon and one of the gluons remains massless, while the orthogonal linear combination and the remainder of the gluons become massive by the Higgs mechanism. The gauge symmetry breaking is $SU(3)_{\text{color}} \otimes U(1)_Q \to U(1)_{\tilde{Q}}$. Thus a "rotated" electromagnetism is present in the CFL color superconducting phase of quark matter. This raises the interesting possibility of having an interface between a vacuum region in which the propagating gauge boson is the usual Q-photon, and

a quark matter region in which it is a different particle, the $\tilde{Q}$-photon, which is a mixture of the photon and a gluon. What will happen to electromagnetic fields, including light beams, that encounter such an interface?

The $U(1) \otimes U(1)$ gauge system arises in various other physical contexts. Electroweak symmetry breaking can be simplified to a $U(1) \otimes U(1)$ system by focussing on the hypercharge and W_3 bosons, which mix to form the photon and Z^0. The $U(1) \otimes U(1)$ gauge system also arises in extensions of the standard model, where an extra $U(1)$ gauge symmetry with a corresponding Z' gauge boson is added. Natural contexts for this include Grand Unified Theories with gauge groups such as $SO(10)$ and E_6, and some string models [52, 53].

In chapter 5 we study the light reflection and transmission properties of a boundary between phases in a $U(1) \otimes U(1)$ gauge theory. There have been previous studies of the behavior of magnetic fields [54] and light beams [55] in the specific case of the interface between the vacuum and CFL quark matter. However, we consider the most general realization of the gauge symmetries that supports propagating gauge bosons. On one side of the boundary both $U(1)$ gauge symmetries may be free, or some linear combination may be Higgsed or confined. On the other side, both $U(1)$ gauge symmetries may be free, or a *different* linear combination may be Higgsed or confined, where the difference is parameterized by a "mismatch angle" α. We calculate the nature and intensity of the reflected and transmitted gauge bosons in each case.

We introduce the $U(1) \otimes U(1)$ model and show how Higgsing or confinement of

a gauge field can be implemented by appropriate boundary conditions at the interface and describe the calculation of the reflection and transmission coefficients for the various types of boundary. We then discuss how they compare with previous calculations, explain some mysterious features, and analyze their compatibility with expectations based on the complementarity principle. We also analyze subleties of the low-frequency limit and a detailed example of complementarity.

Chapter 2

Isospin asymmetry and Cooper pair interactions

Recently, it has been suggested that nuclear matter in neutron stars might be a type-I superconductor. The astrophysical evidence is that certain neutron stars have long precession periods, and it has been suggested that this means the proton supercon-ductivity cannot be type-II [7], although that inference has been contested [8, 9]. A theoretical argument for type-I superconductivity in neutron star cores was then presented by Buckley et. al. in Ref. [10]. These authors assumed that the effective potential for the Cooper pair fields has a $U(2)$ symmetry under rotation of proton and neutron Cooper pairs into each other. Specifically, the effective potential for the Cooper pair fields was assumed to take the form

$$V(|\Delta_{pp}|^2, |\Delta_{nn}|^2) \approx U(|\Delta_{pp}|^2 + |\Delta_{nn}|^2)$$

$$= -\mu_c(|\Delta_{pp}|^2 + |\Delta_{nn}|^2) + a(|\Delta_{pp}|^2 + |\Delta_{nn}|^2)^2 + \cdots$$

(2.1)

The assumption that the potential is approximately a function of $|\Delta_{pp}|^2 + |\Delta_{nn}|^2$ leads to $|\Delta_{pp}|^2|\Delta_{nn}|^2$ cross terms, which provide a strong repulsive interaction between the neutron and proton Cooper pair condensates. It is argued in Ref. [10] that this leads to a long-range attraction between proton flux tubes, i.e. type-I superconductivity.

The assumed $U(2)$ symmetry was justified by invoking the isospin symmetry of the underlying nuclear interaction. The authors of Ref. [10] admit that isospin is severely broken by the constraint of electrical neutrality, which, combined with beta-equilibration, greatly suppresses the proton Fermi momentum relative to the neutron Fermi momentum, but they claim that this does not affect the interaction between the p-p and n-n Cooper pairs. This seems implausible, since it is well known in the theory of superconductivity that the coefficients of the terms in the Landau-Ginzburg effective theory, including the quartic coupling a, depend strongly on the Fermi momenta of the underlying fermions [11]. For example, for a one component Fermi gas, just below the BCS critical point, the effective Landau-Ginzburg potential is

$$V(|\Delta|^2) = -\mu|\Delta|^2 + a|\Delta|^4 + \cdots \tag{2.2}$$

where $\mu \approx N_F(T_c - T)/T_c$, and N_F is the density of states at the Fermi surface, so for non-relativistic fermions $N_F \propto mp_F$ where m is the mass and p_F is the Fermi momentum. The minimum of the potential occurs at $\Delta_0 = \sqrt{\mu/(2a)}$, so the quartic coefficient is $a = \mu/(2\Delta_0^2)$. The binding energy of the condensate is then $V(\Delta_0) = -\frac{1}{2}N_F\Delta_0^2$, a well-known result in the superconductivity literature [12]. We see that μ,

a, and $V(\Delta_0)$ are all very sensitive to the Fermi momenta of the underlying fermions. Clearly for protons and neutrons in a neutron star, which have very different Fermi momenta but similar pairing condensates Δ, this will not give an effective potential of the form (2.1).

In this chapter, we back up our reasoning with a concrete calculation. We work with a very simple microscopic model for nucleon-nucleon interactions, and analyze the pairing using the mean-field approximation. We take into account the requirements of electrical neutrality and equilibration under the weak interactions, which disfavor neutron-proton pairing. At zero temperature the potential is not accurately described by an low-order polynomial like (2.1), but we can expand around the mean field and obtain the quartic coupling between small fluctuations ϕ_{nn}, ϕ_{pp},

$$\Omega(\phi_{pp}, \phi_{nn}) = \cdots + \alpha_{pp}\phi_{pp}^4 + \alpha_{nn}\phi_{nn}^4 + \alpha_{np}\phi_{pp}^2\phi_{nn}^2 + \cdots . \qquad (2.3)$$

By explicitly calculating these couplings we find that they do not obey the $U(2)$ symmetry assumed in Ref. [10]. In fact, in the mean field approximation our result (2.14) shows no interaction at all between the proton and neutron Cooper pairs: $\alpha_{np} = 0$. This appears to be a generic mean-field result, and does not depend on any specific features of the pairing interaction. Further, and as expected from the preceding discussion, we find that $\alpha_{pp} \ll \alpha_{nn}$. We then discuss the lowest-order corrections beyond the mean-field approximation by calculating the effective interaction between neutron and proton Cooper pairs diagrammatically. We show that this interaction is sub-leading in the coupling and is negligible in weak coupling. At temperatures close

to the critical temperature, where Landau-Ginzburg theory can be used to analyze vortex structure, we find that the interaction between the pp condensate and the nn is weak and repulsive, not strong and attractive as Eq. (2.1) would imply.

Our simple model of neutrons and protons is based on the isospin-symmetric Lagrangian

$$\mathcal{L} = \mathcal{L}_{\text{kinetic}} + \mathcal{L}_{\text{int}} ,$$

$$\mathcal{L}_{\text{kinetic}} = N_{\alpha a}^{\dagger} \left(\frac{\partial}{\partial \tau} - \frac{\nabla^2}{2m} - \mu_a \right) N_{\alpha a} , \tag{2.4}$$

$$\mathcal{L}_{\text{int}} = -\frac{G}{2} \left(N_{\alpha a}^{\dagger} N_{\alpha a} \right)^2 .$$

The nucleon field $N_{a\alpha}$ has isospin index $a = n, p$ and spin index $\alpha = \uparrow, \downarrow$. Repeated indices are summed. We immediately generalize the interaction to allow different couplings for protons and neutrons, and Fierz-transform it into the pairing form. We assume that all pairing is in the rotationally invariant s-wave channel, so keeping only those terms we obtain

$$\begin{aligned} \mathcal{L}_{\text{int}} = {} & -G_{pp}\, p_{\uparrow}^{\dagger} p_{\downarrow}^{\dagger} p_{\downarrow} p_{\uparrow} - G_{nn}\, n_{\uparrow}^{\dagger} n_{\downarrow}^{\dagger} n_{\downarrow} n_{\uparrow} \\ & - \tfrac{1}{2} G_{np}\, (p_{\uparrow}^{\dagger} n_{\downarrow}^{\dagger} + n_{\uparrow}^{\dagger} p_{\downarrow}^{\dagger})(n_{\downarrow} p_{\uparrow} + p_{\downarrow} n_{\uparrow}) . \end{aligned} \tag{2.5}$$

The isospin-symmetric case corresponds to $G_{pp} = G_{nn} = G_{np}$. This interaction will lead to pairing of the fermions at their Fermi surfaces, by the usual BCS mechanism. We can calculate the thermodynamic potential of the paired state by a standard Hubbard-Stratonovich transformation that introduces complex bosonic Cooper-pair fields Δ_{nn}, Δ_{pp}, and Δ_{pn} (for a review, see [56]). The Lagrangian then has three parts:

the kinetic term is as before, and the others contain the Cooper pair fields:

$$\mathcal{L} = \mathcal{L}_{kinetic} + \mathcal{L}_\Delta + \mathcal{L}_F,$$

$$\mathcal{L}_\Delta = |\Delta_{nn}|^2/G_{nn} + |\Delta_{pp}|^2/G_{pp} + |\Delta_{pn}|^2/G_{np},$$

$$\mathcal{L}_F = -\Delta_{nn}^* n_\downarrow n_\uparrow - \Delta_{pp}^* p_\downarrow p_\uparrow$$
$$-\frac{1}{\sqrt{2}}\Delta_{pn}^*(p_\downarrow n_\uparrow + n_\downarrow p_\uparrow) + h.c.$$

$$(2.6)$$

By adjusting the phases of the n and p fields we can choose Δ_{nn} and Δ_{pp} to be real, leaving Δ_{pn} complex. As is well known [57], in neutron star matter the mismatch between the proton and neutron Fermi surfaces completely suppresses n-p pairing, so $\Delta_{pn} = 0$ even at small isospin asymmetry, but for now we keep the Δ_{pn} term. In the mean-field approximation, we neglect any space-time variation in the Δ fields and set them equal to their vacuum expectation values. We can then integrate out the fermions, giving us the volume density of the thermodynamic potential or grand canonical potential $\Omega = E/V - \mu N/V = -p$. In the rest of this paper we will loosely refer to this as the "thermodynamic potential". We find

$$\Omega = \mathcal{L}_\Delta - \int \frac{d\omega}{2\pi} \int^\Lambda \frac{d^3k}{(2\pi)^3} \ln \mathrm{Det} M, \qquad (2.7)$$

where we have introduced an ultraviolet cutoff Λ on the three-dimensional momentum integral. To obtain this expression, we wrote the inverse propagator in the Nambu-Gork'ov basis $(p_\uparrow, n_\uparrow, p_\downarrow^\dagger, n_\downarrow^\dagger, p_\downarrow, n_\downarrow, p_\uparrow^\dagger, n_\uparrow^\dagger)$, and observed that it block-diagonalizes

into two identical 4×4 blocks,

$$
M = \begin{pmatrix}
-i\omega + \epsilon_p & 0 & -\Delta_{pp} & -\dfrac{\Delta_{pn}}{\sqrt{2}} \\[2ex]
0 & -i\omega + \epsilon_n & -\dfrac{\Delta_{pn}}{\sqrt{2}} & -\Delta_{nn} \\[2ex]
-\Delta_{pp} & -\dfrac{\Delta_{pn}^*}{\sqrt{2}} & -i\omega - \epsilon_p & 0 \\[2ex]
-\dfrac{\Delta_{pn}^*}{\sqrt{2}} & -\Delta_{nn} & 0 & -i\omega - \epsilon_n
\end{pmatrix}. \tag{2.8}
$$

Note that when $\Delta_{pn} = 0$, M further decomposes into 2×2 blocks, for $(p_\uparrow, p_\downarrow^\dagger)$, $(n_\uparrow, n_\downarrow^\dagger)$ etc, which describe the s-wave pairing of protons and neutrons respectively. In Eq. (2.8), $\epsilon_p \equiv k^2/2m - \mu_p$ and $\epsilon_n \equiv k^2/2m - \mu_n$. The determinant is straightforward to compute and we obtain

$$
\begin{aligned}
\mathrm{Det} M &= (\omega^2 + \epsilon_n^2)(\omega^2 + \epsilon_p^2) + \Delta_{nn}^2(\omega^2 + \epsilon_p^2) \\[1ex]
&+ \Delta_{pp}^2(\omega^2 + \epsilon_n^2) + |\Delta_{pn}|^2(\omega^2 + \epsilon_p\epsilon_n) \\[1ex]
&+ (\Delta_{nn}\Delta_{pp} - \Delta_{pn}^2/2)(\Delta_{nn}\Delta_{pp} - \Delta_{pn}^{*2}/2)
\end{aligned} \tag{2.9}
$$

The requirement that the vacuum expectation values Δ_{pp}, Δ_{nn}, and Δ_{pn} minimize the thermodynamic potential is expressed in the three gap equations,

$$
\begin{aligned}
\frac{\Delta_{nn}}{G_{nn}} &= \int \frac{d\omega d^3 k}{(2\pi)^4} \frac{\Delta_{nn}(\omega^2 + \epsilon_p^2) + \Delta_{pp}(\Delta_{pp}\Delta_{nn} - \mathrm{Re}\Delta_{pn}^2/2)}{\det M} \\[2ex]
\frac{\Delta_{pp}}{G_{pp}} &= \int \frac{d\omega d^3 k}{(2\pi)^4} \frac{\Delta_{pp}(\omega^2 + \epsilon_n^2) + \Delta_{nn}(\Delta_{pp}\Delta_{nn} - \mathrm{Re}\Delta_{pn}^2/2)}{\det M} \\[2ex]
\frac{\Delta_{pn}}{G_{np}} &= \int \frac{d\omega d^3 k}{(2\pi)^4} \frac{\Delta_{pn}(\omega^2 + \epsilon_p\epsilon_n) - \Delta_{pn}^*(\Delta_{pp}\Delta_{nn} - \Delta_{pn}^2/2)}{\det M}
\end{aligned} \tag{2.10}
$$

When $\Delta_{pn} = 0$, as in neutron star matter [57] these equations decouple into independent gap equations for Δ_{pp} and Δ_{nn}.

Because our model interaction is so simple, it predicts pairing gaps that rise with the density of states near the Fermi surface, so Δ rises with p_F. This means that it does not produce realistic neutral nuclear matter, in which the interaction is isospin-symmetric, and $p_{Fp} \ll p_{Fn}$ (from electrical neutrality) but nevertheless $\Delta_{pp} \approx \Delta_{nn}$. In the real world, this happens because the nuclear interaction at short distance is repulsive, so even though $p_{Fn} \gg p_{Fp}$, the neutrons end up with a similar pairing gap to the protons. In our simple model, which is strictly valid only at low density, the four-Fermion coupling only encodes the attractive part of the interaction through the s-wave scattering length. We will choose G_{pp} to be larger than G_{nn} so that in the neutral system the protons and neutrons have the same pairing gap, as in real nuclear matter. It will turn out that our essential conclusion, that there is no $U(2)$ symmetry of the effective potential for the Cooper pair fields, holds irrespective of whether or not the the couplings G_{pp} and G_{nn} are equal. It is then reasonable to guess that G_{np} should have a value somewhere between G_{nn} and G_{pp}. To be specific, we shall employ typical values $\mu_n \sim 60$ MeV ($k_{Fn} \sim 335$ MeV) and $\mu_p \sim 8$ MeV ($k_{Fp} \sim 123$ MeV) and a momentum cut-off $\Lambda = 750$ MeV. For these parameters the four-fermion couplings that gives $\Delta_{nn} \sim 1$ MeV and $\Delta_{pp} \sim 1$ MeV are $G_{nn} \sim 1 \times 10^{-5}$ MeV^2 and $G_{pp} \sim 2 \times 10^{-5}$ MeV^2, respectively.

Since $\Delta_{np} = 0$ in beta-equilibrated neutral nuclear matter, we can write the mean-field thermodynamic potential

$$
\begin{aligned}
\Omega &= \frac{\Delta_{nn}^2}{G_{nn}} + \frac{\Delta_{pp}^2}{G_{pp}} - \int \frac{d\omega}{2\pi} \int^{\Lambda} \frac{d^3k}{(2\pi)^3} \Big(\ln(\omega^2 + \epsilon_n^2 + \Delta_{nn}^2) + \ln(\omega^2 + \epsilon_p^2 + \Delta_{pp}^2) \Big) \quad (2.11) \\
&= \frac{\Delta_{nn}^2}{G_{nn}} - \int^{\Lambda} \frac{d^3k}{(2\pi)^3} \Big(\sqrt{\epsilon_n^2 + \Delta_{nn}^2} - \epsilon_n \Big) + \frac{\Delta_{pp}^2}{G_{pp}} - \int^{\Lambda} \frac{d^3k}{(2\pi)^3} \Big(\sqrt{\epsilon_p^2 + \Delta_{pp}^2} - \epsilon_p \Big) \quad (2.12)
\end{aligned}
$$
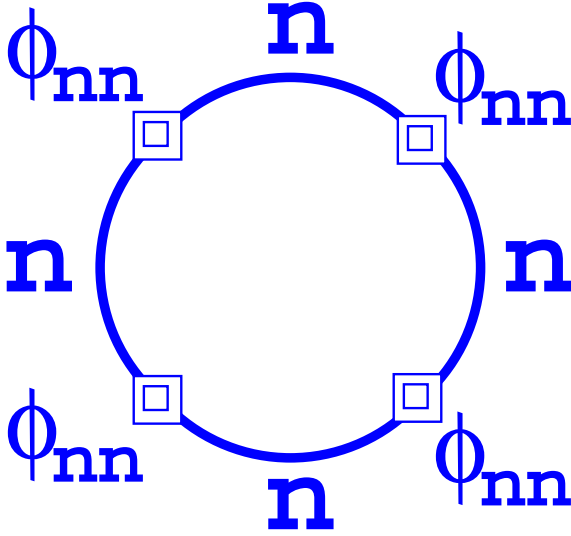
Figure 2.1: The lowest-order mean-field contribution to α_{nn}, the coefficient of the ϕ_{nn}^4 term in the effective potential, which describes scattering between low-momentum fluctuations ϕ_{nn} in the nn condensate. The thick lines are Nambu-Gork'ov neutron propagators. Each double-square vertex is an insertion of the ϕ_{nn} operator. There is a similar diagram for α_{pp}.

We see that this is equal to the sum of the thermodynamic potentials for two species of Cooper pair bosons that do not interact with each other. There are no cross-terms between Δ_{pp} and Δ_{nn}. The effective potential does not take the form (2.1). This result did not depend on the specific form of the interaction. It simply arises from the fact that beta-equilibrium and electrical neutrality require $p_{Fp} \ll p_{Fn}$, and Cooper pairing is suppressed between species with very different Fermi momenta.

We may use Eq. (2.12) to investigate the nature of the quartic terms that describe the coupling between fluctuations in the Cooper-pair densities. Fluctuations in the pairing field ϕ_{nn}, ϕ_{pp} are defined through the following substitutions in Eq. (2.12): $\Delta_{nn} \rightarrow \tilde{\Delta}_{nn} + \phi_{nn}$ and $\Delta_{pp} \rightarrow \tilde{\Delta}_{pp} + \phi_{pp}$ where $\tilde{\Delta}_{nn}$ and $\tilde{\Delta}_{pp}$ are the ground state

expectation values that satisfy the gap equations. For small fluctuations an expansion

of the thermodynamic potential about the mean field ground state is well motivated.

Retaining only the quartic terms

$$\Omega(\phi_{pp}, \phi_{nn}) = \cdots + \alpha_{pp}\phi_{pp}^4 + \alpha_{nn}\phi_{nn}^4 + \alpha_{np}\phi_{pp}^2\phi_{nn}^2 + \cdots . \tag{2.13}$$

From the preceding discussion it is clear that in the mean field approximation there

are no cross-terms. The coefficients α_{nn} and α_{pp} are non zero and depend in general

on the chemical potentials, $\tilde{\Delta}_{nn}$ and $\tilde{\Delta}_{pp}$. Explicitly, by Taylor expanding Eq. (2.12)

we find

$$
\begin{aligned}
\alpha_{np} &= 0 , \\
\alpha_{nn} &= \frac{1}{8} \int \frac{d^3 k}{(2\pi)^3} \frac{1}{E_n^3} - \frac{6\tilde{\Delta}_{nn}^2}{E_n^5} + \frac{5\tilde{\Delta}_{nn}^4}{E_n^7} , \\
\alpha_{pp} &= \frac{1}{8} \int \frac{d^3 k}{(2\pi)^3} \frac{1}{E_p^3} - \frac{6\tilde{\Delta}_{pp}^2}{E_p^5} + \frac{5\tilde{\Delta}_{pp}^4}{E_p^7} ,
\end{aligned}
\tag{2.14}
$$

where $E_n = \sqrt{\epsilon_n^2 + \tilde{\Delta}_{nn}^2}$ and $E_p = \sqrt{\epsilon_p^2 + \tilde{\Delta}_{pp}^2}$. These contributions can also be

calculated in a diagrammatic approach using the Nambu-Gorkov Greens functions

[4]. The diagram for α_{nn} is shown in Fig. 2.1, and there is an analogous one for α_{pp}.

We find

$$\alpha_{nn} = \frac{1}{4} \int \frac{d^3 k}{(2\pi)^3} \ kT \sum_s \ \mathrm{Tr} \ [\mathcal{G}_n(k, i\omega_s)\tau\mathcal{G}_n(k, i\omega_s)\tau\mathcal{G}_n(k, i\omega_s)\tau\mathcal{G}_n(k, i\omega_s)\tau] \ , \tag{2.15}$$

where the finite temperature Nambu-Gorkov Green's function for the neutron super-

fluid, expressed in the $(n_\uparrow, n_\downarrow^\dagger)$ basis (see text after Eq. (2.8)), is

$$\mathcal{G}_n(k, i\omega_s) = \frac{1}{(i\omega_s)^2 - E_n^2(p)} \begin{pmatrix} -i\omega_s + \epsilon_n & -\Delta_{nn} \\ -\Delta_{nn} & -i\omega_s - \epsilon_n \end{pmatrix} , \tag{2.16}$$

and insertions of the fluctuating pairing field are

$$\tau = \begin{pmatrix} 0 & 1 \\ 1 & 0 \end{pmatrix}. \qquad (2.17)$$

The Matsubara frequency is $\omega_s = (2s + 1)\pi kT$. In evaluating these diagrams we ignore any momentum transfer since we are interested only in the low momentum fluctuations. We have explicitly checked that the diagrammatic approach gives the same result as Eq. (2.14). At zero temperature and when $\tilde{\Delta}/\mu$ is small we obtain the following analytic expressions

$$\alpha_{nn} = -\frac{Mk_{Fn}}{24\pi^2\tilde{\Delta}_{nn}^2}\left(1 + O[\frac{\tilde{\Delta}_{nn}^2}{\mu_n^2}]\right), \qquad (2.18)$$

$$\alpha_{pp} = -\frac{Mk_{Fp}}{24\pi^2\tilde{\Delta}_{pp}^2}\left(1 + O[\frac{\tilde{\Delta}_{pp}^2}{\mu_p^2}]\right). \qquad (2.19)$$

We see that the couplings are proportional to the corresponding Fermi momenta, $\alpha_{nn} \propto k_{Fn}$ and $\alpha_{pp} \propto k_{Fp}$, so the scattering of proton condensate fluctuations is much weaker than that of neutron condensate fluctuations, indicating a strong breaking of any symmetry that rotates proton Cooper pairs into neutron Cooper pairs. Further, the sign of α_{nn} and α_{pp} is negative. However, since we are Taylor expanding about the global minimum of the thermodynamic potential, there are lower and higher order terms (not explicitly written in Eq. (2.13)) that ensure that the system is stable with respect to both small and large fluctuations. This is in contrast to the usual Landau-Ginzburg analysis just below T_c, where a Taylor expansion about the normal state is characterized by a negative quadratic coefficient and a positive quartic term.

We now discuss corrections to Eq. (2.12) beyond the mean field approximation.
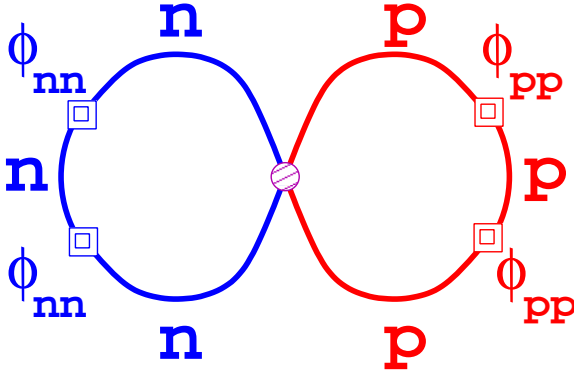
Figure 2.2: The lowest-order contributions beyond mean field to α_{np}, the coefficient of the $\phi_{nn}^2 \phi_{pp}^2$ term in the effective potential, which describes scattering between low-momentum fluctuations ϕ_{nn} and ϕ_{pp} in the nn and pp condensates.   The thick lines are Nambu-Gork'ov neutron or proton propagators. The double square vertices are insertions of the ϕ_{nn} and ϕ_{pp} operators. The hatched vertex is the fundamental $n^\dagger n p^\dagger p$ interaction in the Lagrangian.

The leading order diagram that contributes to the scattering between neutron and proton fluctuations is shown in Fig. 2.2. The important point is that this diagram involves the fundamental four-fermion neutron-proton interaction G_{np}. Evaluating the diagram, we find that the leading-order beyond-mean-field contribution to the effective four-point interaction between the proton and neutron condensate fluctuations is

$$
\begin{aligned}
\alpha_{np} &= \frac{1}{4} \, G_{np} \int \frac{d^4k}{(2\pi)^4} \, \text{Tr} \left[\mathcal{G}_n(k, i\omega) \tau \mathcal{G}_n(k, i\omega) \tau \mathcal{G}_n(k, i\omega) \tau_3 \right] \\
&\quad \times \int \frac{d^4k}{(2\pi)^4} \text{Tr} \left[\mathcal{G}_p(k, i\omega) \tau \mathcal{G}_p(k, i\omega) \tau \mathcal{G}_p(k, i\omega) \tau_3 \right] \qquad (2.20) \\
&= - \, G_{np} \, \frac{k_{Fn}^3 k_{Fp}^3}{64\pi^4 \mu_n^2 \mu_p^2} \, f(\frac{\Delta_{nn}}{\mu_n}) \, f(\frac{\Delta_{pp}}{\mu_p}) \, , \qquad (2.21)
\end{aligned}
$$

where $\mathcal{G}_n(k, i\omega)$ and $\mathcal{G}_p(k, i\omega)$ are the Nambu-Gorkov Green's functions for the neutrons and protons respectively, and $\tau_3 = \text{diag}(1, -1)$ is the diagonal Pauli matrix [4].

The dimensionless function f is defined by the integral

$$f(\delta) = \int_{-1}^{\infty} dx \; x \; \sqrt{x+1} \; \frac{x^2 - 2\delta^2}{(\delta^2 + x^2)^{5/2}} \; . \tag{2.22}$$

For $\delta \ll 1$ we obtain the following analytic relation

$$f(\delta) = -1 + \log \left[\frac{8}{\delta} \right] + \mathcal{O}[\delta^2] \; . \tag{2.23}$$

To see whether beyond-mean-field corrections can raise α_{np} to a value comparable to α_{nn} or α_{pp} we follow Ref. [10] in defining an asymmetry parameter

$$\epsilon = (\alpha_{nn}\alpha_{pp} - \alpha_{np}^2)/(\alpha_{nn}\alpha_{pp}) \; . \tag{2.24}$$

(Ref. [10] expresses ϵ in terms of the quartic couplings a_{pp}, a_{nn}, a_{np} for the expansion around $\Delta = 0$, but it should be equally valid to expand around the mean field, which is the minimum of the thermodynamic potential.) Ref. [10] concluded that type-I superconductivity requires $\epsilon < 1/20$. As we have seen, in the mean-field approximation $\epsilon = 1$. From Eq. (2.21) we find that the beyond-mean-field corrections to ϵ are negligible by several orders of magnitude. ϵ is always within 10^{-4} of unity.

All our calculations so far have been at zero temperature, in which case the expansion of the potential around the mean-field ground state is only valid for small deviations from that state. This makes it impossible to discuss the expected structure of the vortices, in which the pairing fields vary from zero to their vacuum values. In order to be able to say anything about the vortices, we have to work at temperatures close to the critical temperature T_c, where a traditional Landau-Ginzburg analysis is possible, using an expansion around the zero-mean-field state with only the quadratic

and quartic terms,

$$\Omega(T \sim T_c; \phi_{nn}, \phi_{pp}) = -\mu_{nn}^c \phi_{nn}^2 - \mu_{pp}^c \phi_{pp}^2 + a_{pp}^c \phi_{pp}^4 + a_{nn}^c \phi_{nn}^4 + a_{np}^c \phi_{pp}^2 \phi_{nn}^2 + \cdots . \quad (2.25)$$

This analysis was performed by S. Reddy and presented in [13], so it will not be included here. However, we will state the results of the analysis. For our choice of parameters we find that $T_c \simeq 0.6$ MeV. For $T = 0.4$ MeV the coefficients of the effective potential are $\mu_{nn}^c = 5520 \,\mathrm{MeV}^2$, $\mu_{pp}^c = 2010 \,\mathrm{MeV}^2$, $a_{nn}^c = 2627$, $a_{pp}^c = 968$ and $a_{np}^c = -3(G_{np}/G_{nn})$. As before, the asymmetry parameter $\epsilon \simeq 1$ since $a_{np} \ll a_{nn}$ and $a_{np} \ll a_{pp}$. The fact that a_{np}^c is negative implies that the neutron(proton) superfluid density will decrease in the inner core of the proton(neutron) vortex.

Our conclusion is that in neutral nuclear matter, the disparity between the neutron and proton Fermi momenta provides a strong explicit breaking of the $U(2)$ symmetry posited in Ref. [10]. This breaking is far too strong to allow the proposed mechanism for type-I superconductivity to operate. A calculation of the vortex structure is presented in chapter 4, where due to the non-perturbative nature of the interaction between nucleons, we do not exclude the possibility of a strong coupling between the neutron and proton superfluids. In our simple model the attractive interaction between neutrons and protons directly leads to a negative a_{np}^c leading to a depletion of the neutron superfluid in the core of the proton vortex. This result is robust as long as the effective interaction between neutrons and protons is attractive and contradicts the predictions in Ref. [10] where the neutron superfluid density increased inside the proton vortex.

Chapter 3

Flux tubes and the type-I/type-II transition in a superconductor coupled to a superfluid

In this chapter we investigate a system that has both a charged condensate, leading to superconductivity, and a neutral condensate, leading to superfluidity. We focus on the magnetic flux tubes that are associated with the superconducting condensate, and study how they are modified by the presence of the superfluid, assuming that the two condensates can interact with each other via density and gradient ("entrainment") interactions. Nuclear matter is an example of this type of system, which at sufficiently high density undergoes Cooper pairing of both neutrons and protons. We will present our calculations in this context, referring to the charged condensate as the "proton condensate" and the neutral one as the "neutron condensate", and choosing values

appropriate to nuclear matter for our parameters when presenting numerical results.

We study the type I versus type II nature of a (proton) superconductor coupled to a (neutron) superfluid, using an effective theory for the protons and neutrons that contains four-fermion interaction terms which lead to *s*-wave pairing. We do not include higher-angular-momentum pairing, although that would be needed for a more realistic analysis of high-density nuclear matter. Our analysis extends that of Ref. [10] in the following ways: (a) Our model, like that of Ref. [10], contains a coupling a_{np} between the magnitudes of the neutron and proton condensates, and self-couplings a_{nn} and a_{pp}, but we survey the whole range of values of a_{np}, from zero to of order a_{pp}; (b) we also include "entrainment" interactions between the gradients of the proton and neutron condensates; (c) we use a simpler and more direct method to study the type-I/type-II phase boundary, using the energetics of flux tube coalescence/fission: we calculate the energy of flux tubes with a wide range of magnetic fluxes, from one quantum to several hundred quanta, and find which one has the lowest energy per unit flux. As we will see, this has the additional benefit of allowing us to find exotic stable multi-quantum flux tubes, such as have been found in systems of two coupled superconductors [15]. However, as we discuss below, our analysis is not sensitive to minima in the interaction energy at finite separation between flux tubes.

Our analysis is entirely at zero temperature. This is a good approximation for neutron star matter near nuclear saturation density, where the critical temperatures for the superfluid and superconductor are of order MeV [16, 17, 18]. The temperature of a compact star drops below this value within minutes of its formation in a

supernova, and is at or below the keV range after the first 1000 years [19]. When we discuss type-I versus type-II behavior we are referring to the response of the system to a magnetic field at the lower critical value, at $T = 0$.

As far as we know, there has been no previous work on how a flux tube in a superconductor is affected by a gradient coupling to a co-existing superfluid. However, there has been work on possible knot solitons [20], vortices in the $SO(5)$ model of high-temperature superconductivity [21], and on the complementary situation, a superfluid vortex with gradient coupling to a co-existing superconductor. There the coupling leads to the "entrainment" or Andreev-Bashkin effect [22] whereby the proton condensate is dragged along with the neutron condensate, producing a non-zero proton current around the vortex, dressing it with some magnetic flux [23]. It is interesting to note that this flux is not a multiple of the flux quantum for proton flux tubes. This is possible because of the difference between the energetics of a neutron vortex and a proton flux tube. The flux tube has energy density localized to the vicinity of its core. Far from the core the energy density must vanish, which means the proton field must change in phase by a multiple of 2π, and the the vector potential must cancel the resultant gradient, leading to a quantized magnetic flux. A neutron vortex, by contrast, has gradient energy that is not localized to the vicinity of the vortex, and the total energy per unit length diverges in the infinite volume limit. The vector potential is therefore not constrained to cancel any gradient in the proton field, and takes on a value that minimizes the overall energy, with no quantization condition on the resulting magnetic flux.

Returning to the situation that we study, a proton flux tube in a neutron superfluid background, we do not expect a similar behavior. This is because the proton flux tube's energy density is localized around its core, giving it (unlike the neutron vortex) a finite energy per unit length. If the neutron condensate were entrained, and developed non-zero circulation around the flux tube, it would acquire a non-localized energy density, leading to an infinite energy per unit length for the flux tube, which is clearly energetically disfavored. We will see that the effect of gradient couplings on the proton superconductor is more subtle: it leads to metastable regions near the type-I/type-II boundary.

3.1   Stability of flux tubes

Our aim is to explore the response of the proton superconductor to an applied critical magnetic field at zero temperature. We will therefore construct a phase diagram in the space of the coupling constants of the Ginzburg-Landau effective theory. We would like to be able to specify when it is of type II (at the lower critical magnetic field, flux tubes appear, and remain separate, i.e they repel) and when it is of type I (at the critical magnetic field, macroscopic normal regions appear, i.e. the flux tubes attract and coalesce). The simplest way to do this is to calculate the energy per unit length E_n of a flux tube containing n flux quanta. The same approach has been used for vortices in the $SO(5)$ model [58]. It is convenient to work in terms of the energy

per flux quantum,

$$B_n = \frac{E_n}{n} - E_1 \ .$$

(3.1)

When B_n is negative the n-quantum flux tube is stable against fission into many single quantum flux tubes, and it is energetically favorable for n single quantum flux tubes to coalesce into one n-quantum flux tube. When B_n is positive the n-quantum flux tube is unstable against fission, and coalescence is energetically disfavored. If one calculates B_n for all n then the energetically favored value of n is the one that minimizes B_n.

In a traditional type I superconductor, small flux tubes attract each other and amalgamate into large ones and ultimately into macroscopic normal regions, so we would expect to find $B_n < 0$ with its value dropping monotonically as n rises. In a type II superconductor we would expect $B_n > 0$, with its value rising monotonically with n. Our calculations confirm these results for a single superconductor, but we will see that B_n shows more complicated behavior when the superconductor feels interaction with a co-existing superfluid.

Calculations of B_n are straightforward because they always occur in a cylindrically symmetric geometry, so the problem is one-dimensional. For a more detailed understanding of flux tube interactions, one would have to consider two single-quantum flux tubes a distance d apart. Their total energy is $U(d)$, where $U(0) = E_2$ and $U(\infty) = 2E_1$, so $B_2 = \frac{1}{2}(U(0) - U(\infty))$. As expected, $B_2 < 0$ means that the flux tubes have lower energy when they amalgamate, and $B_2 > 0$ means that the flux tubes have lower energy when they separate. If $U(d)$ is monotonic, we can conclude

that flux tubes either coalesce ($B_2 < 0$) or repel to infinite separation ($B_2 > 0$), corresponding to type-I or type-II behavior respectively. However, if there is a minimum in $U(d)$ at some favored intermediate separation $d = d^*$ then irrespective of the sign of B_n, one has a new variety of type II superconductor with some favored Abrikosov lattice spacing d^*. Such behavior has been found to arise from a ϕ^6 term [59] and in the case of two charged condensates [15]. Calculating $U(d)$ in the current context is an interesting but demanding problem which we leave for future work. In this paper we assume that $U(d)$ is monotonic, so to analyze the attractiveness/repulsiveness of the flux tube interactions it is sufficient to calculate B_n, or equivalently E_n/n.

3.2 Flux tubes in the Ginzburg-Landau model

3.2.1 Ginzburg-Landau model

We start by writing down the zero-temperature Ginzburg-Landau effective theory of proton and neutron condensates in the presence of a magnetic field [6, 10]. We denote the proton condensate field by ϕ_p, the neutron condensate field by ϕ_n, and the magnetic vector potential by $\mathbf{A}$. The free energy density is

$$\mathcal{F} = \frac{\hbar^2}{2m_c}(|(\nabla - \frac{iq}{\hbar c}\mathbf{A})\phi_p|^2 + |\nabla\phi_n|^2) + \frac{|\nabla \times \mathbf{A}|^2}{8\pi} + U_{ent}(\phi_p, \phi_n) + V(|\phi_p|^2, |\phi_n|^2) \quad (3.2)$$

where m_c is twice the nucleon mass, q is twice the proton charge, U_{ent} is the entrainment

free energy density (see [6])

$$U_{ent} = -\frac{\hbar^2}{2m_c}\frac{\sigma}{2\langle\phi_p\rangle\langle\phi_n\rangle}\left[\phi_p^*\phi_n^*\left((\nabla-\frac{iq}{\hbar c}\mathbf{A})\phi_p\cdot\nabla\phi_n\right)+\phi_p^*\phi_n\left((\nabla-\frac{iq}{\hbar c}\mathbf{A})\phi_p\cdot\nabla\phi_n^*\right)\right.$$
$$\left.+\phi_p\phi_n\left((\nabla+\frac{iq}{\hbar c}\mathbf{A})\phi_p^*\cdot\nabla\phi_n^*\right)+\phi_p\phi_n^*\left((\nabla+\frac{iq}{\hbar c}\mathbf{A})\phi_p^*\cdot\nabla\phi_n\right)\right] \quad (3.3)$$

and

$$V(|\phi_p|^2,|\phi_n|^2) = -\mu_p|\phi_p|^2 - \mu_n|\phi_n|^2 + \frac{a_{pp}}{2}|\phi_p|^4 + \frac{a_{nn}}{2}|\phi_n|^4 + a_{pn}|\phi_p|^2|\phi_n|^2 \quad (3.4)$$

σ is a parameter characterizing the strength of the gradient coupling, μ_p and μ_n are

the chemical potentials of the proton and neutron condensate excitations, and a_{pp},

a_{nn}, and a_{pn} are the GL quartic couplings.

In zero magnetic field, the condensates would have position-independent bulk

densities $\langle\phi_p\rangle^2$ and $\langle\phi_n\rangle^2$ obtained by minimizing the free energy. This allows us to

eliminate the chemical potentials μ_p, μ_n by writing

$$\mu_p = a_{pp}\langle\phi_p\rangle^2 + a_{pn}\langle\phi_n\rangle^2$$
$$\mu_n = a_{nn}\langle\phi_n\rangle^2 + a_{pn}\langle\phi_p\rangle^2 \quad (3.5)$$

so up to constants involving $\langle\phi_p\rangle$ and $\langle\phi_n\rangle$, the potential V can be expressed in terms

of the deviations of the condensate fields from their bulk values:

$$V(|\phi_p|^2,|\phi_n|^2) = \frac{a_{pp}}{2}\left(|\phi_p|^2 - \langle\phi_p\rangle^2\right)^2 + \frac{a_{nn}}{2}\left(|\phi_n|^2 - \langle\phi_n\rangle^2\right)^2$$
$$+a_{pn}\left(|\phi_p|^2 - \langle\phi_p\rangle^2\right)\left(|\phi_n|^2 - \langle\phi_n\rangle^2\right) \ . \quad (3.6)$$

In a neutron star, electrical neutrality keeps the proton fraction small, in the 5%

to 10% range [60, 61]; we will take $\langle\phi_p\rangle^2/\langle\phi_n\rangle^2 \approx 0.05$. As we now argue, a typical

value for the entrainment coupling is $\sigma \sim 10^{-1}$. We first relate our formalism to the hydrodynamic limit of the free energy, following [6]. We focus on the phases of the fields, $\phi_p = \langle\phi_p\rangle \exp(i\chi_p)$ and $\phi_n = \langle\phi_n\rangle \exp(i\chi_n)$, and assume the fields have constant magnitude, and their phases have gradients

$$\mathbf{v}_p = \frac{\hbar}{2m_p}\nabla\chi_p - \frac{2e}{m_p c}\mathbf{A} \; , \qquad \mathbf{v}_n = \frac{\hbar}{2m_n}\nabla\chi_n \; . \tag{3.7}$$

The free energy density (3.2) then reduces to the hydrodynamic form

$$F = \frac{1}{2}\rho^{pp}\mathbf{v}_p^2 + \frac{1}{2}\rho^{nn}\mathbf{v}_n^2 + \rho^{pn}\mathbf{v}_p \cdot \mathbf{v}_n + V + \frac{\mathbf{B}^2}{8\pi} \; , \tag{3.8}$$

where the symmetric matrix ρ of superfluid densities has elements

$$\rho^{pp} = 2m_p\langle\phi_p\rangle^2 \approx m_c\langle\phi_p\rangle^2 \; , \; \rho^{nn} = 2m_n\langle\phi_n\rangle^2 \approx m_c\langle\phi_n\rangle^2 \; , \; \rho^{pn} = -2m_n\sigma\langle\phi_p\rangle\langle\phi_n\rangle \; . \tag{3.9}$$

Our entrainment parameter σ is therefore related to the parameter ϵ of Ref. [62, 63, 64] by $\sigma = \epsilon\langle\phi_n\rangle/\langle\phi_p\rangle$. Since ϵ is of order 0.03, and $\langle\phi_n\rangle^2/\langle\phi_p\rangle^2 \sim 20$, we expect $\sigma \sim 10^{-1}$. This is consistent with the estimate $\rho^{pn} \approx -\frac{1}{2}\rho^{pp}$ used by [6]. In terms of the Andreev-Bashkin parametrization [22], $\rho_{12} = -\rho^{pn}$, $\rho_1 = \rho^{pp}+\rho^{pn}$, $\rho_2 = \rho^{nn}+\rho^{pn}$, so $\rho_1/\rho_{12} \sim 1$, $\rho_2/\rho_{12} \sim 40$. All the interactions in (3.8), including the entrainment, have their ultimate origin in the strong interaction between the nucleons, which is isospin symmetric, and hence does not distinguish protons from neutrons.

3.2.2   Flux tube solutions

To study a flux tube containing n flux quanta, we assume a cylindrically symmetric field configuration in which the proton condensate field winds (in a covariantly

constant way) around the z-axis with a net phase $2\pi n$,

$$\phi_p = \langle\phi_p\rangle \, f(r)e^{in\theta} \tag{3.10}$$

$$\phi_n = \langle\phi_n\rangle \, g(r) \tag{3.11}$$

$$\mathbf{A} = \frac{n\hbar c}{q}\frac{a(r)}{r}\hat{\theta} \tag{3.12}$$

We have defined ϕ_n as a real field, because, as noted in chapter 1, any net phase change in the neutron condensate when it circles the flux tube would cost an infinite energy per unit length. Inserting the ansatz in (3.2) we obtain

$$
\begin{aligned}
\mathcal{F} =\ & \frac{\hbar^2}{2m_c}\left[\langle\phi_p\rangle^2\left((f')^2 + \frac{n^2 f^2(1-a)^2}{r^2}\right) + \langle\phi_n\rangle^2(g')^2 - 2\sigma\langle\phi_p\rangle\langle\phi_n\rangle f \cdot g \cdot f' \cdot g'\right] \\
& + \frac{n^2\hbar^2 c^2}{8\pi q^2}\frac{(a')^2}{r^2} + \frac{a_{pp}\langle\phi_p\rangle^4}{2}\left(f^2 - 1\right)^2 + \frac{a_{nn}\langle\phi_n\rangle^4}{2}\left(g^2 - 1\right)^2 \\
& + a_{pn}\langle\phi_p\rangle^2\langle\phi_n\rangle^2\left(f^2 - 1\right)\left(g^2 - 1\right)
\end{aligned}
\tag{3.13}
$$

Generating the Euler-Lagrange equations using the standard procedure, we obtain a set of coupled differential equations for f, g and a:

$$
\begin{aligned}
\frac{\hbar^2}{2m_c a_{pp}\langle\phi_p\rangle^2}\left[f'' + \frac{f'}{r} - \frac{n^2(1-a)^2 f}{r^2} \right. & \left. - \sigma\frac{\langle\phi_n\rangle}{\langle\phi_p\rangle}\left[f \cdot g\left(g'' + \frac{g'}{r}\right) + f\,(g')^2\right]\right] \\
& = f(f^2 - 1) + \frac{a_{pn}}{a_{pp}}\frac{\langle\phi_n\rangle^2}{\langle\phi_p\rangle^2}f(g^2 - 1) \\
\frac{\hbar^2}{2m_c a_{pp}\langle\phi_p\rangle^2}\left[g'' + \frac{g'}{r} \right. & \left. - \sigma\frac{\langle\phi_p\rangle}{\langle\phi_n\rangle}\left[f \cdot g\left(f'' + \frac{f'}{r}\right) + g\,(f')^2\right]\right] \\
& = \frac{a_{nn}}{a_{pp}}\frac{\langle\phi_n\rangle^2}{\langle\phi_p\rangle^2}g(g^2 - 1) + \frac{a_{pn}}{a_{pp}}g(f^2 - 1) \\
\frac{m_c c^2}{4\pi q^2\langle\phi_p\rangle^2}\left(a'' - \frac{a'}{r}\right) & = -(1 - a)f^2
\end{aligned}
\tag{3.14}
$$

At this point we recall the definition of the Ginzburg-Landau parameter $\kappa = \lambda/\xi$, where the London penetration depth λ and superconducting coherence length ξ are

(see [65])

$$\lambda \equiv \sqrt{\frac{m_c c^2}{4\pi q^2 \langle \phi_p \rangle^2}} = \sqrt{\frac{m_c c^2}{16\pi \hbar c \alpha_{EM} \langle \phi_p \rangle^2}}$$

$$\xi \equiv \sqrt{\frac{\hbar^2}{2m_c a_{pp} \langle \phi_p \rangle^2}} \tag{3.15}$$

To further simplify the equations, we then change variables to a dimensionless radial

coordinate $\tilde{r} = r/\xi$, obtaining

$$
\begin{aligned}
f'' &+ \frac{f'}{\tilde{r}} - \frac{n^2(1-a)^2 f}{\tilde{r}^2} - \sigma \frac{\langle \phi_n \rangle}{\langle \phi_p \rangle} \left[f \cdot g \left(g'' + \frac{g'}{\tilde{r}} \right) + f(g')^2 \right] \\
&= f(f^2 - 1) + \frac{a_{pn}}{a_{pp}} \frac{\langle \phi_n \rangle^2}{\langle \phi_p \rangle^2} f(g^2 - 1) \\
g'' &+ \frac{g'}{\tilde{r}} - \sigma \frac{\langle \phi_p \rangle}{\langle \phi_n \rangle} \left[f \cdot g \left(f'' + \frac{f'}{\tilde{r}} \right) + g(f')^2 \right] \\
&= \frac{a_{nn}}{a_{pp}} \frac{\langle \phi_n \rangle^2}{\langle \phi_p \rangle^2} g(g^2 - 1) + \frac{a_{pn}}{a_{pp}} g(f^2 - 1) \\
a'' &- \frac{a'}{\tilde{r}} = -\frac{1}{\kappa^2}(1-a)f^2
\end{aligned}
\tag{3.16}
$$

The free energy per unit length of the flux tube, in terms of the variable $\tilde{r}$, is

$$
\begin{aligned}
E_n &= 2\pi a_{pp} \langle \phi_p \rangle^4 \xi^2 \int_0^\infty (\tilde{r} d\tilde{r}) \Bigg\{ (f')^2 + \frac{n^2 f^2(1-a)^2}{\tilde{r}} + \frac{\langle \phi_n \rangle^2}{\langle \phi_p \rangle^2}(g')^2 - 2\sigma \frac{\langle \phi_n \rangle}{\langle \phi_p \rangle} f \cdot g \cdot f' \cdot g' \\
&\quad + n^2 \kappa^2 \frac{(a')^2}{\tilde{r}^2} + \frac{1}{2}\left(f^2 - 1\right)^2 + \frac{1}{2}\frac{a_{nn}}{a_{pp}} \frac{\langle \phi_n \rangle^4}{\langle \phi_p \rangle^4}\left(g^2 - 1\right)^2 + \frac{a_{pn}}{a_{pp}}\frac{\langle \phi_n \rangle^2}{\langle \phi_p \rangle^2}\left(f^2 - 1\right)\left(g^2 - 1\right) \Bigg\}
\end{aligned}
\tag{3.17}
$$

In addition to the system of equations, we require boundary conditions on the fields

at the origin and at ∞. Far from the flux tube core, the fields will go to their

uniform condensate value, so $f(\infty) = g(\infty) = a(\infty) = 1$. Near the origin, $f(r) \propto$

r^n, $a(r) \propto r^2$ and $g(r)$ is a constant. Therefore we have the conditions $f(0) = 0$,

$a(0) = 0$ and $g'(0) = 0$. To obtain the energy of a flux tube we numerically solve the

ODE system for the neutron and proton condensate and magnetic potential profile

functions, then calculate the free energy of the system by inserting the results into

(3.17) and integrating.

The system has five independent parameters: a_{pp}, a_{nn}/a_{pp}, a_{pn}/a_{pp}, σ, and $\langle\phi_n\rangle/\langle\phi_p\rangle$. In neutral nuclear matter, the density of protons (neutrons) is proportional to $\langle\phi_p\rangle^2$ ($\langle\phi_n\rangle^2$), and the proton density is approximately 5% of the total baryon number density [6], so we set $\langle\phi_p\rangle^2/\langle\phi_n\rangle^2 = .05$ in most of our analysis. Following [10, 13] we set $a_{nn} = a_{pp}$, and use (3.15) to exchange the parameter a_{pp} for κ, which is the conventional parameter used in condensed matter studies of superconductivity. Our reduced set of parameters is therefore κ, the proton-neutron gradient coupling σ, and the proton-neutron density coupling $\beta \equiv a_{pn}/a_{pp}$. We also study some effects of varying $\langle\phi_p\rangle^2/\langle\phi_n\rangle^2$.

3.3   Numerical Results

3.3.1   Flux tube solutions

For given values of $\langle\phi_p\rangle^2/\langle\phi_n\rangle^2$, κ, the proton-neutron gradient coupling σ, and the proton-neutron amplitude coupling $\beta \equiv a_{pn}/a_{pp}$ we numerically solved the equations of motion (3.16) giving the field profiles for flux tubes with various numbers n of flux quanta. We obtained the solutions using a finite-element relaxation method, which is much less sensitive to initial conditions than the traditional "shooting" method, and better suited to repeatedly solving the equations for different sets of parameters. Next, we insert the solution for each profile into our expression for the free energy

Profiles with nonzero density coupling
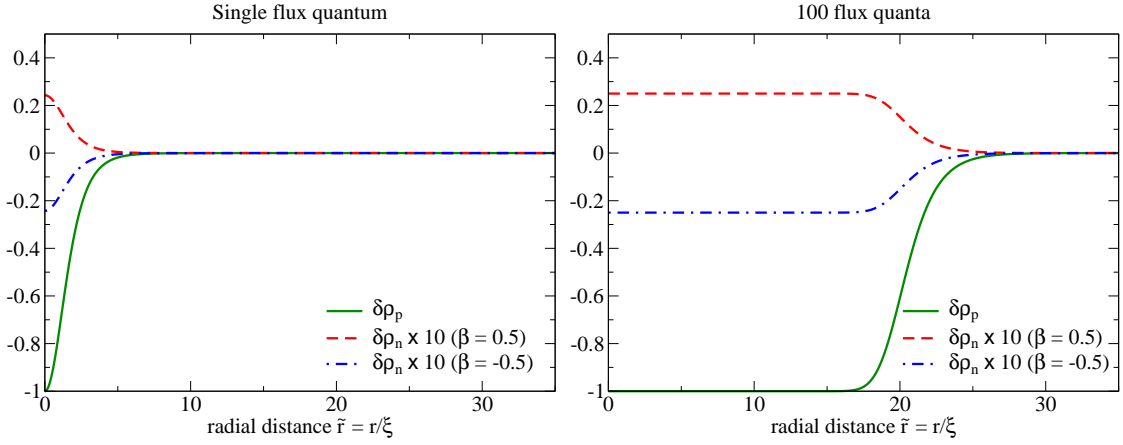
Figure 3.1: (Color online) Profile of flux tube with $n = 1$ units of flux (left) and $n = 100$ units of flux (right) showing the effect of density coupling β between neutron and proton condensates. The plot shows the deviation $\delta\rho$ of the condensates from their vacuum values (3.18). With no coupling between the condensates ($\beta = \sigma = 0$), the neutrons are undisturbed ($\delta\rho_n = 0$). With a non-zero density coupling β, the neutron condensate (broken lines) is significantly perturbed by the flux tube. Note that the neutron $\delta\rho_n$'s are multiplied by 10 (not by 100 as in Fig. 3.2) to make them visible. The other parameters are $\kappa = 3.0$, $\sigma = 0.0$, and $\langle\phi_p\rangle^2/\langle\phi_n\rangle^2 = .05$.

(3.17) and numerically integrate it to obtain a value for E_n.

To estimate the numerical errors in our results, we varied the convergence criterion in the finite-element relaxation calculation, the spacing of the radial grid of points, and the radius out to which the grid extended. We found that the resultant variation in E_n/n was of order 10^{-6}, so numerical errors are invisible on the scale of the plots shown in Fig. 3.3.

Having obtained E_n we then plot the series B_n to determine whether the system is type I or type II for the chosen point in parameter space. In this way we find the

Profiles with nonzero gradient coupling
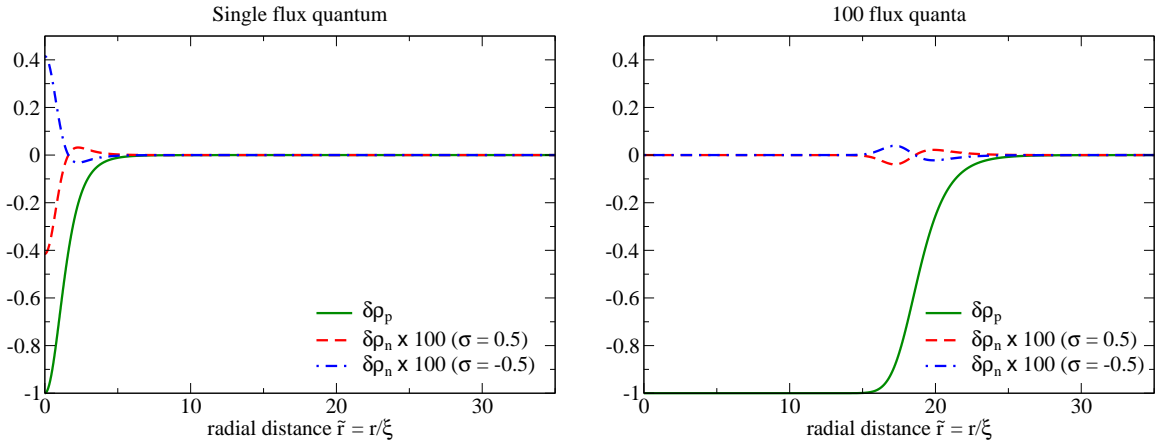
Figure 3.2: Profile of flux tube with $n = 1$ units of flux (left) and $n = 100$ units of flux (right) showing the effect of gradient coupling σ between neutrons and protons. The plot shows the deviation $\delta\rho$ of the condensates from their vacuum values (3.18). With no coupling between the condensates ($\beta = \sigma = 0$), the neutrons are undisturbed ($\delta\rho_n = 0$). With a non-zero gradient coupling σ, the neutron condensate (broken lines) is slightly perturbed by the flux tube. Note that the neutron $\delta\rho_n$'s are multiplied by 100 to make them visible. The other parameters are $\kappa = 3.0$, $\beta = 0.0$, and $\langle\phi_p\rangle^2/\langle\phi_n\rangle^2 = .05$.

points in parameter space where the system changes from a type I state to a type II state. Taking various slices through the parameter space, we can generate phase diagrams that show the boundary curves between the various phases.

Figs. 3.1 and 3.2 each show a profile for a flux tube with a single flux quantum $n = 1$ on the left, and a profile for a flux tube with 100 flux quanta on the right. Fig. 3.1 shows the effect of non-zero density coupling β and Fig. 3.2 shows the effect of non-zero gradient coupling σ. We have plotted the normalized difference in density

of the pair fields from their condensate values,

$$
\begin{aligned}
\delta\rho_p(\tilde{r}) &\equiv \frac{\phi_p^2(\tilde{r}) - \langle\phi_p\rangle^2}{\langle\phi_p\rangle^2} = f^2(\tilde{r}) - 1 \\
\delta\rho_n(\tilde{r}) &\equiv \frac{\phi_n^2(\tilde{r}) - \langle\phi_n\rangle^2}{\langle\phi_n\rangle^2} = g^2(\tilde{r}) - 1
\end{aligned}
\tag{3.18}
$$

No coupling to neutrons

We do not show a plot of the flux tube profile for a simple superconductor, since this is well known: in a core region whose area rises as the number of flux quanta n, the proton condensate is suppressed; in a wall region the condensate returns to its vacuum value. At the Bogomolnyi point [66], $\kappa = 1/\sqrt{2}$, the energy per flux quantum is independent of n [67], but on either side of this value there are area and perimeter contributions to the energy [68], so for κ close to $1/\sqrt{2}$ we expect the energy of a flux tube in a simple superconductor to have the following dependence on n,

$$
E_n^{(sc)}(\kappa) = nE_{\mathrm{Bog}} + \delta\kappa\, M\left(n - c_{\frac{1}{2}}\sqrt{n} + c_1 + \cdots\right) .
\tag{3.19}
$$

This is an expansion around $n = \infty$, but our numerical results will show that it works down to $n = 1$. We define $\delta\kappa \equiv \kappa - 1/\sqrt{2}$. E_{Bog} is the energy per unit flux at $\delta\kappa = 0$. By convention we take the parameter M, which has dimensions of energy, to be positive. The value of $c_{\frac{1}{2}}$ is then positive, ensuring that for $\delta\kappa > 0$, $n = \infty$ is disfavored (type-II), and for $\delta\kappa < 0$, $n = \infty$ is favored (type-I). We will see this behavior in our numerical results (Sec. 3.3.2 and upper left plot of Fig. 3.3).

Density coupling to neutrons

For positive β, which corresponds to positive a_{np}, equations (3.2) and (3.4) indicate that there is a repulsion between the neutron and proton condensates, so in the center of the flux tube, where the proton condensate is suppressed, the neutron condensate will be enhanced. That is exactly what we see in Fig. 3.1, where the dashed curve, showing the perturbation to the neutron density ρ_n, rises inside the flux tube. For negative β there is attraction between the two condensates, and the neutron condensate is suppressed inside the flux tube (dash-dotted line). We therefore expect that the leading correction due to the interaction will be proportional to the core area, i.e proportional to n. The energy of an n-quantum flux tube is then

$$E_n(\kappa, \beta) \approx E_n^{(\text{sc})}(\kappa) + M_\beta(-n + b_{\frac{1}{2}}\sqrt{n} + b_1 + \cdots) \, , \tag{3.20}$$

where $E_n^{(sc)}(\kappa)$ is the energy for an n-quantum flux tube in a pure superconductor, with no coupling to a superfluid (3.19). The leading correction is $-M_\beta n$, which should be negative and quadratic in β for small β (see Sec. 3.3.1), so the interaction energy parameter M_β is positive and proportional to β^2. The sub-leading term proportional to $\sqrt{n}$ arises from the energy cost of the gradient in ρ_n at the edge of the flux tube, where it must return to its vacuum value, so we expect this term to be positive: $b_{\frac{1}{2}} > 0$. We do not have an *a priori* expectation for the sign of the sub-sub-leading term b_1.

Gradient coupling to neutrons

For positive σ, we expect from (3.2) and (3.3) that the positive gradient in ρ_p at the wall of the flux tube will induce a positive gradient in ρ_n in the same range of radii, which lowers the energy of the system. This is exactly what we see in Fig. 3.2, where the dashed curve showing the perturbation to ρ_n has a positive slope in the range of radii where the solid curve (ρ_p) has the largest positive slope. On either side of that region it has a negative slope, as it returns to its unperturbed value. For negative σ the effect is reversed: the dash-dotted curve shows ρ_n having a negative slope where ρ_p has the largest positive slope.

We therefore expect that in the presence of a gradient coupling, the correction to the energy of a flux tube has a dominant core-perimeter term proportional to $\sqrt{n}$,

$$E_n(\kappa, \sigma) \approx E_n^{(\mathrm{sc})}(\kappa) + M_\sigma(-s_{\frac{1}{2}}\sqrt{n} + s_1 + \cdots) . \tag{3.21}$$

The energy correction is negative and quadratic in σ for small σ (see Sec. 3.3.1), so the interaction energy parameter M_σ is proportional to σ^2; choosing it to be positive by convention requires $s_{\frac{1}{2}}$ to be positive. We do not have an *a priori* expectation for the sign of s_1.

Symmetry under change of sign of couplings

It is clear from Figs. 3.1 and 3.2 that for couplings β and σ of order 0.5 the modification of the field configuration due to the interaction between the condensates is extremely small, so it is reasonable to treat its effects perturbatively. (At the end of Sec. 3.3.3 we

will discuss the limit of small neutron condensate, where the perturbative approach becomes questionable.)

When we evaluate the perturbative correction to the energy of the flux tube, there is no linear term in β and σ. Such a term would arise from evaluating the β and σ terms from the Hamiltonian in the unperturbed field configuration. But in that configuration the neutron condensate sits at its vacuum value, so both terms evaluate to zero ($g = 1$, $g' = 0$ in (3.17)).

We therefore expect the change in the energy of the flux tube to be quadratic in the couplings β and σ. Firstly, this correction must be negative. This is a well-known result from perturbation theory: the second-order correction arises from the change in the configuration in response to the perturbation, which only occurs because it is driven by a resultant lowering of the energy. Secondly, the change in the energy will in general contain β^2, σ^2, and $\beta\sigma$ terms. This means it will be even in β when $\sigma = 0$ and even in σ when $\beta = 0$, so we expect $M_\beta \propto \beta^2$ and $M_\sigma \propto \sigma^2$ in Eqs. (3.20) and (3.21).

However, if both β and σ are nonzero, then the $\beta\sigma$ terms spoil the symmetry of the energy under negation of the couplings. This is clear from Figs. 3.1 and 3.2. For example, suppose that as well as non-zero β we have a very small non-zero σ. Now consider sending $\beta \rightarrow -\beta$. From Fig. 3.1 we see that this changes the sign of the slope of ρ_n in the wall region where ρ_p has positive slope. If σ is nonzero then these two configurations will have different energies, since the gradient of ρ_n is then coupled to the gradient of ρ_p.
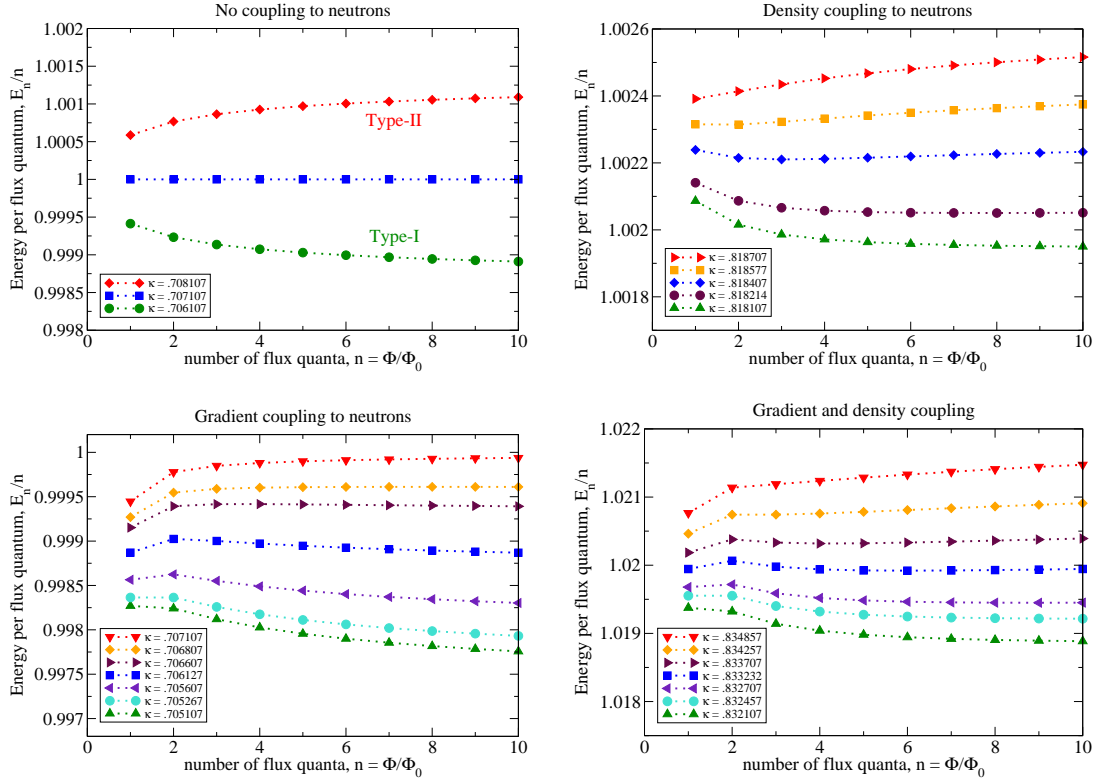
Figure 3.3: (Color online) The energy per flux quantum E_n/n, in units of E_{Bog} (see Eq. (3.19)), as a function of the number n of units of flux in the flux tube. Top left, simple proton superconductor with neutrons completely decoupled ($\beta = \sigma = 0$); top right, density coupling between condensates ($\beta = .5, \sigma = 0$); bottom left, gradient coupling between condensates ($\beta = 0, \sigma = .5$); bottom right, both couplings ($\beta = \sigma = .5$).

3.3.2 Energetic stability of flux tubes

In Fig. 3.3, the energy per flux unit (E_n/n) is plotted against n for various values of the Ginzburg-Landau parameters, namely κ, the density coupling β, and the gradient coupling σ. We fixed $\langle \phi_p \rangle^2 / \langle \phi_n \rangle^2 = 0.05$ (Sec. 3.2.1).

No coupling to neutrons

The upper left plot of Fig. 3.3 shows $E_n^{(sc)}(\kappa)/n$, the energy per flux quantum when there are no interactions between the neutron and proton pairs. We see that the only possible phases are the standard type I and type II, with a transition at the Bogomolnyi point, $\kappa = 1/\sqrt{2}$, where the favored value of n jumps from 1 to infinity. The lower line (κ just below $1/\sqrt{2}$) corresponds to type-I, where the lowest energy/flux is at $n = \infty$, so flux tubes attract. The upper line (κ just above $1/\sqrt{2}$) corresponds to type-II, where the lowest energy/flux is at $n = 1$, so flux tubes always repel each other. The middle line corresponds to the transition point ($\kappa = 1/\sqrt{2}$), where there is no interaction between flux tubes [66]. Our numerical results are consistent with the expected form (3.19): when $\delta\kappa > 0$ the asymptotic value of E_n/n is increased, and E_n/n rises monotonically towards that asymptotic value, and conversely when $\delta\kappa < 0$ the asymptotic value of E_n/n is decreased, and E_n/n falls monotonically towards that asymptotic value. It is clear that $c_{\frac{1}{2}}$ in (3.19) must be positive to obtain this behavior at large n. From fits to our numerical calculations we find that c_1 is always positive, so it "fights against" the leading $c_{\frac{1}{2}}/\sqrt{n}$ term, but for all $n \geqslant 1$ it is overwhelmed. In fact, we find that (3.19) gives an excellent fit to our results down to $n = 1$, without any higher order terms.

In the remaining panels of Fig. 3.3, we explore the effect of density and gradient couplings between the proton superconductor and the neutron superfluid.

Density coupling to neutrons

The upper right panel of Fig. 3.3 shows the effect of a density coupling between the condensates. From (3.19) and (3.20) we expect

$$E_n/n = E_{\text{Bog}} + (M\delta\kappa - M_\beta) + \frac{M_\beta b_{\frac{1}{2}} - \delta\kappa M c_{\frac{1}{2}}}{\sqrt{n}} + \frac{M_\beta b_1 + \delta\kappa M c_1}{n} + \cdots \quad (3.22)$$

The first point to notice is that the density coupling shifts the critical κ to a larger value. The transition between type-I and type-II occurs when the asymptotic behavior at large n changes from rising to falling, i.e. when the coefficient of the $1/\sqrt{n}$ term changes sign. This occurs for some positive value of $\delta\kappa$

$$\delta\kappa_{\text{crit}}(\beta) = \frac{M_\beta \, b_{\frac{1}{2}}}{M c_{\frac{1}{2}}} \quad \propto \beta^2 \quad (3.23)$$

which rises as β^2 because M, M_β, $b_{\frac{1}{2}}$, and $c_{\frac{1}{2}}$ are all positive, and $M_\beta \propto \beta^2$ when $\sigma = 0$ (Sec. 3.3.1). Thus in the upper right panel of Fig. 3.3 we had to increase κ from around 0.707 to around 0.818 in order to find the transition.

The other important point is the presence of a minimum in E_n/n when κ is just above the new type-I/type-II boundary, indicating that the favored value of n may be neither 1 (standard type-II) nor infinity (type-I) but some intermediate value. This is consistent with (3.22), as long as we assume that the coefficient b_1 from (3.20) is either positive, or negative and of sufficiently small magnitude, so that the $1/n$ term in (3.22) has a positive coefficient (recall that M_β, M, and c_1 are all positive, and $\delta\kappa$ is also positive in this region). The minimum will then arise from competition between the positive $1/n$ term, which dominates at smaller n, giving a negative slope, and

the $1/\sqrt{n}$ term which has a negative coefficient (because $\delta\kappa$ is just above the new critical value) and dominates at larger n giving a positive slope. However, as $\delta\kappa$ is reduced the negative coefficient of $1/\sqrt{n}$ becomes smaller and smaller, and the minimum moves out to arbitrarily large n, so the energetically favored value of n does not jump suddenly from 1 to ∞ as in the standard case, but increases in steps from 1 to infinity as we lower κ through a range of values down to the new critical value. This creates an infinite number of "type-II(n)" phases, each with a different flux in the favored flux tube, and when that flux becomes infinite the superconductor becomes type-I. This behavior is seen in our numerical results (Fig. 3.4).

Gradient coupling to neutrons

The lower left panel of Fig. 3.3 shows the effect of a gradient interaction with the superfluid. From (3.19) and (3.20) we expect

$$E_n/n = E_{\text{Bog}} + M\delta\kappa + \frac{-M_\sigma s_{\frac{1}{2}} - \delta\kappa M c_{\frac{1}{2}}}{\sqrt{n}} + \frac{-M_\sigma s_1 + \delta\kappa M c_1}{n} + \cdots \qquad (3.24)$$

Here we see that the gradient coupling shifts the critical κ to a smaller value. The transition between type-I and type-II occurs when the coefficient of the $1/\sqrt{n}$ term changes sign, which in this case happens for small negative $\delta\kappa$,

$$\delta\kappa_{\text{crit}}(\sigma) = -\frac{M_\sigma s_{\frac{1}{2}}}{M c_{\frac{1}{2}}} \quad \propto -\sigma^2 \qquad (3.25)$$

which is proportional to $-\sigma^2$ because M, M_σ, $s_{\frac{1}{2}}$, and $c_{\frac{1}{2}}$ are all positive, and $M_\sigma \propto \sigma^2$ when $\beta = 0$ (Sec. 3.3.1).

The other important feature of this plot is the presence of a maximum in E_n/n when κ is close to the type-I/type-II boundary. This is consistent with (3.24), as long as we assume that the coefficient s_1 from (3.21) is either positive, or negative and of sufficiently small magnitude, so that the $1/n$ term in (3.24) has a negative coefficient. The maximum will then arise from competition between the negative $1/n$ term, which dominates at smaller n, giving a positive slope, and the $1/\sqrt{n}$ term, which dominates at larger n giving a negative slope.

The presence of this maximum allows for the possibility of metastable flux configurations. If we scan down in κ, we start in a type-II region where E_n/n has its minimum at $n = 1$ and rises monotonically with n. But at some point a metastable minimum at $n = \infty$ appears, which drops to become degenerate with the minimum at $n = 1$. At this point there is a first-order transition: at the critical field, $n = 1$ flux tubes would co-exist with macroscopic normal regions (i.e. flux tubes with $n = \infty$) but not with flux tubes of intermediate size. Reducing κ further, the $n = 1$ flux tube becomes energetically metastable, and finally unstable.

Density and gradient coupling to neutrons

The lower right panel of Fig. 3.3 shows the effect of a combination of gradient and density interactions. As κ is decreased, a metastable energy minimum emerges at finite n; it drops and becomes a new global minimum at $n = n^*$, yielding a sharp transition from $n = 1$ type-II to $n = n^*$ type-II. As κ is reduced further the favored number of flux quanta in a flux tube rises in integer steps from n^* to infinity, at which

point the superconductor becomes type-I.
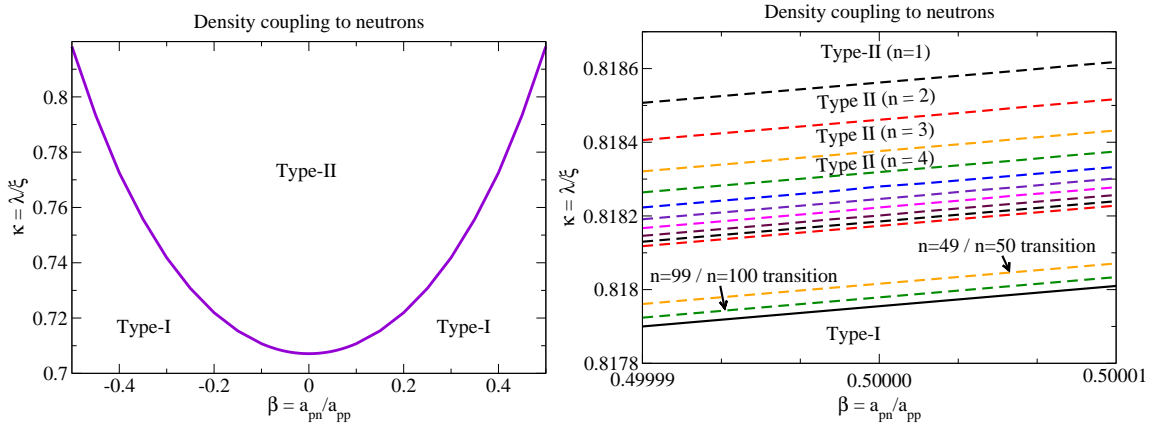
Figure 3.4: (Color online) Effect on the superconductor of density coupling β to a superfluid, displayed as a phase diagram in the κ-β plane, with no gradient coupling ($\sigma = 0$) and $\langle \phi_p \rangle^2 / \langle \phi_n \rangle^2 = 0.05$. The left panel shows how non-zero β causes an increase in $\kappa_{\mathrm{critical}}$. In the right panel we magnify the transition region near $\beta = 0.5$, illustrating that on the type-II side there is a sequence of "type-II(n)" bands in which the number of flux quanta in the favored flux tube rises, reaching infinity when the superconductor becomes type I.

3.3.3   Phase diagrams

Figures 3.4–3.7 illustrate the additional structure in the phase diagram of the superconductor induced by the couplings to a superfluid. Each diagram is a two-dimensional slice through the parameter space.

Figure 3.4 shows the consequences of a density coupling β between the superfluid and superconductor. We see that the density coupling, irrespective of its sign, favors type-I superconductivity, pushing the the critical κ for the type-I/type-II transition up to higher values, forming a parabolic phase boundary in the β-κ plane, as expected
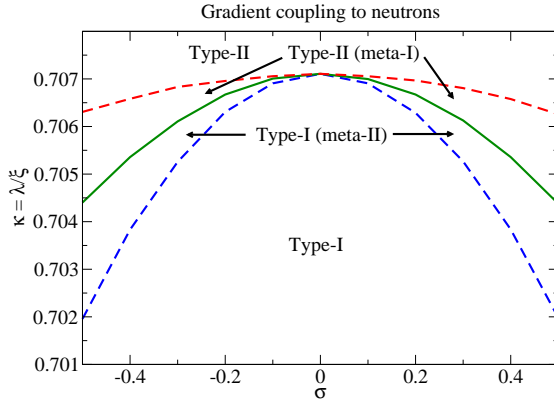
Figure 3.5: (Color online) Effect on the superconductor of gradient coupling σ to a superfluid, displayed as a phase diagram in the κ-σ plane, with no density coupling ($\beta = 0$) and $\langle \phi_p \rangle^2 / \langle \phi_n \rangle^2 = 0.05$. The gradient coupling causes a decrease in κ_{critical}, and creates metastable states on either side of the transition, with spinodal lines as shown.

from (3.23). This can be thought of as arising from the fact that nonzero β lowers the energy per flux of the core of large flux tubes (see (3.22)), which favors type-I superconductivity.

In the right panel we zoom in on the transition line near $\beta = 0.5$ to show the substructure in the phase transition region that is invisibly small in the left panel. As one would expect from our discussion of Figure 3.3 (upper right panel), on the type-II side of the transition there is a series of bands distinguished by the number of flux quanta n in the energetically favored flux tube. "Type-II ($n = 1$)" is the standard type-II superconductor. With decreasing κ we find transitions to Type-II ($n = 2$), Type-II ($n = 3$), and on up to $n = \infty$ which is a type-I superconductor.

In Figure 3.5 we show the consequences of a gradient coupling σ between the superfluid and superconductor. We see that the gradient coupling, irrespective of its
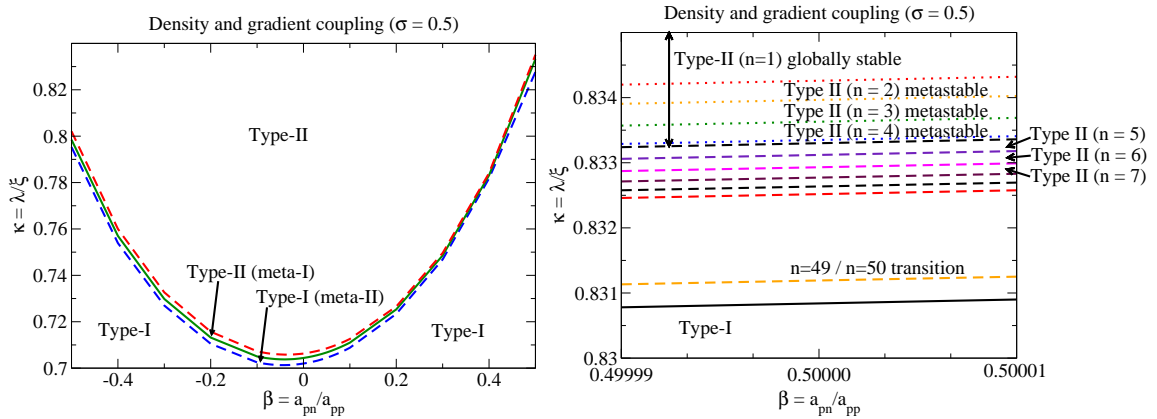
Figure 3.6: (Color online) Phase diagram for combined density and gradient interactions: the κ-β plane for $\sigma = 0.5$ and $\langle\phi_p\rangle^2/\langle\phi_n\rangle^2 = 0.05$. The type-I/type-II boundary is no longer symmetric under $\beta \to -\beta$. In the right panel we magnify the transition region near $\beta = 0.5$, illustrating that on the type-II side as κ decreases the number of flux quanta in the favored flux tube jumps from 1 to a finite value (in this case $n = 5$) and then there is a sequence of bands in which n rises to infinity, at which point the superconductor becomes type I.

sign, favors type-II superconductivity, pushing the critical κ for the type-I/type-II transition down to lower values, forming an inverted parabolic phase boundary in the σ-κ plane, as expected from (3.25). It also makes the phase transition first order, with spinodal lines where the unfavored phase becomes metastable. Both these effects arise from the lowering of the energy of the wall of the vortex, as explained in Sec. 3.3.2.

In Figure 3.6 we show phase diagrams for the combination of both density and gradient couplings, fixing $\sigma = 0.5$ and varying β. As discussed in Sec. 3.3.1, we expect that when $\sigma \neq 0$ the $\beta \to -\beta$ symmetry is now broken. In the right panel we magnify the transition region near $\beta = 0.5$, illustrating that on the type-II side as κ decreases the number of flux quanta in the favored flux tube jumps from 1 to a finite
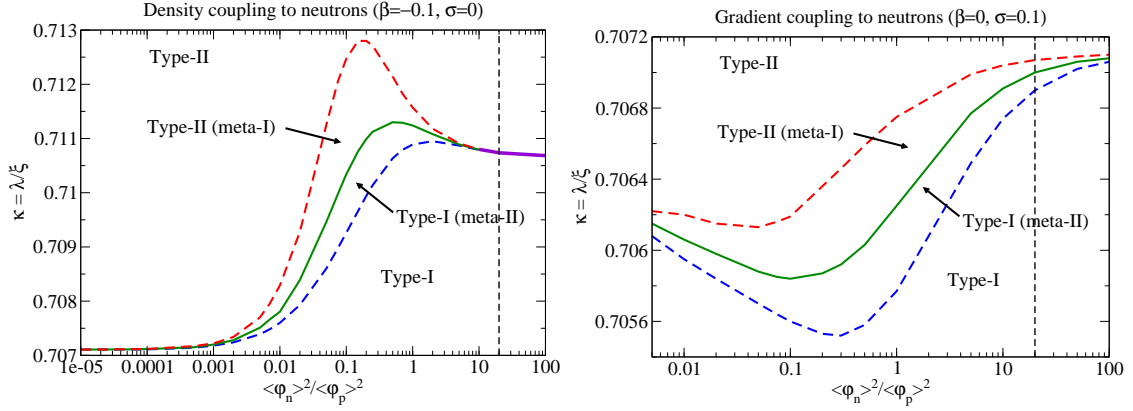
Figure 3.7: (Color online) Phase diagrams in the κ vs. $\langle\phi_n\rangle^2/\langle\phi_p\rangle^2$ plane. Vertical dashed lines show $\langle\phi_n\rangle^2/\langle\phi_p\rangle^2 = 20$, the value used for other figures in this paper. The left panel is for density coupling $\beta = -0.1$, but no gradient coupling ($\sigma = 0$). The right panel is for gradient coupling $\sigma = 0.1$, but no density coupling ($\beta = 0$). In both cases, we see that the type-I/type-II transition converges to $\kappa = 1/\sqrt{2}$ as the neutron condensate disappears. For the case of a density coupling, as the neutron condensate decreases, the type-I/type-II boundary changes at $\langle\phi_n\rangle^2/\langle\phi_p\rangle^2 \sim 10$ from a narrow region of type-II(n) phase bands (thick line) to wider metastable regions.

value $n = 5$, and then there is a sequence of bands in which n rises, reaching infinity when the superconductor becomes type I. This is the expected behavior, based on our discussion in Sec. 3.3.2.

Finally, in Figure 3.7, we anticipate one direction in which this work could be extended, by exploring the consequences of varying the ratio of the superfluid density to the superconductor density, which up to now was fixed to $\langle\phi_n\rangle^2/\langle\phi_p\rangle^2 = 20$, an appropriate value for neutral beta-equilibrated nuclear matter, of the type we expect to find inside neutron stars. Figure 3.7 shows phase diagrams in the plane of κ and $\langle\phi_n\rangle^2/\langle\phi_p\rangle^2$ for a system with a density coupling (left panel) and with a gradient coupling (right panel).

For the case of a density coupling we use a negative value of the coupling, because this corresponds to an attractive interaction, which gives smooth behavior in the limit where the neutron condensate disappears, $\langle\phi_n\rangle^2/\langle\phi_p\rangle^2 \to 0$. As is clear from the plot, the type-I/type-II transition then converges to the standard value for a single-component superconductor, $\kappa = 1/\sqrt{2}$. For a repulsive interaction, the $\langle\phi_n\rangle^2/\langle\phi_p\rangle^2 \to 0$ limit is singular: we discuss this in more detail below. It is interesting to note that the effects of the density coupling change dramatically with the relative densities of the neutrons and protons. At $\langle\phi_n\rangle^2/\langle\phi_p\rangle^2 \gtrsim 10$ the density coupling produces a thin region of multi-flux-quantum "type-II(n)" phases, as was illustrated in Fig. 3.4. But for lower values, it has a similar effect to a gradient coupling, inducing metastable regions on either side of the type-I/type-II boundary. This should be understandable in terms of the dependence of the coefficients $b_{\frac{1}{2}}$ and b_1 (Eqn. (3.20)) on $\langle\phi_n\rangle^2/\langle\phi_p\rangle^2$. In Sec. 3.3.2 we argued that if b_1 is large enough then the E_n/n curve has a minimum at finite n, yielding a type-II(n) phase. We conjecture that as $\langle\phi_n\rangle^2/\langle\phi_p\rangle^2$ gets smaller, b_1 becomes sufficiently negative that this is no longer the case, and instead there is a maximum, leading to metastability of the $n = 0$ and $n = \infty$ states in spinodal regions around the type-I/type-II boundary. This is a topic for future investigation.

For the case of a gradient coupling (right panel of Fig. 3.7) the effects of varying $\langle\phi_n\rangle^2/\langle\phi_p\rangle^2$ are less dramatic. It is interesting that, as for a density coupling, the variation is non-monotonic. Again, we conjecture that this could be understood in terms of variation of the coefficients $s_{\frac{1}{2}}$ and s_1 (Eqn. (3.21)) with $\langle\phi_n\rangle^2/\langle\phi_p\rangle^2$. As the superfluid density drops to zero, its effects become negligible, and the critical value

of κ converges towards $1/\sqrt{2}$ as one would expect.

Finally, we discuss the singularity of the $\langle\phi_n\rangle^2/\langle\phi_p\rangle^2 \to 0$ limit for a positive β, i.e. a repulsive density coupling between the neutron and proton condensates. From (3.6) we see that the expectation value of the neutron condensate is $\langle\phi_n\rangle + \frac{1}{2}\beta(\langle\phi_p\rangle - \phi_p)$, so far from the flux tube, where ϕ_p is $\langle\phi_p\rangle$, it is $\langle\phi_n\rangle$. But in the core of the condensate it is larger (there is less proton condensate to repel it). In fact, even if the parameter $\langle\phi_n\rangle^2$ were zero or slightly negative, there would be a positive neutron condensate in the core of the flux tube. This shows that for positive β the neutrons do *not* decouple and become irrelevant in the limit $\langle\phi_n\rangle \to 0$. We note two consequences of this. Firstly, for small $\langle\phi_n\rangle$ the $\beta \to -\beta$ symmetry discussed in Sec. 3.3.1 is no longer present, because the effect of the flux tube on the neutron condensate is no longer a small perturbation. Secondly, in a system where $\langle\phi_n\rangle^2$ is small and negative (i.e. the neutrons just barely fail to condense in the presence of the proton condensate) flux tubes could have superfluid cores, which is another topic that we leave for future investigation.

3.4 Conclusion

We conclude that coupling a superconductor to a co-existing superfluid causes significant modification of the energetics of the flux tubes. On the basis of calculations restricted to the cylindrical geometry of n-quantum flux tubes, we conclude that a coupling between the densities of the condensates shifts the type-I/type-II boundary

to larger κ, and, if the superfluid density is high enough, appears to create an infinite number of new "type-II(n)" phases whose most stable flux tubes contain multiples of the basic flux quantum. A gradient coupling between the condensates leads to metastable regions surrounding the transition between type-I and type-II superconductivity.

As discussed in Section 3.1, our calculation corresponds to comparing the energy at zero and infinite separation of flux tubes with varying numbers of flux quanta. This leaves open the possibility that there might be additional minima at finite separation. It is therefore possible that in parts of the phase diagram there might be a different phase from the ones we identify, namely an alternative type of type-II superconductor in which the spacing between flux tubes is fixed by the microscopic physics rather than by the strength of the applied field. To resolve this question will require calculation of the free energy of a pair of flux tubes at arbitrary separation. Such calculations have been performed for large separation [69, 70, 71], and by perturbing about the Bogomolnyi point [59] and by numerical computation [72]. In particular, the numerical methods that have been used recently to follow the interaction and annihilation or vortex-antivortex pairs [73] would be readily applicable to the simpler time-independent calculation of the interaction potential of flux tubes. Another natural generalization of our calculation would be to allow for non-s-wave pairing, such as the $^3P_2$ pairing that is believed to occur in the neutron superfluid in the core of a neutron star.

Our results add another example to the class of two-component Ginzburg-Landau

models with non-standard superconducting behavior. Previous work in this area includes the $SO(5)$ model of high-temperature superconductivity, which has flux tubes described by a two-component GL model, where each component carries a different $U(1)$ charge, and only one of them condenses in the vacuum [21]. Another example is the case of a two-component GL model where both components have electric charge, very different mass, and nearly the same Fermi energy. This system was found to have non-monotonic $E(n)/n$ and intermediate minima in the interaction potential [15].

The exotic phenomena that we predict are localized to the region around the type-I/type-II transition, so they may not turn out to be relevant for the inner core of a neutron star, which is believed to be well inside the type-II regime [5]. However, given the extremely impressive recent progress in creating exotic systems such as multi-component superfluids of trapped cold atoms, it seems quite conceivable that a material that is both a superconductor and a superfluid might be created in the laboratory, and could be studied under controlled conditions. Our results would be directly relevant to such a material.

Chapter 4

Leptonic contribution to the bulk viscosity of nuclear matter

The bulk viscosity of nuclear matter plays an important role in the damping of oscillations in neutron stars. One well-known example is r-modes, which, if the interior of the star is a perfect (dissipationless) fluid, become unstable with respect to the emission of gravitational waves [24, 25, 26]. This emission acts as a brake on the rotation of the star. However, r-mode spindown will not occur if the r-mode is sufficiently strongly damped, for example by shear or bulk viscosity of the matter in the interior of the star. It is therefore important to calculate of the bulk viscosity of the various candidate phases in a neutron star. Several calculations exist in the literature, for nuclear [27, 28, 29, 30, 31, 32] and hyperonic [33, 34, 35] as well as for unpaired quark matter [36, 37, 38] and various color-superconducting phases [39, 40, 41, 42, 43, 44].

In this chapter we will study β-equilibrated nuclear matter. We will assume

that the density is high enough that the negative-charge chemical potential μ_l is greater than the mass of the muon, so the matter consists of neutrons, protons, electrons and muons. Such matter is expected to exist in the core of the star. In previous calculations of bulk viscosity of $npe\mu$ nuclear matter the focus has been on the contribution from interconversion of neutrons and protons via weak interactions. But nuclear matter at neutron-star densities is expected to show Cooper pairing of protons (superconductivity) or neutrons (superfluidity) [16, 17, 46] either of which will suppress interconversion by a factor of order $\exp(-\Delta/T)$, where Δ is the energy gap at the Fermi surface. This opens up the possibility that, in superfluid or superconducting phases, the dominant contribution to the bulk viscosity might come from purely leptonic processes. The relevant process is conversion of electrons to muons (and vice versa) via either the direct Urca process or the modified Urca process. The direct Urca leptonic conversion process is forbidden by energy and momentum conservation: in converting an electron near its Fermi surface to a muon near its Fermi surface, the change in free energy is very small (of order T), so the emitted neutrinos carry momentum and energy of this order. But the change of momentum of the charged lepton is large, at least $\mu_l - \sqrt{\mu_l^2 - m_\mu^2}$, and the low-energy neutrino cannot carry this much momentum. However, the modified Urca process can occur; for example, two electrons with energy slightly above the Fermi energy can scatter to an electron and a muon with energies near the Fermi energy, or an electron and muon can scatter to two muons. The strongest interaction between leptons is electromagnetism, so this process proceeds via exchange of a photon, whose propagator should include the

effects of screening by the nuclear medium. As the temperature decreases, the process will become suppressed as the Fermi distributions assume their zero-temperature step function profiles, but at finite temperature the modified Urca process will result in a non-zero contribution to the bulk viscosity.

We calculate the leptonic bulk viscosity arising from the processes $e + \ell \rightleftharpoons \mu + \ell + \nu + \bar{\nu}$, where $\ell = e$ or μ. We conclude that, if the protons and neutrons are both ungapped, i.e if there is neither superfluidity nor superconductivity, then the bulk viscosity from these purely leptonic processes is several orders of magnitude smaller than that from the nucleonic processes. However, once the temperature drops below the critical value for Cooper pairing of the protons or neutrons, the nucleonic bulk viscosity at frequencies $\gtrsim 10\,\mathrm{Hz}$ is strongly suppressed, and leptonic processes become the dominant source of bulk viscosity at those frequencies.

In this chapter, we lay out the process for calculating the bulk viscosity of a two-component leptonic system under application of a periodic volume and pressure perturbation. A crucial component of this calculation is the conversion rate between electrons and muons, which is discussed in great detail. We show the numerical results of our calculations and how they compare to the bulk viscosity resulting from modified Urca equilibration of the nucleon population.

4.1   Bulk viscosity of leptons

First we write down a general expression for bulk viscosity in a two-species system, arising from interconversion of the two species. Then we specialize to the case of electrons and muons in nuclear matter.

4.1.1   Bulk viscosity of a two-species system

We assume that the system experiences a small-amplitude driving oscillation

$$V(t) = \bar{V} + \mathrm{Re}(\delta V\, e^{i\omega t})$$

$$p(t) = \bar{p} + \mathrm{Re}(\delta p\, e^{i\omega t}) \tag{4.1}$$

where the volume amplitude $\delta V \ll \bar{V}$ is real by convention, and the resultant pressure oscillation $p(t)$ is complex. The average power dissipated per unit volume is

$$\frac{dE}{dt} = -\frac{1}{\tau \bar{V}} \int_0^\tau p(t) \frac{dV}{dt} dt = -\frac{1}{2}\omega\, \mathrm{Im}(\delta p)\, \frac{\delta V}{\bar{V}} \ , \tag{4.2}$$

where $\tau = 2\pi/\omega$, so the bulk viscosity is [37]

$$\zeta = \frac{2\bar{V}^2}{\omega^2(\delta V)^2} \frac{dE}{dt} = -\frac{\mathrm{Im}(\delta p)}{\delta V} \frac{\bar{V}}{\omega} \ . \tag{4.3}$$

We will determine $\mathrm{Im}(\delta p)$, which will be negative. We will assume that heat arising from dissipation is conducted away quickly, so the whole calculation is performed at constant temperature T. We assume that our system contains two particle species e and μ, and the state of the system is determined by the corresponding chemical potentials μ_e and μ_μ. The total number of electrons and muons is conserved, and

equilibrium is established via the conversion process $e \leftrightarrow \mu$. For simplicity of presentation and of the final expressions, it is better to work in terms of charged lepton number l and electron-muon asymmetry a, so pressure is a function of μ_l and μ_a, where

$$
\begin{aligned}
\mu_l &= \tfrac{1}{2}(\mu_e + \mu_\mu) & n_l &= n_e + n_\mu = \left.\frac{\partial p}{\partial \mu_l}\right|_{\mu_a} \\
\mu_a &= \tfrac{1}{2}(\mu_e - \mu_\mu) & n_a &= n_e - n_\mu = \left.\frac{\partial p}{\partial \mu_a}\right|_{\mu_l}
\end{aligned}
\tag{4.4}
$$

From now on all partial derivatives with respect to μ_l will be assumed to be at constant μ_a, and vice versa. In beta-equilibrium, μ_a is zero. The variations in the chemical potentials are expressed in terms of complex amplitudes $\delta\mu_l$, and $\delta\mu_a$,

$$
\begin{aligned}
\mu_l(t) &= \bar{\mu}_l + \mathrm{Re}(\delta\mu_l\, e^{i\omega t}) \ , \\
\mu_a(t) &= \mathrm{Re}(\delta\mu_a e^{i\omega t}) \ .
\end{aligned}
\tag{4.5}
$$

The pressure amplitude is then

$$
\delta p = \left.\frac{\partial p}{\partial \mu_l}\right|_{\mu_a} \delta\mu_l + \left.\frac{\partial p}{\partial \mu_a}\right|_{\mu_l} \delta\mu_a = n_l \delta\mu_l + n_a \delta\mu_a \ ,
\tag{4.6}
$$

From (4.6) and (4.3) we find

$$
\zeta = -\frac{1}{\omega}\frac{\bar{V}}{\delta V}\left(\bar{n}_l \mathrm{Im}(\delta\mu_l) + \bar{n}_a \mathrm{Im}(\delta\mu_a)\right) \ .
\tag{4.7}
$$

To obtain the imaginary parts of the chemical potential amplitudes, we write down the rate of change of the corresponding conserved quantities,

$$
\begin{aligned}
\frac{dn_l}{dt} &= \frac{\partial n_l}{\partial \mu_l}\frac{d\mu_l}{dt} + \frac{\partial n_l}{\partial \mu_a}\frac{d\mu_a}{dt} = -\frac{n_l}{\bar{V}}\frac{dV}{dt} \ , \\
\frac{dn_a}{dt} &= \frac{\partial n_a}{\partial \mu_l}\frac{\partial \mu_l}{dt} + \frac{\partial n_a}{\partial \mu_a}\frac{d\mu_a}{dt} = -\frac{n_a}{\bar{V}}\frac{dV}{dt} - \Gamma_{e\to\mu}^{\text{total}} \ .
\end{aligned}
\tag{4.8}
$$

65

All the partial derivatives are evaluated at equilibrium, $\mu_l = \bar{\mu}_l$ and $\mu_a = 0$. The right hand term on the first line expresses the fact that charge is conserved, so when a volume is compressed, the density of charged leptons rises. On the second line, there is such a term from the compression of the existing population of particles, but there is also a rate of conversion $\Gamma^{\text{total}}_{e \to \mu}$ of electrons to muons, which reflects the fact that weak interactions will push the lepton densities towards their equilibrium value. For small deviations from equilibrium we expect $\Gamma^{\text{total}}_{e \to \mu}$ to be linear in μ_a, so it is convenient to write the rate in terms of an average width γ_a, which is defined in terms of the total rate by writing

$$\Gamma^{\text{total}}_{e \to \mu} = \gamma_a \frac{\partial n_a}{\partial \mu_a} \mu_a \ . \tag{4.9}$$

We now substitute the assumed oscillations (4.1) and (4.5) in to (4.8), and solve to obtain the amplitudes $\delta\mu_l$ and $\delta\mu_a$ in terms of the amplitude δV and frequency ω of the driving oscillation. Inserting their imaginary parts in (4.7) we obtain the bulk viscosity, which is conveniently expressed in terms of the susceptibilities

$$
\begin{aligned}
\chi_{ll} &= \frac{\partial n_l}{\partial \mu_l} \ , \\[2mm]
\chi_{la} &= \frac{\partial n_l}{\partial \mu_a} = \frac{\partial n_a}{\partial \mu_l} \ , \\[2mm]
\chi_{aa} &= \frac{\partial n_a}{\partial \mu_a} \ ,
\end{aligned}
\tag{4.10}
$$

all evaluated at equilibrium, $\mu_l = \bar{\mu}_l$, $\mu_a = 0$. Note that χ_{al} is the same as χ_{la} from

(4.4). Defining

$$
\begin{aligned}
\gamma_{\text{eff}} &= \frac{\chi_{ll}\chi_{aa}}{\chi_{ll}\chi_{aa} - \chi_{la}^2}\gamma_a = \frac{\chi_{ll}}{\chi_{ll}\chi_{aa} - \chi_{la}^2}\frac{\partial\Gamma_{e\to\mu}^{\text{total}}}{\partial\mu_a}\bigg|_{\mu_a=0}, \\[2mm]
C &= \frac{(\chi_{ll}n_a - \chi_{la}n_l)^2}{\chi_{ll}(\chi_{ll}\chi_{aa} - \chi_{la}^2)} ,
\end{aligned}
\tag{4.11}
$$

we obtain the final result for the bulk viscosity in a two-species system,

$$
\zeta = C\frac{\gamma_{\text{eff}}}{\omega^2 + \gamma_{\text{eff}}^2} .
\tag{4.12}
$$

From (4.12) we can already see how the bulk viscosity of a two-species system depends on the frequency ω of the oscillation and the effective equilibration rate γ_{eff}.

At fixed equilibration rate, the bulk viscosity decreases monotonically as the oscillation frequency rises; it is roughly constant for $\omega \lesssim \gamma_{\text{eff}}$, and then drops off quickly as $1/\omega^2$ for $\omega \gg \gamma_{\text{eff}}$.

At fixed oscillation frequency ω, the bulk viscosity is a non-monotonic function of the rate γ_{eff}. It is peaked at $\gamma_{\text{eff}} = \omega$, with a value

$$
\zeta_{\text{max}} = \tfrac{1}{2}C/\omega .
\tag{4.13}
$$

For $\gamma_{\text{eff}} \ll \omega$ or $\gamma_{\text{eff}} \gg \omega$ the bulk viscosity tends to zero. Thus very fast and very slow processes are not an important source of bulk viscosity. As we will see below, for leptons in nuclear matter the equilibration rate is sensitive to temperature but the coefficient C is not, so we expect $\zeta(T)$ to be peaked at $\gamma_{\text{eff}}(T) = \omega$, where the oscillation frequency ω is of order kHz for typical oscillation modes of neutron stars.

4.1.2 Leptons in nuclear matter

In nuclear matter the leptonic chemical potential $\mu_l = \mu_e = \mu_\mu$ is much greater than the temperature and the electron mass, so we can evaluate the susceptibilities (4.10) at $m_e = T = 0$. Temperature dependence will come in only via the equilibration rate γ_a. Treating the electrons and muons as free fermions, we find

$$\gamma_{\text{eff}} = \gamma_a \frac{(\mu_l + p_F)^2}{4\mu_l p_F} ,$$

$$C = \frac{1}{9\pi^2} m_\mu^2 p_F (\mu_l - p_F) .$$

(4.14)

where the muon Fermi momentum is given by $p_F^2 = \mu_l^2 - m_\mu^2$. Note that the bulk viscosity goes to zero as $m_\mu \to 0$ ($m_\mu \to m_e$, really). This is because if the muons and electrons have equal mass then under compression their relative densities do not change, and there is no need for any equilibrating process, so the pressure is always in phase with the volume and no dissipation occurs.

Even without calculating the rate of lepton number equilibration, we can now estimate the amount of bulk viscosity that could possibly arise from leptons. If the equilibrating weak interaction at some temperature happened to have a rate that matched the typical oscillation frequency of the star, $\omega \approx 2\pi \times 1000$ Hz, and the lepton chemical potential had a relatively moderate value of about 120 MeV, we would obtain from (4.13), $\zeta_{\text{max}} = 5.5 \times 10^{22}$ MeV$^3 = 7.5 \times 10^{27}$ g s^{-1}cm^{-1}. This is at the upper end of typical nuclear bulk viscosities which range up to 10^{28}g s^{-1}cm^{-1} [27]. This motivates us to proceed with the calculation of the rate of conversion of muons to and from electrons via the weak interaction.

4.2   Muon-electron conversion rate

The muon-electron conversion rate $\Gamma_{e\to\mu}^{\text{total}}$ consists of two partial rates,

$$\Gamma_{e\to\mu}^{\text{total}} = \Gamma_{ee\to e\mu}^{\text{total}} + \Gamma_{e\mu\to\mu\mu}^{\text{total}} \tag{4.15}$$

The partial rates are

$$\Gamma_{ab\to cd}^{\text{total}} = \int \frac{d^3p_1 d^3p_2 d^3p_3 d^3p_4 d^3k_1 d^3k_2}{64(2\pi)^{14}\omega_1\omega_2\omega_3\omega_4\Omega_1\Omega_2}\delta^4(p_1+p_2-p_3-p_4-k_1-k_2)W_{ab\to cd}(p_1p_2\to p_3p_4k_1k_2)$$

$$\times \left[f_a(\omega_1)f_b(\omega_2)\left(1-f_c(\omega_3)\right)\left(1-f_d(\omega_4)\right)-f_c(\omega_1)f_d(\omega_2)\left(1-f_a(\omega_3)\right)\left(1-f_b(\omega_4)\right)\right] \tag{4.16}$$

where a,b,c,d are either e or μ, $W_{ab\to cd}$ is the spin-summed and averaged matrix element. The charged lepton of flavor j has energy $\omega_j = \sqrt{\mathbf{p}_j^2 + m_j^2}$, the neutrino of flavor j has energy $\Omega_j = |k_j|$, and $f_b(\omega_j)$ is the Fermi distribution function

$$f_b(\omega_j) = \left[1 + \exp\left(\frac{\omega_j - \mu_b}{T}\right)\right]^{-1} \tag{4.17}$$

Using the previous definitions for μ_l and μ_a, we have

$$\mu_e = \mu_l + \mu_a, \quad \mu_\mu = \mu_l - \mu_a \tag{4.18}$$

and since μ_a is small, to first order in μ_a we have

$$f_e(\omega_1)f_e(\omega_2)\left(1-f_e(\omega_3)\right)\left(1-f_\mu(\omega_4)\right)-f_e(\omega_1)f_\mu(\omega_2)\left(1-f_e(\omega_3)\right)\left(1-f_e(\omega_4)\right) = F(\omega_1,\omega_2,\omega_3,\omega_4)\frac{\mu_a}{T}$$

$$\tag{4.19}$$

and

$$f_\mu(\omega_1)f_e(\omega_2)\left(1-f_\mu(\omega_3)\right)\left(1-f_\mu(\omega_4)\right)-f_\mu(\omega_1)f_\mu(\omega_2)\left(1-f_\mu(\omega_3)\right)\left(1-f_e(\omega_4)\right) = F(\omega_1,\omega_2,\omega_3,\omega_4)\frac{\mu_a}{T}$$

$$\tag{4.20}$$

$$F(\omega_1,\omega_2,\omega_3,\omega_4) \equiv \frac{2\exp\left[(\omega_3+\omega_4-2\mu_l)/T\right]\left[1+2\exp\left[(\omega_2-\mu_l)/T\right]+\exp\left[(\omega_2+\omega_4-2\mu_l)/T\right]\right]}{(1+\exp[(\omega_1-\mu_l)/T])\,(1+\exp[(\omega_2-\mu_l)/T])^2\,(1+\exp[(\omega_3-\mu_l)/T])\,(1+\exp[(\omega_4-\mu_l)/T])^2} \tag{4.21}$$
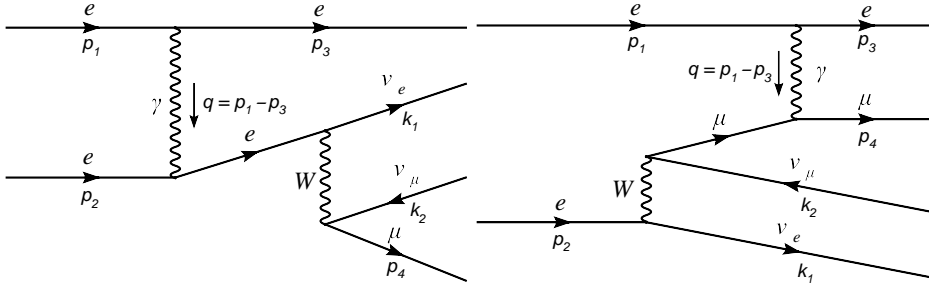
Figure 4.1: Feynman diagrams for the process $e + e \rightarrow e + \mu + \bar{\nu}_\mu + \nu_e$. There are an additional two diagrams which are obtained from these by exchanging $p_1 \leftrightarrow p_2$.
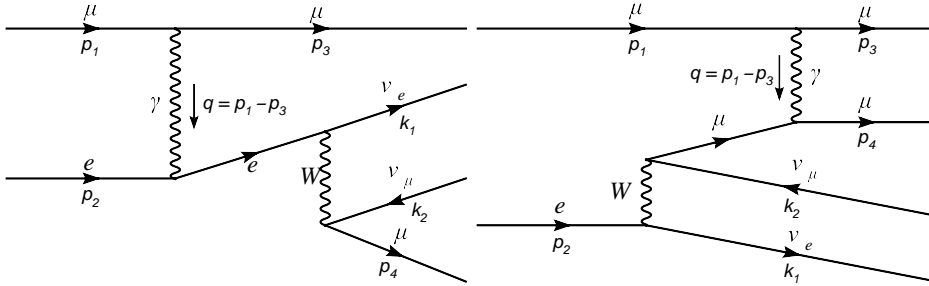
Figure 4.2: Feynman diagrams for the process $e + \mu \rightarrow \mu + \mu + \bar{\nu}_\mu + \nu_e$. There are an additional two diagrams which are obtained from these by exchanging $p_3 \leftrightarrow p_4$.

To determine the content of the matrix elements, we draw the Feynman diagrams for each possible way the reaction can occur. We can draw two different diagrams for each process, depending on the whether the weak conversion of the electron to muon occurs before the electromagnetic scattering, or in the reverse order (Fig. 4.1, Fig. 4.2). However, because there are identical particles involved, and we are integrating over all initial and final momenta, we need to add two additional diagrams for each process. For the process $e + e \rightleftharpoons \mu + e + \nu + \bar{\nu}$, we must add two diagrams where the labels on the initial state electron momenta are reversed; and for the process $e + \mu \rightleftharpoons \mu + \mu + \nu + \bar{\nu}$, we must add two diagrams where the labels on the final state muon momenta are reversed. These diagrams get an additional negative sign for the interchange of fermions [74]. For similar calculations, see [75, 76].

Since we have four diagrams for each process, the spin summed-and-averaged matrix elements are

$$
\begin{aligned}
W_{ee \to e\mu} &= \frac{1}{8} \sum_{spins} |E_1 + E_2 - E_3 - E_4|^2 \\
W_{e\mu \to \mu\mu} &= \frac{1}{8} \sum_{spins} |M_1 + M_2 - M_3 - M_4|^2
\end{aligned}
\tag{4.22}
$$

Here E_1, E_2, E_3, E_4 are the amplitudes corresponding to the diagrams of Fig. 4.1, and

M_1, M_2, M_3, M_4 are the amplitudes corresponding to the diagrams of Fig. 4.2 [77]:

$$
\begin{aligned}
E_1 &= \frac{e^2 G_F}{\sqrt{2}(q^2 - q_s^2)} \bar{e}(p_3)\gamma^\mu e(p_1)\bar{\nu}_e(k_1)\gamma^\lambda \left(1-\gamma^5\right) \frac{\not{p}_2 + \not{q} + m_e}{(p_2+q)^2 - m_e^2} \gamma_\mu e(p_2)\bar{\mu}(p_4)\gamma_\lambda \left(1-\gamma^5\right) \nu_\mu(k_2) \\
E_2 &= \frac{e^2 G_F}{\sqrt{2}(q^2 - q_s^2)} \bar{e}(p_3)\gamma^\mu e(p_1)\bar{\nu}_e(k_1)\gamma^\lambda \left(1-\gamma^5\right) e(p_2)\bar{\mu}(p_4)\gamma_\mu \frac{\not{p}_4 - \not{q} + m_\mu}{(p_4-q)^2 - m_\mu^2} \gamma_\lambda \left(1-\gamma^5\right) \nu_\mu(k_2) \\
E_3 &= \frac{e^2 G_F}{\sqrt{2}(w^2 - q_s^2)} \bar{e}(p_3)\gamma^\mu e(p_2)\bar{\nu}_e(k_1)\gamma^\lambda \left(1-\gamma^5\right) \frac{\not{p}_1 + \not{w} + m_e}{(p_1+w)^2 - m_e^2} \gamma_\mu e(p_1)\bar{\mu}(p_4)\gamma_\lambda \left(1-\gamma^5\right) \nu_\mu(k_2) \\
E_4 &= \frac{e^2 G_F}{\sqrt{2}(w^2 - q_s^2)} \bar{e}(p_3)\gamma^\mu e(p_2)\bar{\nu}_e(k_1)\gamma^\lambda \left(1-\gamma^5\right) e(p_1)\bar{\mu}(p_4)\gamma_\mu \frac{\not{p}_4 - \not{w} + m_\mu}{(p_4-w)^2 - m_\mu^2} \gamma_\lambda \left(1-\gamma^5\right) \nu_\mu(k_2)
\end{aligned}
$$

$$(4.23)$$

$$
\begin{aligned}
M_1 &= \frac{e^2 G_F}{\sqrt{2}(q^2 - q_s^2)} \bar{\mu}(p_3)\gamma^\mu \mu(p_1)\bar{\nu}_e(k_1)\gamma^\lambda \left(1-\gamma^5\right) \frac{\not{p}_2 + \not{q} + m_e}{(p_2+q)^2 - m_e^2} \gamma_\mu e(p_2)\bar{\mu}(p_4)\gamma_\lambda \left(1-\gamma^5\right) \nu_\mu(k_2) \\
M_2 &= \frac{e^2 G_F}{\sqrt{2}(q^2 - q_s^2)} \bar{\mu}(p_3)\gamma^\mu \mu(p_1)\bar{\nu}_e(k_1)\gamma^\lambda \left(1-\gamma^5\right) e(p_2)\bar{\mu}(p_4)\gamma_\mu \frac{\not{p}_4 - \not{q} + m_\mu}{(p_4-q)^2 - m_\mu^2} \gamma_\lambda \left(1-\gamma^5\right) \nu_\mu(k_2) \\
M_3 &= \frac{e^2 G_F}{\sqrt{2}(s^2 - q_s^2)} \bar{\mu}(p_4)\gamma^\mu \mu(p_1)\bar{\nu}_e(k_1)\gamma^\lambda \left(1-\gamma^5\right) \frac{\not{p}_2 + \not{s} + m_e}{(p_2+s)^2 - m_e^2} \gamma_\mu e(p_2)\bar{\mu}(p_3)\gamma_\lambda \left(1-\gamma^5\right) \nu_\mu(k_2) \\
M_4 &= \frac{e^2 G_F}{\sqrt{2}(s^2 - q_s^2)} \bar{\mu}(p_4)\gamma^\mu \mu(p_1)\bar{\nu}_e(k_1)\gamma^\lambda \left(1-\gamma^5\right) e(p_2)\bar{\mu}(p_3)\gamma_\mu \frac{\not{p}_3 - \not{s} + m_\mu}{(p_3-s)^2 - m_\mu^2} \gamma_\lambda \left(1-\gamma^5\right) \nu_\mu(k_2)
\end{aligned}
$$

$$(4.24)$$

where $w = p_2 - p_3$, and $s = p_1 - p_4$.

The only parameter in our calculation that depends on details of the baryonic matter in the neutron star is the plasma screening momentum q_s. In a full treatment one would have to use the appropriate in-medium propagator which is a complicated function of the photon momentum involving Debye screening of longitudinal photons, and Landau damping and possible Meissner screening of transverse photons [78, 79] In this paper we greatly simplify the calculation by assuming that the longitudinal and transverse photons have a common screening mass

$$q_s^2 = 5\alpha\mu_l^2 \ . \tag{4.25}$$

For the longitudinal photons, this is a reasonable estimate of the square of the Debye mass M_D^2 for $\mu_l > m_\mu$. The electron contribution to M_D^2 is $4\alpha\mu_l^2/\pi \approx \alpha\mu_l^2$ [80]; the muon contribution is smaller when $\mu_l \sim m_\mu$ and equal when $\mu_l \gg m_\mu$, and there is also a proton contribution that is enhanced by m_N/μ_l. If we treat the system as a gas of free nucleons and leptons then (4.25) differs from M_D^2 by less than a factor of 2 for $\mu_l > m_\mu$.

For the transverse photons, (4.25) is an overestimate of their screening. In the low-momentum (London) limit, proton superconductivity would give a Meissner mass $M_M^2 = 4/(3\pi)\alpha p_{F,p}^3/m_p$ (see, e.g., Ref. [12]), and overall charge neutrality requires that $p_{F,p} \approx \mu_l$ (assuming that electrons are the main source of negative charge), so $M_M^2 \approx \alpha\mu_l^2(\mu_l/m_N)$; (4.25) would then overestimate M_M^2 by a factor of between 10 and 50 depending on μ_l. Moreover, in modified Urca processes the photon momentum is well above the proton inverse coherence length, so the magnetic screening is reduced below the London value [81, 80].

However, the sensitivity of our results to the precise screening of the photons is limited by the fact that the photon always carries enough momentum to move a lepton between the muon and electron Fermi surfaces, and its energy is negligible in comparison to its momentum. So in the transverse photon propagator M_M^2 is added to κ^2 where the minimum value of κ is $p_{Fe} - p_{F\mu}$ which varies from about 80 MeV at $\mu_l = 110$ MeV to 20 MeV at $\mu_l = 300$ MeV. There is therefore no singularity at very small values of M_M: the photon propagator becomes independent of M_M when $M_M \ll \kappa$. Our approximation (4.25) corresponds to assuming a value of M_M that, in the range

$m_\mu < \mu_l < 300$ MeV, is unphysically large but of the same order of magnitude as the minimum momentum transfer κ. So using (4.25) is a conservative approximation that should give a reasonable order-of-magnitude estimate of the leptonic equilibration rate, with a tendency to underestimate it because the contribution of transverse photons is overly suppressed.

To obtain the equilibration rates, we first multiply out the right hand sides of (4.22) and define partial matrix elements by

$$
\begin{aligned}
W_{ee \to e\mu} &= \sum_{i,j \leq i} W^{ij}_{ee \to e\mu}, \; W_{e\mu \to \mu\mu} = \sum_{i,j \leq i} W^{ij}_{e\mu \to \mu\mu} \\
W^{11}_{ee \to e\mu} &= \frac{1}{8} \sum_{spins} |E_1|^2, \; W^{12}_{ee \to e\mu} = \frac{1}{8} \sum_{spins} (E_1^\dagger E_2 + E_2^\dagger E_1), \\
W^{13}_{ee \to e\mu} &= -\frac{1}{8} \sum_{spins} (E_1^\dagger E_3 + E_3^\dagger E_1), \; \text{etc.}
\end{aligned}
\tag{4.26}
$$

The traces resulting from the spin sums are easily evaluated with a computer algebra package; we used the FeynCalc package for Mathematica [82]. The traces are listed in section 4.5. In the next few paragraphs, we will describe the steps used to analytically integrate 10 of the 18 integrals, and list the expressions that we subsequently integrated numerically in section 4.4.

We make use of the fact that the neutrino energies are $\sim T \ll \mu_e, \mu_\mu$ by approximating the momentum and energy conserving delta functions as

$$
\delta^4(p_1 + p_2 - p_3 - p_4 - k_1 - k_2) \approx \delta(\omega_1 + \omega_2 - \omega_3 - \omega_4 - \Omega_1 - \Omega_2)\delta^3(\mathbf{p}_1 + \mathbf{p}_2 - \mathbf{p}_3 - \mathbf{p}_4) \tag{4.27}
$$

We then note that k_1 and k_2 occur exactly once in each term, dotted into one of the

other 4-momenta p_i. Writing

$$k_j = \Omega_j \left(1, \sin \xi_j \cos \eta_j, \sin \xi_j \sin \eta_j, \cos \xi_j\right) \tag{4.28}$$

then any dot product with another 4-momentum p_i is

$$p_i \cdot k_j = \Omega_j \left(\omega_i - (p_i)_x \sin \xi_j \cos \eta_j - (p_i)_y \sin \xi_j \sin \eta_j - (p_i)_z \cos \xi_j\right) \tag{4.29}$$

The result of this operation is that the integrals over the k_1 and k_2 angular variables

become trivial:

$$\int \frac{d^3 k_j}{\Omega_j} p_i \cdot k_j \rightarrow \int k_j^2 dk_j d(\cos \xi_j) d\eta_j p_i \cdot \hat{k}_j \rightarrow 4\pi\omega_i \int_0^\infty \Omega_j^2 d\Omega_j \tag{4.30}$$

because all of the integrations over one of the angles ξ_j or η_j are zero.

The energy-momentum conserving delta function allows us to use relations like

$p_1 - p_3 = p_4 - p_2$ to rewrite some of the denominators of the matrix elements. For

example, in $W_{ee \rightarrow e\mu}$ we can substitute variables so that p_3 does not appear in the

denominators of any of the terms; then we can integrate out the p_3 3-momentum

variables easily. Similarly, in $W_{e\mu \rightarrow \mu\mu}$ we can substitute variables so that p_2 does

not appear in the denominators and integrate out the p_2 3-momentum variables.

However, our matrix elements have many terms containing the four-momentum p_3

(p_2), so it would be easier if we could integrate over $d^4 p_3$ $(d^4 p_2)$. This is accomplished

by replacing

$$\int \frac{d^3 p_3}{\omega_3} = \int \frac{d^4 p_3}{(p_3)_0} \delta \left((p_3)_0 - \sqrt{\mathbf{p}_3^2 + m_\mu^2}\right) \approx \int \frac{d^4 p_3}{(p_3)_0} \delta \left((p_3)_0 - \mu_l\right) \tag{4.31}$$

in $W_{ee \rightarrow e\mu}$ and similarly for p_2 in $W_{e\mu \rightarrow \mu\mu}$. In the last approximation we are using

the fact that the Fermi distribution function is sharply peaked at low temperatures. Then we integrate over $d^4 p_3$ ($d^4 p_2$) using four of the delta functions.

We can further approximate that the medium is isotropic, by taking one of the remaining momentum variables to be in a fixed direction (the z-axis for convenience). The electrons are relativistic, so $\omega_i = |\mathbf{p}_i|$ and $d^3 p_i = \omega_i^2 d\omega_i d\cos\theta_i d\phi_i$ when particle i is an electron. The muons may not be relativistic, so $\omega_i = \sqrt{\mathbf{p}_i^2 + m_\mu^2}$ and $d^3 p_i = \omega_i \sqrt{\omega_i^2 - m_\mu^2} d\omega_i d\cos\theta_i d\phi_i$ when particle i is a muon. We then use the remaining delta function to integrate over the magnitude of this isotropic momentum variable.

The remainder of the integrations are performed numerically. The only further approximation made was to again take advantage of the sharply peaked Fermi distribution function, and set $\omega_i = \mu_l$ everywhere inside the integral, except for inside the Fermi function itself. This allows a separation of the eight-dimensional integral into a four-dimensional energy integral and a four-dimensional integral over the angular variables. The integration variables are also changed to dimensionless variables by scaling them with respect to μ_l.

The final expression for each term in the rate has the form

$$\Gamma^{ij}_{e\ell \to \mu\ell} = \frac{e^4 G_F^2 \mu_l^{12}}{128\pi^{11} m_\mu^4} \left(\frac{\mu_a}{T}\right) \times I_\omega^\ell \times I_{d\Omega}^{\ell ij} \tag{4.32}$$

where ℓ is the species of the spectator lepton, and I_ω^ℓ and $I_{d\Omega}^{\ell ij}$ are dimensionless energy and angular integrals, respectively. These integrals are listed in section 4.4.

4.3   Numerical results and conclusions

The remaining part of the rate calculation is performed numerically. The dimensionless energy integrals are nearly the same; a power-law fit of the results yields

$$I_\omega^e \approx 78.86 \left(\frac{T}{\mu_l}\right)^8, \quad I_\omega^\mu \approx 78.62 \left(\frac{T}{\mu_l}\right)^8 \tag{4.33}$$

In our approximation, the angular integrals only have dependence on μ_l. We determined an analytical fit for the μ_l-dependence of $I_{d\Omega}^{eij}$ and $I_{d\Omega}^{\mu ij}$ (accurate within 5%) over the range $120\,\mathrm{MeV} < \mu_l < 300\,\mathrm{MeV}$ by curve-fitting the numerical data with sixth-order polynomials:

$$\sum_{ij} I_{d\Omega}^{eij} \approx \left(1 - \frac{m_\mu^2}{\mu_l^2}\right)^{1/2} \sum_{i=0}^{6} c_i \left(\frac{\mu_l}{m_\mu}\right)^i,$$

$$c_0 = -1.7363 \times 10^4, c_1 = 5.0189 \times 10^4, c_2 = -4.7644 \times 10^4, c_3 = 1.3224 \times 10^4,$$

$$c_4 = 4.4203 \times 10^3, c_5 = -2.7199 \times 10^3, c_6 = 3.5119 \times 10^2 \tag{4.34}$$

$$\sum_{ij} I_{d\Omega}^{\mu ij} \approx \left(1 - \frac{m_\mu^2}{\mu_l^2}\right)^{3/2} \sum_{i=0}^{6} c_i \left(\frac{\mu_l}{m_\mu}\right)^i,$$

$$c_0 = 1.2433 \times 10^6, c_1 = -3.6329 \times 10^6, c_2 = 4.4365 \times 10^6, c_3 = -2.8702 \times 10^6,$$

$$c_4 = 1.0354 \times 10^6, c_5 = -1.9728 \times 10^5, c_6 = 1.5507 \times 10^4 \tag{4.35}$$

Fig. 4.3 shows the μ_l dependence of the effective rate γ_{eff} defined in (4.11). As μ_l approaches m_μ, the rate quickly drops to zero as the muon population disappears. The overall T^7 dependence is also illustrated in the sizable difference in order of magnitude of the rate for the three different temperatures.

Fig. 4.4 shows the temperature dependence of the bulk viscosity ζ as defined in (4.12), for a neutron star with oscillation frequency $\omega = 2\pi \times 1\mathrm{kHz}$. The straight
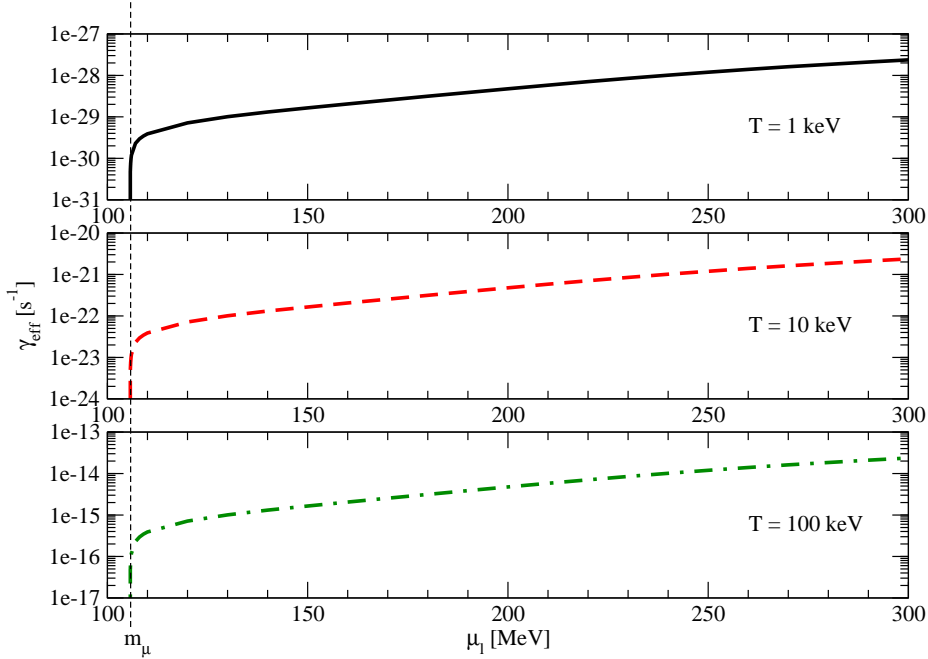
Figure 4.3: (Color online) Dependence of the effective rate of electron/muon conversion γ_{eff} (see (4.11)) on the charged-lepton chemical potential μ_l at three different temperatures. As μ_l drops towards m_μ, the muon population decreases and the conversion rate drops to zero. The temperature dependence is T^7, hence γ_{eff} is much larger at higher temperatures.

dashed, dotted and dot-dashed lines on the log-log plot illustrate the power-law dependence on T for three different values of μ_l. Also plotted is the nucleonic bulk viscosity using the results of [28]. These results are for a model where neutrons are superfluid, pairing in the spin triplet state, and the protons are superconducting, pairing in the spin singlet state; also, it is assumed that only modified Urca processes are available for damping of pulsations (although direct Urca processes would become possible at higher densities) and the critical temperature for both the neutron superfluidity and proton superconductivity was chosen to be $10^{10}\,\mathrm{K} \approx 0.86$ MeV. Above the critical temperature for proton superfluidity, the bulk viscosity for 1 kHz oscillations due to leptons is several orders of magnitude less than the bulk viscosity due to nucleons; below the critical temperature, the nucleonic bulk viscosity quickly decreases and at a low enough temperature, the leptonic contribution becomes dominant. Based on our calculations, this crossover temperature appears to be of order 0.01 to 0.1 MeV (10^8 to 10^9 K) for an oscillation frequency in the kHz range. Such a suppression of the nucleonic contribution can arise either from superfluidity of neutrons or superconductivity of protons. It is therefore quite possible that for many cold neutron stars, the bulk viscosity of the superconducting or superfluid region comes mainly from leptonic processes.

The viscosity curves in Fig. 4.4 all slope upwards because the equilibration rate $\gamma_{\mathrm{eff}}(T)$ is well below the oscillation frequency ω, so we are in the slow-equilibration
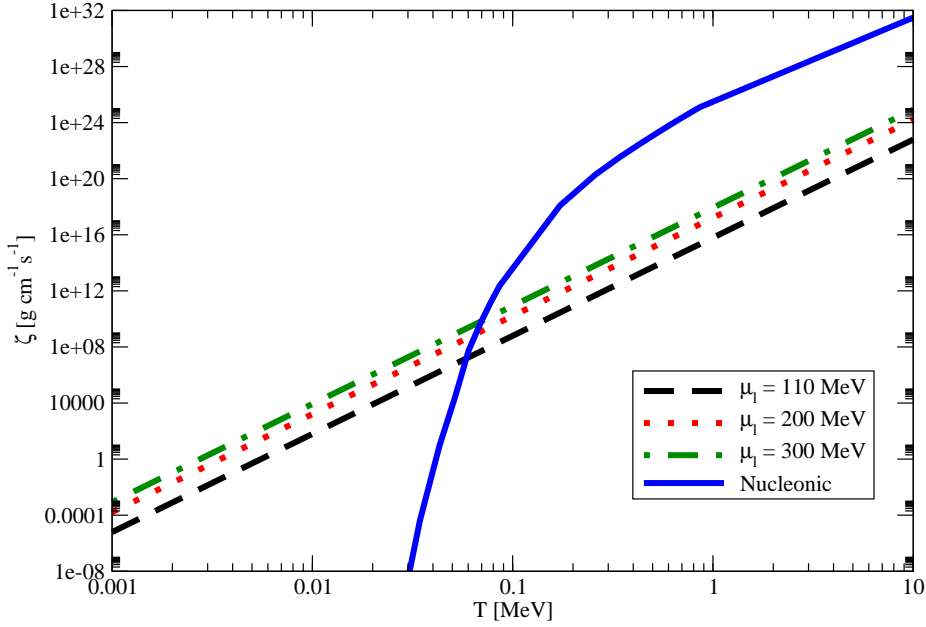
Figure 4.4: (Color online) Dependence of the leptonic bulk viscosity ζ on temperature for three different values of the lepton chemical potential, and an oscillation frequency of $1\,\mathrm{kHz}$; for frequency dependence, see the discussion after (4.36). The solid line is the nucleonic bulk viscosity [28] due to modified-Urca processes. The protons are superconducting at $T < 0.86\,\mathrm{MeV}\,(10^{10}\,\mathrm{K})$.

(high frequency) regime of (4.12), where

$$\zeta \approx C \frac{\gamma_{\text{eff}}(T)}{\omega^2} \ .$$

(4.36)

This is true for both leptonic and nuclear viscosities. In this regime one can simply add the two bulk viscosities to get the total bulk viscosity (see, for example, appendix A of Ref. [40]). As the temperature rises, the equilibration rate and hence the bulk viscosity rise. When $\gamma_{\text{eff}}(T)$ comes close to ω, (4.36) becomes a poor approximation to (4.12): ζ reaches a maximum when $\gamma_{\text{eff}}(T) = \omega$. Those maxima, for both leptonic and nuclear bulk viscosities, are beyond the right hand limit of Fig. 4.4; for $\mu_l = 200$ MeV, the peak occurs at $T \approx 40$ MeV.

We can now see how our results depend on the frequency of the oscillations. Decreasing ω moves each $\zeta(T)$ curve to the left, shifting the viscosity curves in Fig. 4.4 upwards. The largest value we find for the leptonic effective rate γ_{eff} (at $T = 10$ MeV, for $\mu_l = 300$ MeV) is $\gamma_{\text{eff}} \sim 2$ rad/s, so for the leptonic bulk viscosity (4.36) is valid for oscillation frequencies well above this value. For example, if we reduced the oscillation frequency from 1000 Hz to 100 Hz then all the viscosity curves in Fig. 4.4 would be shifted upwards by a factor of 100. Decreasing the frequency still further would bring us to the regime where, in the temperature range of interest, either the nuclear and leptonic rate was comparable to the oscillation frequency (so one or both bulk viscosity curves would show a resonant peak in our plot). Then one may not be able to simply add the bulk viscosities. At extremely low oscillation frequencies, both peaks would shift to very low temperatures, the bulk viscosity curves in our

plot would all slope downwards, the nucleonic contribution dominates, and the bulk viscosities could again be added.

It will be interesting to see whether the leptonic contribution that we have calculated here has any impact on oscillations of neutron stars. In the case of r-modes, shear viscosity becomes the dominant source of damping in the low temperature regime, so the leptonic contributions to the bulk viscosity at low temperature are not likely to be an important source of r-mode damping. However, for other modes such as radial pulsations [83] they might be the main source of damping. We argued (after (4.25)) that our approximations lead to a result that is of the correct order of magnitude, tending to err on the conservative side of underestimating the leptonic equilibration rate. If a more precise estimate of the bulk viscosity were required, one could improve on our treatment by replacing the approximation (4.25) with separate propagators for the transverse and longitudinal photons, incorporating their separate screening mechanisms [81]. It should be noted that our calculation is limited to the small-amplitude regime ($\mu_a \ll T$). If the leptonic bulk viscosity is insufficient to damp an unstable oscillation such as an r-mode then the amplitude will rise and it will be necessary to repeat our calculation in the large-amplitude ("supra-thermal") regime [84] to see whether leptonic bulk viscosity can stop the growth of the mode once it reaches a large enough amplitude.

4.4   Partial Rate Integrals

The following abbreviations are used throughout this appendix:

$$x_m = \frac{m_\mu}{\mu_l}, \; x_s = \frac{q_s}{\mu_l}, \; t = \frac{T}{\mu_l}$$

$$C_{12} = 1 - \cos\theta_2, \; C_{14} = 1 - \sqrt{1-x_m^2}\cos\theta_4$$

$$C_{24} = 1 - \sqrt{1-x_m^2}\left(\sin\theta_2\sin\theta_4(\sin\phi_2\sin\phi_4+\cos\phi_2\cos\phi_4)+\cos\theta_2\cos\theta_4\right)$$

$$\bar{C}_{13} = 1 - (1-x_m^2)\left(\sin\theta_1\sin\theta_3(\sin\phi_1\sin\phi_3+\cos\phi_1\cos\phi_3)+\cos\theta_1\cos\theta_3\right)$$

$$\bar{C}_{14} = 1 - (1-x_m^2)\cos\theta_1, \; \bar{C}_{34} = 1 - (1-x_m^2)\cos\theta_3 \tag{4.37}$$

$$F(x_a,x_b,x_c,x_d) = \frac{2\exp\left[(x_c+x_d-2)/t\right]\left[1+2\exp\left[(x_b-1)/t\right]+\exp\left[(x_b+x_d-2)/t\right]\right]}{(1+\exp[(x_a-1)/t])\,(1+\exp[(x_b-1)/t])^2\,(1+\exp[(x_c-1)/t])\,(1+\exp[(x_d-1)/t])^2} \tag{4.38}$$

$$I_\omega^e = \int dx_2 dx_4 dy_1 dy_2 \; y_1^2 \, y_2^2 \; F(x_4+y_1+y_2-x_2+1, x_2, 1, x_4)$$

$$I_\omega^\mu = \int dx_1 dx_3 dy_1 dy_2 \; y_1^2 \, y_2^2 \; F(x_1, 1, x_3, x_1-x_3-y_1-y_2+1) \tag{4.39}$$

$$I_{d\Omega}^{e11} = \sqrt{1-x_m^2}\int d\Omega_2 d\Omega_4 \frac{4C_{12}C_{14}+2C_{12}C_{24}-2C_{14}C_{24}-4x_m^2 C_{12}+x_m^2 C_{24}}{(x_m^2-2C_{24}-x_s^2)^2} \tag{4.40}$$

$$I_{d\Omega}^{e12} = -\sqrt{1-x_m^2}\int d\Omega_2 d\Omega_4 \left[\frac{-2C_{12}C_{24}^2+2C_{14}C_{24}^2+8C_{12}C_{14}+4C_{12}C_{24}-4C_{12}C_{14}C_{24}-4C_{14}C_{24}}{(x_m^2-2C_{24}-x_s^2)^2}\right.$$
$$\left. + \frac{x_m^2\left(4C_{12}^2-8C_{12}+4C_{14}+C_{12}C_{24}-C_{14}C_{24}\right)-x_m^4}{(x_m^2-2C_{24}-x_s^2)^2}\right] \tag{4.41}$$

$$I_{d\Omega}^{e13} = -\sqrt{1-x_m^2}\int d\Omega_2 d\Omega_4 \frac{-4C_{12}C_{14}-4C_{12}C_{24}+6x_m^2 C_{12}}{(x_m^2-2C_{24}-x_s^2)(x_m^2-2C_{14}-x_s^2)} \tag{4.42}$$

$$
I_{d\Omega}^{e14} = \sqrt{1-x_m^2} \int d\Omega_2 d\Omega_4 \left[\frac{2C_{12}C_{14}^2 - 4C_{12}C_{14} - 4C_{12}C_{24} + 2C_{12}C_{14}C_{24}}{(x_m^2 - 2C_{24} - x_s^2)(x_m^2 - 2C_{14} - x_s^2)} \right.
$$
$$
\left. + \frac{x_m^2(-C_{12}^2 + 6C_{12} - 2C_{12}C_{14} + 2C_{14} - 2C_{24}) + x_m^4/2}{(x_m^2 - 2C_{24} - x_s^2)(x_m^2 - 2C_{14} - x_s^2)} \right] \quad (4.43)
$$

$$
I_{d\Omega}^{e22} = \sqrt{1-x_m^2} \int d\Omega_2 d\Omega_4 \frac{4C_{12}C_{14} + 2C_{12}C_{24} - 2C_{14}C_{24} - 4x_m^2 C_{12} + 4x_m^2 C_{14} + x_m^2 C_{24} - x_m^4}{(x_m^2 - 2C_{24} - x_s^2)^2}
$$
$$
(4.44)
$$

$$
I_{d\Omega}^{e23} = \sqrt{1-x_m^2} \int d\Omega_2 d\Omega_4 \left[\frac{2C_{12}C_{24}^2 - 4C_{12}C_{14} - 4C_{12}C_{24} + 2C_{12}C_{14}C_{24}}{(x_m^2 - 2C_{24} - x_s^2)(x_m^2 - 2C_{14} - x_s^2)} \right.
$$
$$
\left. + \frac{x_m^2(-C_{12}^2 + 6C_{12} - 2C_{12}C_{24} - 2C_{14} + 2C_{24}) + x_m^4 C_{12}/2}{(x_m^2 - 2C_{24} - x_s^2)(x_m^2 - 2C_{14} - x_s^2)} \right] \quad (4.45)
$$

$$
I_{d\Omega}^{e24} = -\sqrt{1-x_m^2} \int d\Omega_2 d\Omega_4 \left[\frac{2C_{12}^2 C_{14} - 4C_{12}C_{14} + 2C_{12}^2 C_{24} - 4C_{12}C_{24}}{(x_m^2 - 2C_{24} - x_s^2)(x_m^2 - 2C_{14} - x_s^2)} \right.
$$
$$
\left. + \frac{x_m^2(-4C_{12}^2 + 5C_{12} + C_{12}C_{14} + C_{12}C_{24} + C_{14} + C_{24})}{(x_m^2 - 2C_{24} - x_s^2)(x_m^2 - 2C_{14} - x_s^2)} \right] \quad (4.46)
$$

$$
I_{d\Omega}^{e33} = \sqrt{1-x_m^2} \int d\Omega_2 d\Omega_4 \frac{2C_{12}C_{14} + 4C_{12}C_{24} - 2C_{14}C_{24} + x_m^2(-4C_{12} + C_{14})}{(x_m^2 - 2C_{14} - x_s^2)^2} \quad (4.47)
$$

$$
I_{d\Omega}^{e34} = -\sqrt{1-x_m^2} \int d\Omega_2 d\Omega_4 \left[\frac{-2C_{12}C_{14}^2 + 4C_{12}C_{14} + 2C_{14}^2 C_{24} + 8C_{12}C_{24} - 4C_{12}C_{14}C_{24} - 4C_{14}C_{24}}{(x_m^2 - 2C_{14} - x_s^2)^2} \right.
$$
$$
\left. + \frac{x_m^2(2C_{12}^2 - 8C_{12} + C_{12}C_{14} - C_{14}C_{24} + 4C_{24}) - x_m^4}{(x_m^2 - 2C_{14} - x_s^2)^2} \right] \quad (4.48)
$$

$$
I_{d\Omega}^{e44} = \sqrt{1-x_m^2} \int d\Omega_2 d\Omega_4 \frac{2C_{12}C_{14} + 4C_{12}C_{24} - 2C_{14}C_{24} + x_m^2(-4C_{12} + C_{14} + 4C_{24}) - x_m^4}{(x_m^2 - 2C_{14} - x_s^2)^2}
$$
$$
(4.49)
$$

$$
I_{d\Omega}^{\mu11} = \left(1-x_m^2\right)^{3/2} \int d\Omega_1 d\Omega_3 \frac{-2\bar{C}_{13}\bar{C}_{14} + 2\bar{C}_{13}\bar{C}_{34} + 4\bar{C}_{14}\bar{C}_{34} + x_m^2(3\bar{C}_{14} - 5\bar{C}_{34}) - x_m^4}{(2x_m^2 - 2\bar{C}_{13} - x_s^2)^2} \quad (4.50)
$$

$$
I_{d\Omega}^{\mu12} = -\left(1-x_m^2\right)^{3/2} \int d\Omega_1 d\Omega_3 \left[\frac{-2\bar{C}_{13}\bar{C}_{14}^2 + 4\bar{C}_{14}^2 - 2\bar{C}_{13}\bar{C}_{34}^2 - 4\bar{C}_{34}^2 + 8\bar{C}_{13}\bar{C}_{34} + 8\bar{C}_{14}\bar{C}_{34}}{(2x_m^2 - 2\bar{C}_{13} - x_s^2)^2} \right.
$$
$$
+ \frac{x_m^2(4\bar{C}_{14}^2 + 4\bar{C}_{34}^2 - 8\bar{C}_{13} + 2\bar{C}_{13}\bar{C}_{14} - 8\bar{C}_{14} - 2\bar{C}_{13}\bar{C}_{34} - 4\bar{C}_{14}\bar{C}_{34} - 8\bar{C}_{34})}{(2x_m^2 - 2\bar{C}_{13} - x_s^2)^2}
$$
$$
\left. + \frac{x_m^4(3\bar{C}_{13} - 2\bar{C}_{14} + 2\bar{C}_{34} + 10) - 3x_m^6}{(2x_m^2 - 2\bar{C}_{13} - x_s^2)^2} \right] \quad (4.51)
$$

$$I_{d\Omega}^{\mu 13} = -\left(1-x_m^2\right)^{3/2} \int d\Omega_1 d\Omega_3 \left[\frac{2\bar{C}_{13}\bar{C}_{34}^2 + 2\bar{C}_{14}\bar{C}_{34}^2 - 4\bar{C}_{13}\bar{C}_{34} - 4\bar{C}_{14}\bar{C}_{34}}{(2x_m^2 - 2\bar{C}_{13} - x_s^2)(2x_m^2 - 2\bar{C}_{14} - x_s^2)} \right.$$

$$+ \frac{x_m^2(-4\bar{C}_{34}^2 + 5\bar{C}_{13} + 5\bar{C}_{14} + \bar{C}_{13}\bar{C}_{34} + \bar{C}_{14}\bar{C}_{34} + 5\bar{C}_{34})}{(2x_m^2 - 2\bar{C}_{13} - x_s^2)(2x_m^2 - 2\bar{C}_{14} - x_s^2)}$$

$$\left. + \frac{x_m^4(-3\bar{C}_{13}/2 - 3\bar{C}_{14}/2 - \bar{C}_{34} - 6) + 2x_m^6}{(2x_m^2 - 2\bar{C}_{13} - x_s^2)(2x_m^2 - 2\bar{C}_{14} - x_s^2)} \right] \tag{4.52}$$

$$I_{d\Omega}^{\mu 14} = \left(1-x_m^2\right)^{3/2} \int d\Omega_1 d\Omega_3 \left[\frac{2\bar{C}_{13}\bar{C}_{34}^2 + 4\bar{C}_{34}^2 - 8\bar{C}_{13}\bar{C}_{34} - 8\bar{C}_{14}\bar{C}_{34}}{(2x_m^2 - 2\bar{C}_{13} - x_s^2)(2x_m^2 - 2\bar{C}_{14} - x_s^2)} \right.$$

$$+ \frac{x_m^2(-\bar{C}_{14}^2 - 3\bar{C}_{34}^2 + 6\bar{C}_{13} + 8\bar{C}_{14} + 2\bar{C}_{13}\bar{C}_{34} + 2\bar{C}_{14}\bar{C}_{34} + 8\bar{C}_{34})}{(2x_m^2 - 2\bar{C}_{13} - x_s^2)(2x_m^2 - 2\bar{C}_{14} - x_s^2)}$$

$$\left. + \frac{x_m^4(-3\bar{C}_{13}/2 - 2\bar{C}_{34} - 9) + 3x_m^6/2}{(2x_m^2 - 2\bar{C}_{13} - x_s^2)(2x_m^2 - 2\bar{C}_{14} - x_s^2)} \right] \tag{4.53}$$

$$I_{d\Omega}^{\mu 22} = \left(1-x_m^2\right)^{3/2} \int d\Omega_1 d\Omega_3 \frac{2\bar{C}_{14}^2 - 2\bar{C}_{34}^2 + 4\bar{C}_{13}\bar{C}_{34} + 4\bar{C}_{14}\bar{C}_{34} + x_m^2(-4\bar{C}_{13} - 4\bar{C}_{34}) + 4x_m^4}{(2x_m^2 - 2\bar{C}_{13} - x_s^2)^2} \tag{4.54}$$

$$I_{d\Omega}^{\mu 23} = \left(1-x_m^2\right)^{3/2} \int d\Omega_1 d\Omega_3 \left[\frac{2\bar{C}_{14}\bar{C}_{34}^2 + 4\bar{C}_{34}^2 - 8\bar{C}_{13}\bar{C}_{34} - 8\bar{C}_{14}\bar{C}_{34}}{(2x_m^2 - 2\bar{C}_{13} - x_s^2)(2x_m^2 - 2\bar{C}_{14} - x_s^2)} \right.$$

$$+ \frac{x_m^2(-\bar{C}_{13}^2 - 3\bar{C}_{34}^2 + 10\bar{C}_{13} + \bar{C}_{13}\bar{C}_{14} + 6\bar{C}_{14} + 2\bar{C}_{13}\bar{C}_{34} + 2\bar{C}_{14}\bar{C}_{34} + 8\bar{C}_{34})}{(2x_m^2 - 2\bar{C}_{13} - x_s^2)(2x_m^2 - 2\bar{C}_{14} - x_s^2)}$$

$$\left. + \frac{x_m^4(-\bar{C}_{13} - 2\bar{C}_{14} - 2\bar{C}_{34} - 10) + 2x_m^6}{(2x_m^2 - 2\bar{C}_{13} - x_s^2)(2x_m^2 - 2\bar{C}_{14} - x_s^2)} \right] \tag{4.55}$$

$$I_{d\Omega}^{\mu 24} = -\left(1-x_m^2\right)^{3/2} \int d\Omega_1 d\Omega_3 \frac{4\bar{C}_{34}^2 - 8\bar{C}_{13}\bar{C}_{34} - 8\bar{C}_{14}\bar{C}_{34} + x_m^2(8\bar{C}_{13} + 8\bar{C}_{14} + 8\bar{C}_{34}) - 8x_m^4}{(2x_m^2 - 2\bar{C}_{13} - x_s^2)(2x_m^2 - 2\bar{C}_{14} - x_s^2)} \tag{4.56}$$

$$I_{d\Omega}^{\mu 33} = \left(1-x_m^2\right)^{3/2} \int d\Omega_1 d\Omega_3 \frac{-2\bar{C}_{14}^2 + 2\bar{C}_{14}\bar{C}_{34} + x_m^2(\bar{C}_{13} + 6\bar{C}_{14} - 3\bar{C}_{34}) - 3x_m^4}{(2x_m^2 - 2\bar{C}_{14} - x_s^2)^2} \tag{4.57}$$

$$I_{d\Omega}^{\mu 34} = -\left(1-x_m^2\right)^{3/2} \int d\Omega_1 d\Omega_3 \left[\frac{2\bar{C}_{13}^2 - 2\bar{C}_{13}\bar{C}_{14}^2 + 2\bar{C}_{13}\bar{C}_{14} - 2\bar{C}_{13}\bar{C}_{34} + 2\bar{C}_{13}\bar{C}_{14}\bar{C}_{34}}{(2x_m^2 - 2\bar{C}_{14} - x_s^2)^2} \right.$$

$$+ \frac{x_m^2(-\bar{C}_{13}^2 - \bar{C}_{34}^2 + 2\bar{C}_{13} + 4\bar{C}_{13}\bar{C}_{14} + 2\bar{C}_{14})}{(2x_m^2 - 2\bar{C}_{14} - x_s^2)^2}$$

$$\left. + \frac{x_m^4(-2\bar{C}_{13} - 2\bar{C}_{14} - 2) + 2x_m^6}{(2x_m^2 - 2\bar{C}_{14} - x_s^2)^2} \right] \tag{4.58}$$

85

$$I^{\mu 44}_{d\Omega} = \left(1 - x^2_m\right)^{3/2} \int d\Omega_1 d\Omega_3 \frac{2\bar{C}^2_{13} - 2\bar{C}^2_{34} + 4\bar{C}_{13}\bar{C}_{34} + 4\bar{C}_{14}\bar{C}_{34} + x^2_m(-4\bar{C}_{14} - 4\bar{C}_{34}) + 4x^4_m}{(2x^2_m - 2\bar{C}_{14} - x^2_s)^2}$$

$$(4.59)$$

4.5   Partial Matrix Elements

$$W^{11}_{ee \to e\mu} = \frac{e^4 G^2_F}{16\left(q^2 - q^2_s\right)^2 (p_1 + p_2 - p_3)^4} \times$$

$$\Big[-4096(k_1 \cdot p_4)(k_2 \cdot p_3)(p_1 \cdot p_2)^2 + 4096(k_1 \cdot p_4)(k_2 \cdot p_1)(p_1 \cdot p_2)(p_1 \cdot p_3)$$

$$+ 4096(k_1 \cdot p_4)(k_2 \cdot p_2)(p_1 \cdot p_2)(p_1 \cdot p_3) + 4096(k_1 \cdot p_4)(k_2 \cdot p_1)(p_1 \cdot p_2)(p_2 \cdot p_3)$$

$$+ 8192(k_1 \cdot p_4)(k_2 \cdot p_2)(p_1 \cdot p_2)(p_2 \cdot p_3) - 4096(k_1 \cdot p_4)(k_2 \cdot p_3)(p_1 \cdot p_2)(p_2 \cdot p_3)$$

$$- 4096(k_1 \cdot p_4)(k_2 \cdot p_2)(p_1 \cdot p_3)(p_2 \cdot p_3) + 4096(k_1 \cdot p_4)(k_2 \cdot p_3)(p_1 \cdot p_3)(p_2 \cdot p_3)$$

$$+ 4096(k_1 \cdot p_4)(k_2 \cdot p_1)(p_2 \cdot p_3)^2 \Big]$$

$$(4.60)$$

$$W^{12}_{ee \to e\mu} = \frac{e^4 G_F^2}{16 \left(q^2 - q_s^2\right)^2 \left(p_1 + p_2 - p_3\right)^2 \left[\left(p_3 + p_4 - p_1\right)^2 - m_\mu^2\right]} \times$$

$$\Big[4096(k_1 \cdot p_3)(k_2 \cdot p_4)(p_1 \cdot p_2)(p_1 \cdot p_3) + 4096(k_1 \cdot p_4)(k_2 \cdot p_4)(p_1 \cdot p_2)(p_1 \cdot p_3)$$

$$+ 4096(k_1 \cdot p_3)(k_2 \cdot p_2)(p_1 \cdot p_2)(p_1 \cdot p_4) - 8192(k_1 \cdot p_3)(k_2 \cdot p_3)(p_1 \cdot p_2)(p_1 \cdot p_4)$$

$$- 4096(k_1 \cdot p_4)(k_2 \cdot p_3)(p_1 \cdot p_2)(p_1 \cdot p_4) - 4096(k_1 \cdot p_2)(k_2 \cdot p_2)(p_1 \cdot p_3)(p_1 \cdot p_4)$$

$$+ 4096(k_1 \cdot p_2)(k_2 \cdot p_3)(p_1 \cdot p_3)(p_1 \cdot p_4) + 4096(k_1 \cdot p_1)(k_2 \cdot p_4)(p_1 \cdot p_3)(p_2 \cdot p_3)$$

$$- 4096(k_1 \cdot p_4)(k_2 \cdot p_4)(p_1 \cdot p_3)(p_2 \cdot p_3) + 8192(k_1 \cdot p_3)(k_2 \cdot p_1)(p_1 \cdot p_4)(p_2 \cdot p_3)$$

$$+ 4096(k_1 \cdot p_4)(k_2 \cdot p_1)(p_1 \cdot p_4)(p_2 \cdot p_3) + 4096(k_1 \cdot p_3)(k_2 \cdot p_2)(p_1 \cdot p_4)(p_2 \cdot p_3)$$

$$+ 8192(k_1 \cdot p_4)(k_2 \cdot p_2)(p_1 \cdot p_4)(p_2 \cdot p_3) - 4096(k_1 \cdot k_2)(p_1 \cdot p_3)(p_1 \cdot p_4)(p_2 \cdot p_3)$$

$$- 4096(k_1 \cdot p_3)(k_2 \cdot p_1)(p_1 \cdot p_3)(p_2 \cdot p_4) - 4096(k_1 \cdot p_4)(k_2 \cdot p_1)(p_1 \cdot p_3)(p_2 \cdot p_4)$$

$$+ 4096(k_1 \cdot p_1)(k_2 \cdot p_2)(p_1 \cdot p_3)(p_2 \cdot p_4) - 4096(k_1 \cdot p_3)(k_2 \cdot p_2)(p_1 \cdot p_3)(p_2 \cdot p_4)$$

$$- 8192(k_1 \cdot p_4)(k_2 \cdot p_2)(p_1 \cdot p_3)(p_2 \cdot p_4) - 4096(k_1 \cdot p_1)(k_2 \cdot p_3)(p_1 \cdot p_3)(p_2 \cdot p_4)$$

$$+ 4096(k_1 \cdot p_4)(k_2 \cdot p_3)(p_1 \cdot p_3)(p_2 \cdot p_4) - 4096(k_1 \cdot p_1)(k_2 \cdot p_2)(p_1 \cdot p_2)(p_3 \cdot p_4)$$

$$+ 8192(k_1 \cdot p_4)(k_2 \cdot p_2)(p_1 \cdot p_2)(p_3 \cdot p_4) + 8192(k_1 \cdot p_1)(k_2 \cdot p_3)(p_1 \cdot p_2)(p_3 \cdot p_4)$$

$$- 4096(k_1 \cdot p_4)(k_2 \cdot p_3)(p_1 \cdot p_2)(p_3 \cdot p_4) + 4096(k_1 \cdot p_2)(k_2 \cdot p_1)(p_1 \cdot p_3)(p_3 \cdot p_4)$$

$$+ 4096(k_1 \cdot p_2)(k_2 \cdot p_2)(p_1 \cdot p_3)(p_3 \cdot p_4) - 4096(k_1 \cdot k_2)(p_1 \cdot p_2)(p_1 \cdot p_3)(p_3 \cdot p_4)$$

$$- 8192(k_1 \cdot p_1)(k_2 \cdot p_1)(p_2 \cdot p_3)(p_3 \cdot p_4) + 4096(k_1 \cdot p_4)(k_2 \cdot p_1)(p_2 \cdot p_3)(p_3 \cdot p_4)$$

$$- 4096(k_1 \cdot p_1)(k_2 \cdot p_2)(p_2 \cdot p_3)(p_3 \cdot p_4) \Big] \tag{4.61}$$

$$W^{13}_{ee \to e\mu} = -\frac{e^4 G_F^2}{16 \left(q^2 - q_s^2\right)\left(w^2 - q_s^2\right)\left(p_1 + p_2 - p_3\right)^4} \times$$

$$\left[8192(k_1 \cdot p_4)(k_2 \cdot p_3)(p_1 \cdot p_2)^2 - 8192(k_1 \cdot p_4)(k_2 \cdot p_1)(p_1 \cdot p_2)(p_1 \cdot p_3)\right.$$

$$-8192(k_1 \cdot p_4)(k_2 \cdot p_2)(p_1 \cdot p_2)(p_1 \cdot p_3) - 8192(k_1 \cdot p_4)(k_2 \cdot p_1)(p_1 \cdot p_2)(p_2 \cdot p_3)$$

$$\left.-8192(k_1 \cdot p_4)(k_2 \cdot p_2)(p_1 \cdot p_2)(p_2 \cdot p_3)\right] \tag{4.62}$$

$$W^{14}_{ee \to e\mu} = -\frac{e^4 G_F^2}{16 \left(q^2 - q_s^2\right)\left(w^2 - q_s^2\right)\left(p_1 + p_2 - p_3\right)^2 \left[(p_3 + p_4 - p_2)^2 - m_\mu^2\right]} \times$$

$$\left[-4096(k_1 \cdot p_3)(k_1 \cdot p_4)(p_1 \cdot p_2)(p_2 \cdot p_3) - 4096(k_1 \cdot p_4)(k_1 \cdot p_4)(p_1 \cdot p_2)(p_2 \cdot p_3)\right.$$

$$+4096(k_1 \cdot p_3)(k_1 \cdot p_1)(p_1 \cdot p_4)(p_2 \cdot p_3) + 4096(k_1 \cdot p_4)(k_1 \cdot p_1)(p_1 \cdot p_4)(p_2 \cdot p_3)$$

$$+4096(k_1 \cdot p_3)(k_1 \cdot p_2)(p_1 \cdot p_4)(p_2 \cdot p_3) + 4096(k_1 \cdot p_4)(k_1 \cdot p_2)(p_1 \cdot p_4)(p_2 \cdot p_3)$$

$$+4096(k_1 \cdot p_3)(k_1 \cdot p_3)(p_1 \cdot p_2)(p_2 \cdot p_4) + 4096(k_1 \cdot p_4)(k_1 \cdot p_3)(p_1 \cdot p_2)(p_2 \cdot p_4)$$

$$-4096(k_1 \cdot p_3)(k_1 \cdot p_1)(p_1 \cdot p_3)(p_2 \cdot p_4) - 4096(k_1 \cdot p_4)(k_1 \cdot p_1)(p_1 \cdot p_3)(p_2 \cdot p_4)$$

$$-4096(k_1 \cdot p_3)(k_1 \cdot p_2)(p_1 \cdot p_3)(p_2 \cdot p_4) - 4096(k_1 \cdot p_4)(k_1 \cdot p_2)(p_1 \cdot p_3)(p_2 \cdot p_4)$$

$$-4096(k_1 \cdot p_4)(k_1 \cdot p_1)(p_1 \cdot p_2)(p_3 \cdot p_4) - 4096(k_1 \cdot p_2)(k_1 \cdot p_3)(p_1 \cdot p_2)(p_3 \cdot p_4)$$

$$+4096(k_1 \cdot p_2)(k_1 \cdot p_1)(p_1 \cdot p_3)(p_3 \cdot p_4) + 4096(k_1 \cdot p_2)(k_1 \cdot p_2)(p_1 \cdot p_3)(p_3 \cdot p_4)$$

$$-4096(k_1 \cdot p_1)(k_1 \cdot p_1)(p_2 \cdot p_3)(p_3 \cdot p_4) - 4096(k_1 \cdot p_1)(k_1 \cdot p_2)(p_2 \cdot p_3)(p_3 \cdot p_4)$$

$$\left.+4096(k_1 \cdot k_2)(p_1 \cdot p_2)(p_2 \cdot p_3)(p_3 \cdot p_4)\right.$$

$$\tag{4.63}$$

$$W_{ee\to e\mu}^{22} = \frac{e^4 G_F^2}{16\,(q^2-q_s^2)^2\left[(p_3+p_4-p_1)^2 - m_\mu^2\right]^2} \times$$

$$\Big[4096(k_1\cdot p_1)(k_2\cdot p_2)(p_1\cdot p_3)(p_1\cdot p_4) - 4096(k_1\cdot p_4)(k_2\cdot p_2)(p_1\cdot p_3)(p_1\cdot p_4)$$

$$+4096(k_1\cdot p_3)(k_2\cdot p_2)(p_1\cdot p_4)^2 + 4096(k_1\cdot p_3)(k_2\cdot p_2)(p_1\cdot p_3)(p_3\cdot p_4)$$

$$+4096(k_1\cdot p_4)(k_2\cdot p_2)(p_1\cdot p_3)(p_3\cdot p_4) - 4096(k_1\cdot p_1)(k_2\cdot p_2)(p_1\cdot p_4)(p_3\cdot p_4)$$

$$+4096(k_1\cdot p_3)(k_2\cdot p_2)(p_1\cdot p_4)(p_3\cdot p_4) + 8192(k_1\cdot p_4)(k_2\cdot p_2)(p_1\cdot p_4)(p_3\cdot p_4)$$

$$-4096(k_1\cdot p_1)(k_2\cdot p_2)(p_3\cdot p_4)^2 + 4096(k_1\cdot p_1)(k_2\cdot p_2)(p_1\cdot p_3)m_\mu^2$$

$$-4096(k_1\cdot p_3)(k_2\cdot p_2)(p_1\cdot p_3)m_\mu^2 - 4096(k_1\cdot p_4)(k_2\cdot p_2)(p_1\cdot p_3)m_\mu^2\Big] \quad (4.64)$$

$$W_{ee\to e\mu}^{23} = -\frac{e^4 G_F^2}{16\,(q^2-q_s^2)\,(w^2-q_s^2)\left[(p_3+p_4-p_1)^2 - m_\mu^2\right](p_1+p_2-p_3)^2} \times$$

$$\Big[-4096\,(k_1\cdot p_3)\,(k_2\cdot p_4)\,(p_1\cdot p_2)\,(p_1\cdot p_3) - 4096\,(k_1\cdot p_4)\,(k_2\cdot p_4)\,(p_1\cdot p_2)\,(p_1\cdot p_3)$$

$$+4096\,(k_1\cdot p_3)\,(k_2\cdot p_3)\,(p_1\cdot p_2)\,(p_1\cdot p_4) + 4096\,(k_1\cdot p_4)\,(k_2\cdot p_3)\,(p_1\cdot p_2)\,(p_1\cdot p_4)$$

$$-4096\,(k_1\cdot p_3)\,(k_2\cdot p_1)\,(p_1\cdot p_4)\,(p_2\cdot p_3) - 4096\,(k_1\cdot p_4)\,(k_2\cdot p_1)\,(p_1\cdot p_4)\,(p_2\cdot p_3)$$

$$-4096\,(k_1\cdot p_3)\,(k_2\cdot p_2)\,(p_1\cdot p_4)\,(p_2\cdot p_3) - 4096\,(k_1\cdot p_4)\,(k_2\cdot p_2)\,(p_1\cdot p_4)\,(p_2\cdot p_3)$$

$$+4096\,(k_1\cdot p_3)\,(k_2\cdot p_1)\,(p_1\cdot p_3)\,(p_2\cdot p_4) + 4096\,(k_1\cdot p_4)\,(k_2\cdot p_1)\,(p_1\cdot p_3)\,(p_2\cdot p_4)$$

$$+4096\,(k_1\cdot p_3)\,(k_2\cdot p_2)\,(p_1\cdot p_3)\,(p_2\cdot p_4) + 4096\,(k_1\cdot p_4)\,(k_2\cdot p_2)\,(p_1\cdot p_3)\,(p_2\cdot p_4)$$

$$-4096\,(k_1\cdot p_4)\,(k_2\cdot p_2)\,(p_1\cdot p_2)\,(p_3\cdot p_4) - 4096\,(k_1\cdot p_1)\,(k_2\cdot p_3)\,(p_1\cdot p_2)\,(p_3\cdot p_4)$$

$$-4096\,(k_1\cdot p_2)\,(k_2\cdot p_1)\,(p_1\cdot p_3)\,(p_3\cdot p_4) - 4096\,(k_1\cdot p_2)\,(k_2\cdot p_2)\,(p_1\cdot p_3)\,(p_3\cdot p_4)$$

$$+4096\,(k_1\cdot k_2)\,(p_1\cdot p_2)\,(p_1\cdot p_3)\,(p_3\cdot p_4) + 4096\,(k_1\cdot p_1)\,(k_2\cdot p_1)\,(p_2\cdot p_3)\,(p_3\cdot p_4)$$

$$+4096\,(k_1\cdot p_1)\,(k_2\cdot p_2)\,(p_2\cdot p_3)\,(p_3\cdot p_4)\Big] \quad (4.65)$$

$$
\begin{aligned}
W^{24}_{ee \to e\mu} = &-\frac{e^4 G_F^2}{16 \left(q^2 - q_s^2\right)\left(w^2 - q_s^2\right)\left[(p_3 + p_4 - p_1)^2 - m_\mu^2\right]\left[(p_3 + p_4 - p_2)^2 - m_\mu^2\right]} \times \\
&\Big[-4096\,(k_1 \cdot p_3)(k_2 \cdot p_3)(p_1 \cdot p_2)(p_3 \cdot p_4) - 4096\,(k_1 \cdot p_4)(k_2 \cdot p_3)(p_1 \cdot p_2)(p_3 \cdot p_4) \\
&- 4096\,(k_1 \cdot p_3)(k_2 \cdot p_4)(p_1 \cdot p_2)(p_3 \cdot p_4) - 4096\,(k_1 \cdot p_4)(k_2 \cdot p_4)(p_1 \cdot p_2)(p_3 \cdot p_4) \\
&+ 4096\,(k_1 \cdot p_3)(k_2 \cdot p_2)(p_1 \cdot p_3)(p_3 \cdot p_4) + 4096\,(k_1 \cdot p_4)(k_2 \cdot p_2)(p_1 \cdot p_3)(p_3 \cdot p_4) \\
&+ 4096\,(k_1 \cdot p_3)(k_2 \cdot p_2)(p_1 \cdot p_4)(p_3 \cdot p_4) + 4096\,(k_1 \cdot p_4)(k_2 \cdot p_2)(p_1 \cdot p_4)(p_3 \cdot p_4) \\
&+ 4096\,(k_1 \cdot p_3)(k_2 \cdot p_1)(p_2 \cdot p_3)(p_3 \cdot p_4) + 4096\,(k_1 \cdot p_4)(k_2 \cdot p_1)(p_2 \cdot p_3)(p_3 \cdot p_4) \\
&+ 4096\,(k_1 \cdot p_3)(k_2 \cdot p_1)(p_2 \cdot p_4)(p_3 \cdot p_4) + 4096\,(k_1 \cdot p_4)(k_2 \cdot p_1)(p_2 \cdot p_4)(p_3 \cdot p_4) \\
&- 4096\,(k_1 \cdot p_2)(k_2 \cdot p_1)(p_3 \cdot p_4)^2 - 4096\,(k_1 \cdot p_1)(k_2 \cdot p_2)(p_3 \cdot p_4)^2 \\
&+ 4096\,(k_1 \cdot k_2)(p_1 \cdot p_2)(p_3 \cdot p_4)^2 + 4096\,(k_1 \cdot p_3)(k_2 \cdot p_3)(p_1 \cdot p_2)m_\mu^2 \\
&+ 2048\,(k_1 \cdot p_4)(k_2 \cdot p_3)(p_1 \cdot p_2)m_\mu^2 - 4096\,(k_1 \cdot p_3)(k_2 \cdot p_2)(p_1 \cdot p_3)m_\mu^2 \\
&- 2048\,(k_1 \cdot p_4)(k_2 \cdot p_2)(p_1 \cdot p_3)m_\mu^2 - 4096\,(k_1 \cdot p_3)(k_2 \cdot p_1)(p_2 \cdot p_3)m_\mu^2 \\
&- 2048\,(k_1 \cdot p_4)(k_2 \cdot p_1)(p_2 \cdot p_3)m_\mu^2 \Big] \tag{4.66}
\end{aligned}
$$

$$
\begin{aligned}
W^{33}_{ee \to e\mu} = &\ \frac{e^4 G_F^2}{16 \left(w^2 - q_s^2\right)^2 \left(p_1 + p_2 - p_3\right)^4} \times \\
&\Big[-4096\,(k_1 \cdot p_4)\,(k_2 \cdot p_3)\,(p_1 \cdot p_2)^2 + 8192\,(k_1 \cdot p_4)\,(k_2 \cdot p_1)\,(p_1 \cdot p_2)\,(p_1 \cdot p_3) \\
&+ 4096\,(k_1 \cdot p_4)\,(k_2 \cdot p_2)\,(p_1 \cdot p_2)\,(p_1 \cdot p_3) - 4096\,(k_1 \cdot p_4)\,(k_2 \cdot p_3)\,(p_1 \cdot p_2)\,(p_1 \cdot p_3) \\
&+ 4096\,(k_1 \cdot p_4)\,(k_2 \cdot p_2)\,(p_1 \cdot p_3)^2 + 4096\,(k_1 \cdot p_4)\,(k_2 \cdot p_1)\,(p_1 \cdot p_2)\,(p_2 \cdot p_3) \\
&+ 4096\,(k_1 \cdot p_4)\,(k_2 \cdot p_2)\,(p_1 \cdot p_2)\,(p_2 \cdot p_3) - 4096\,(k_1 \cdot p_4)\,(k_2 \cdot p_1)\,(p_1 \cdot p_3)\,(p_2 \cdot p_3) \\
&+ 4096\,(k_1 \cdot p_4)\,(k_2 \cdot p_3)\,(p_1 \cdot p_3)\,(p_2 \cdot p_3) \Big] \tag{4.67}
\end{aligned}
$$

$$W_{ee \to e\mu}^{34} = \frac{e^4 G_F^2}{16 \left(w^2 - q_s^2\right)^2 (p_1 + p_2 - p_3)^2 \left[(p_3 + p_4 - p_2)^2 - m_\mu^2\right]} \times$$

$$\begin{aligned}
\Big[&4096 \, (k_1 \cdot p_3)(k_2 \cdot p_4)(p_1 \cdot p_2)(p_2 \cdot p_3) + 4096 \, (k_1 \cdot p_4)(k_2 \cdot p_4)(p_1 \cdot p_2)(p_2 \cdot p_3) \\[4pt]
&+ 4096 \, (k_1 \cdot p_2)(k_2 \cdot p_4)(p_1 \cdot p_3)(p_2 \cdot p_3) - 4096 \, (k_1 \cdot p_4)(k_2 \cdot p_4)(p_1 \cdot p_3)(p_2 \cdot p_3) \\[4pt]
&+ 4096 \, (k_1 \cdot p_2)(k_2 \cdot p_1)(p_1 \cdot p_4)(p_2 \cdot p_3) - 4096 \, (k_1 \cdot p_3)(k_2 \cdot p_1)(p_1 \cdot p_4)(p_2 \cdot p_3) \\[4pt]
&- 8192 \, (k_1 \cdot p_4)(k_2 \cdot p_1)(p_1 \cdot p_4)(p_2 \cdot p_3) - 4096 \, (k_1 \cdot p_3)(k_2 \cdot p_2)(p_1 \cdot p_4)(p_2 \cdot p_3) \\[4pt]
&- 4096 \, (k_1 \cdot p_4)(k_2 \cdot p_2)(p_1 \cdot p_4)(p_2 \cdot p_3) - 4096 \, (k_1 \cdot p_2)(k_2 \cdot p_3)(p_1 \cdot p_4)(p_2 \cdot p_3) \\[4pt]
&+ 4096 \, (k_1 \cdot p_4)(k_2 \cdot p_3)(p_1 \cdot p_4)(p_2 \cdot p_3) + 4096 \, (k_1 \cdot p_3)(k_2 \cdot p_1)(p_1 \cdot p_2)(p_2 \cdot p_4) \\[4pt]
&- 8192 \, (k_1 \cdot p_3)(k_2 \cdot p_3)(p_1 \cdot p_2)(p_2 \cdot p_4) - 4096 \, (k_1 \cdot p_4)(k_2 \cdot p_3)(p_1 \cdot p_2)(p_2 \cdot p_4) \\[4pt]
&+ 4096 \, (k_1 \cdot p_3)(k_2 \cdot p_1)(p_1 \cdot p_3)(p_2 \cdot p_4) + 8192 \, (k_1 \cdot p_4)(k_2 \cdot p_1)(p_1 \cdot p_3)(p_2 \cdot p_4) \\[4pt]
&+ 8192 \, (k_1 \cdot p_3)(k_2 \cdot p_2)(p_1 \cdot p_3)(p_2 \cdot p_4) + 4096 \, (k_1 \cdot p_4)(k_2 \cdot p_2)(p_1 \cdot p_3)(p_2 \cdot p_4) \\[4pt]
&- 4096 \, (k_1 \cdot p_1)(k_2 \cdot p_1)(p_2 \cdot p_3)(p_2 \cdot p_4) + 4096 \, (k_1 \cdot p_1)(k_2 \cdot p_3)(p_2 \cdot p_3)(p_2 \cdot p_4) \\[4pt]
&- 4096 \, (k_1 \cdot k_2)(p_1 \cdot p_3)(p_2 \cdot p_3)(p_2 \cdot p_4) - 4096 \, (k_1 \cdot p_2)(k_2 \cdot p_1)(p_1 \cdot p_2)(p_3 \cdot p_4) \\[4pt]
&+ 8192 \, (k_1 \cdot p_4)(k_2 \cdot p_1)(p_1 \cdot p_2)(p_3 \cdot p_4) + 8192 \, (k_1 \cdot p_2)(k_2 \cdot p_3)(p_1 \cdot p_2)(p_3 \cdot p_4) \\[4pt]
&- 4096 \, (k_1 \cdot p_4)(k_2 \cdot p_3)(p_1 \cdot p_2)(p_3 \cdot p_4) - 4096 \, (k_1 \cdot p_2)(k_2 \cdot p_1)(p_1 \cdot p_3)(p_3 \cdot p_4) \\[4pt]
&- 8192 \, (k_1 \cdot p_2)(k_2 \cdot p_2)(p_1 \cdot p_3)(p_3 \cdot p_4) + 4096 \, (k_1 \cdot p_4)(k_2 \cdot p_2)(p_1 \cdot p_3)(p_3 \cdot p_4) \\[4pt]
&+ 4096 \, (k_1 \cdot p_1)(k_2 \cdot p_1)(p_2 \cdot p_3)(p_3 \cdot p_4) + 4096 \, (k_1 \cdot p_1)(k_2 \cdot p_2)(p_2 \cdot p_3)(p_3 \cdot p_4) \\[4pt]
&- 4096 \, (k_1 \cdot k_2)(p_1 \cdot p_2)(p_2 \cdot p_3)(p_3 \cdot p_4) \Big]
\end{aligned}$$

$$\tag{4.68}$$

$$W^{44}_{ee\to e\mu} = \frac{e^4 G_F^2}{16\,(w^2-q_s^2)^2 \left[(p_3+p_4-p_1)^2 - m_\mu^2\right]^2} \times$$

$$\Big[4096\,(k_1\cdot p_2)\,(k_2\cdot p_1)\,(p_2\cdot p_3)\,(p_2\cdot p_4) - 4096\,(k_1\cdot p_4)\,(k_2\cdot p_1)\,(p_2\cdot p_3)\,(p_2\cdot p_4)$$

$$+4096\,(k_1\cdot p_3)\,(k_2\cdot p_1)\,(p_2\cdot p_4)^2 + 4096\,(k_1\cdot p_3)\,(k_2\cdot p_1)\,(p_2\cdot p_3)\,(p_3\cdot p_4)$$

$$+4096\,(k_1\cdot p_4)\,(k_2\cdot p_1)\,(p_2\cdot p_3)\,(p_3\cdot p_4) - 4096\,(k_1\cdot p_2)\,(k_2\cdot p_1)\,(p_2\cdot p_4)\,(p_3\cdot p_4)$$

$$+4096\,(k_1\cdot p_3)\,(k_2\cdot p_1)\,(p_2\cdot p_4)\,(p_3\cdot p_4) + 8192\,(k_1\cdot p_4)\,(k_2\cdot p_1)\,(p_2\cdot p_4)\,(p_3\cdot p_4)$$

$$-4096\,(k_1\cdot p_2)\,(k_2\cdot p_1)\,(p_3\cdot p_4)^2 + 4096\,(k_1\cdot p_2)\,(k_2\cdot p_1)\,(p_2\cdot p_3)\,m_\mu^2$$

$$-4096\,(k_1\cdot p_3)\,(k_2\cdot p_1)\,(p_2\cdot p_3)\,m_\mu^2 - 4096\,(k_1\cdot p_4)\,(k_2\cdot p_1)\,(p_2\cdot p_3)\,m_\mu^2 \Big] \quad (4.69)$$

$$W^{11}_{e\mu\to\mu\mu} = \frac{e^4 G_F^2}{16\,(q^2-q_s^2)^2\,(p_1+p_2-p_3)^4} \times$$

$$\Big[-4096\,(k_1\cdot p_4)\,(k_2\cdot p_3)\,(p_1\cdot p_2)^2 + 4096\,(k_1\cdot p_4)\,(k_2\cdot p_1)\,(p_1\cdot p_2)\,(p_1\cdot p_3)$$

$$+4096\,(k_1\cdot p_4)\,(k_2\cdot p_2)\,(p_1\cdot p_2)\,(p_1\cdot p_3) + 4096\,(k_1\cdot p_4)\,(k_2\cdot p_1)\,(p_1\cdot p_2)\,(p_2\cdot p_3)$$

$$+8192\,(k_1\cdot p_4)\,(k_2\cdot p_2)\,(p_1\cdot p_2)\,(p_2\cdot p_3) - 4096\,(k_1\cdot p_4)\,(k_2\cdot p_3)\,(p_1\cdot p_2)\,(p_2\cdot p_3)$$

$$-4096\,(k_1\cdot p_4)\,(k_2\cdot p_2)\,(p_1\cdot p_3)\,(p_2\cdot p_3) + 4096\,(k_1\cdot p_4)\,(k_2\cdot p_3)\,(p_1\cdot p_3)\,(p_2\cdot p_3)$$

$$+4096\,(k_1\cdot p_4)\,(k_2\cdot p_1)\,(p_2\cdot p_3)^2 - 8192\,(k_1\cdot p_4)\,(k_2\cdot p_1)\,(p_1\cdot p_2)\,m_\mu^2$$

$$-4096\,(k_1\cdot p_4)\,(k_2\cdot p_2)\,(p_1\cdot p_2)\,m_\mu^2 + 4096\,(k_1\cdot p_4)\,(k_2\cdot p_3)\,(p_1\cdot p_2)\,m_\mu^2$$

$$-4096\,(k_1\cdot p_4)\,(k_2\cdot p_2)\,(p_1\cdot p_3)\,m_\mu^2 + 4096\,(k_1\cdot p_4)\,(k_2\cdot p_1)\,(p_2\cdot p_3)\,m_\mu^2$$

$$+4096\,(k_1\cdot p_4)\,(k_2\cdot p_2)\,(p_2\cdot p_3)\,m_\mu^2 - 8192\,(k_1\cdot p_4)\,(k_2\cdot p_3)\,(p_2\cdot p_3)\,m_\mu^2$$

$$+4096\,(k_1\cdot p_4)\,(k_2\cdot p_2)\,m_\mu^4 \Big] \quad (4.70)$$

$$W^{12}_{e\mu\to\mu\mu} = \frac{e^4 G_F^2}{16\,(q^2-q_s^2)^2\,(p_1+p_2-p_3)^2\,\left[(p_3+p_4-p_1)^2 - m_\mu^2\right]} \times$$

$$\Big[4096\,(k_1\cdot p_3)\,(k_2\cdot p_4)\,(p_1\cdot p_2)\,(p_1\cdot p_3)+4096\,(k_1\cdot p_4)\,(k_2\cdot p_4)\,(p_1\cdot p_2)\,(p_1\cdot p_3)$$

$$+4096\,(k_1\cdot p_3)\,(k_2\cdot p_2)\,(p_1\cdot p_2)\,(p_1\cdot p_4)-8192\,(k_1\cdot p_3)\,(k_2\cdot p_3)\,(p_1\cdot p_2)\,(p_1\cdot p_4)$$

$$-4096\,(k_1\cdot p_4)\,(k_2\cdot p_3)\,(p_1\cdot p_2)\,(p_1\cdot p_4)-4096\,(k_1\cdot p_2)\,(k_2\cdot p_2)\,(p_1\cdot p_3)\,(p_1\cdot p_4)$$

$$+4096\,(k_1\cdot p_2)\,(k_2\cdot p_3)\,(p_1\cdot p_3)\,(p_1\cdot p_4)+4096\,(k_1\cdot p_1)\,(k_2\cdot p_4)\,(p_1\cdot p_3)\,(p_2\cdot p_3)$$

$$-4096\,(k_1\cdot p_4)\,(k_2\cdot p_4)\,(p_1\cdot p_3)\,(p_2\cdot p_3)+8192\,(k_1\cdot p_3)\,(k_2\cdot p_1)\,(p_1\cdot p_4)\,(p_2\cdot p_3)$$

$$+4096\,(k_1\cdot p_4)\,(k_2\cdot p_1)\,(p_1\cdot p_4)\,(p_2\cdot p_3)+4096\,(k_1\cdot p_3)\,(k_2\cdot p_2)\,(p_1\cdot p_4)\,(p_2\cdot p_3)$$

$$+8192\,(k_1\cdot p_4)\,(k_2\cdot p_2)\,(p_1\cdot p_4)\,(p_2\cdot p_3)-4096\,(k_1\cdot k_2)\,(p_1\cdot p_3)\,(p_1\cdot p_4)\,(p_2\cdot p_3)$$

$$-4096\,(k_1\cdot p_3)\,(k_2\cdot p_1)\,(p_1\cdot p_3)\,(p_2\cdot p_4)-4096\,(k_1\cdot p_4)\,(k_2\cdot p_1)\,(p_1\cdot p_3)\,(p_2\cdot p_4)$$

$$+4096\,(k_1\cdot p_1)\,(k_2\cdot p_2)\,(p_1\cdot p_3)\,(p_2\cdot p_4)-4096\,(k_1\cdot p_3)\,(k_2\cdot p_2)\,(p_1\cdot p_3)\,(p_2\cdot p_4)$$

$$-8192\,(k_1\cdot p_4)\,(k_2\cdot p_2)\,(p_1\cdot p_3)\,(p_2\cdot p_4)-4096\,(k_1\cdot p_1)\,(k_2\cdot p_3)\,(p_1\cdot p_3)\,(p_2\cdot p_4)$$

$$+4096\,(k_1\cdot p_4)\,(k_2\cdot p_3)\,(p_1\cdot p_3)\,(p_2\cdot p_4)-4096\,(k_1\cdot p_1)\,(k_2\cdot p_2)\,(p_1\cdot p_2)\,(p_3\cdot p_4)$$

$$+8192\,(k_1\cdot p_4)\,(k_2\cdot p_2)\,(p_1\cdot p_2)\,(p_3\cdot p_4)+8192\,(k_1\cdot p_1)\,(k_2\cdot p_3)\,(p_1\cdot p_2)\,(p_3\cdot p_4)$$

$$-4096\,(k_1\cdot p_4)\,(k_2\cdot p_3)\,(p_1\cdot p_2)\,(p_3\cdot p_4)+4096\,(k_1\cdot p_2)\,(k_2\cdot p_1)\,(p_1\cdot p_3)\,(p_3\cdot p_4)$$

$$+4096\,(k_1\cdot p_2)\,(k_2\cdot p_2)\,(p_1\cdot p_3)\,(p_3\cdot p_4)-4096\,(k_1\cdot k_2)\,(p_1\cdot p_2)\,(p_1\cdot p_3)\,(p_3\cdot p_4)$$

$$-8192\,(k_1\cdot p_1)\,(k_2\cdot p_1)\,(p_2\cdot p_3)\,(p_3\cdot p_4)+4096\,(k_1\cdot p_4)\,(k_2\cdot p_1)\,(p_2\cdot p_3)\,(p_3\cdot p_4)$$

$$-4096\,(k_1\cdot p_1)\,(k_2\cdot p_2)\,(p_2\cdot p_3)\,(p_3\cdot p_4)-4096\,(k_1\cdot p_3)\,(k_2\cdot p_2)\,(p_1\cdot p_2)\,m_\mu^2$$

$$+2048\,(k_1\cdot p_1)\,(k_2\cdot p_3)\,(p_1\cdot p_2)\,m_\mu^2+2048\,(k_1\cdot p_3)\,(k_2\cdot p_3)\,(p_1\cdot p_2)\,m_\mu^2$$

$$-4096\,(k_1\cdot p_1)\,(k_2\cdot p_4)\,(p_1\cdot p_2)\,m_\mu^2-4096\,(k_1\cdot p_4)\,(k_2\cdot p_4)\,(p_1\cdot p_2)\,m_\mu^2$$

$$+2048\,(k_1\cdot p_2)\,(k_2\cdot p_1)\,(p_1\cdot p_3)\,m_\mu^2+4096\,(k_1\cdot p_2)\,(k_2\cdot p_2)\,(p_1\cdot p_3)\,m_\mu^2$$

$$-2048\,(k_1\cdot p_2)\,(k_2\cdot p_3)\,(p_1\cdot p_3)\,m_\mu^2-8192\,(k_1\cdot p_2)\,(k_2\cdot p_4)\,(p_1\cdot p_3)\,m_\mu^2$$

$$-2048\,(k_1 \cdot k_2)\,(p_1 \cdot p_2)\,(p_1 \cdot p_3)\,m_\mu^2 - 4096\,(k_1 \cdot p_2)\,(k_2 \cdot p_1)\,(p_1 \cdot p_4)\,m_\mu^2$$

$$+4096\,(k_1 \cdot p_2)\,(k_2 \cdot p_2)\,(p_1 \cdot p_4)\,m_\mu^2 + 4096\,(k_1 \cdot k_2)\,(p_1 \cdot p_2)\,(p_1 \cdot p_4)\,m_\mu^2$$

$$-2048\,(k_1 \cdot p_1)\,(k_2 \cdot p_1)\,(p_2 \cdot p_3)\,m_\mu^2 - 2048\,(k_1 \cdot p_3)\,(k_2 \cdot p_1)\,(p_2 \cdot p_3)\,m_\mu^2$$

$$-4096\,(k_1 \cdot p_1)\,(k_2 \cdot p_2)\,(p_2 \cdot p_3)\,m_\mu^2 - 4096\,(k_1 \cdot p_3)\,(k_2 \cdot p_4)\,(p_2 \cdot p_3)\,m_\mu^2$$

$$+4096\,(k_1 \cdot p_4)\,(k_2 \cdot p_4)\,(p_2 \cdot p_3)\,m_\mu^2 + 2048\,(k_1 \cdot k_2)\,(p_1 \cdot p_3)\,(p_2 \cdot p_3)\,m_\mu^2$$

$$+4096\,(k_1 \cdot p_1)\,(k_2 \cdot p_1)\,(p_2 \cdot p_4)\,m_\mu^2 + 4096\,(k_1 \cdot p_4)\,(k_2 \cdot p_1)\,(p_2 \cdot p_4)\,m_\mu^2$$

$$-4096\,(k_1 \cdot p_1)\,(k_2 \cdot p_2)\,(p_2 \cdot p_4)\,m_\mu^2 + 4096\,(k_1 \cdot p_3)\,(k_2 \cdot p_2)\,(p_2 \cdot p_4)\,m_\mu^2$$

$$+8192\,(k_1 \cdot p_4)\,(k_2 \cdot p_2)\,(p_2 \cdot p_4)\,m_\mu^2 + 4096\,(k_1 \cdot p_3)\,(k_2 \cdot p_3)\,(p_2 \cdot p_4)\,m_\mu^2$$

$$-4096\,(k_1 \cdot p_4)\,(k_2 \cdot p_3)\,(p_2 \cdot p_4)\,m_\mu^2 + 8192\,(k_1 \cdot k_2)\,(p_1 \cdot p_3)\,(p_2 \cdot p_4)\,m_\mu^2$$

$$-4096\,(k_1 \cdot p_2)\,(k_2 \cdot p_2)\,(p_3 \cdot p_4)\,m_\mu^2 - 4096\,(k_1 \cdot p_2)\,(k_2 \cdot p_3)\,(p_3 \cdot p_4)\,m_\mu^2$$

$$+4096\,(k_1 \cdot k_2)\,(p_2 \cdot p_3)\,(p_3 \cdot p_4)\,m_\mu^2 - 2048\,(k_1 \cdot p_2)\,(k_2 \cdot p_1)\,m_\mu^4 - 4096\,(k_1 \cdot p_2)\,(k_2 \cdot p_2)\,m_\mu^4$$

$$+2048\,(k_1 \cdot p_2)\,(k_2 \cdot p_3)\,m_\mu^4 + 8192\,(k_1 \cdot p_2)\,(k_2 \cdot p_4)\,m_\mu^4 + 2048\,(k_1 \cdot k_2)\,(p_1 \cdot p_2)\,m_\mu^4$$

$$\left. -2048\,(k_1 \cdot k_2)\,(p_2 \cdot p_3)\,m_\mu^4 - 8192\,(k_1 \cdot k_2)\,(p_2 \cdot p_4)\,m_\mu^4 \right] \tag{4.71}$$

$$W^{13}_{e\mu\to\mu\mu} = -\frac{e^4 G_F^2}{16\,(q^2-q_s^2)\,(s^2-q_s^2)\,(p_1+p_2-p_3)^2\,(p_1+p_2-p_4)^2} \times$$

$$\Big[-4096\,(k_1\cdot p_4)\,(k_2\cdot p_3)\,(p_1\cdot p_2)^2 - 4096\,(k_1\cdot p_3)\,(k_2\cdot p_4)\,(p_1\cdot p_2)^2$$

$$+4096\,(k_1\cdot p_4)\,(k_2\cdot p_1)\,(p_1\cdot p_2)\,(p_1\cdot p_3)+4096\,(k_1\cdot p_4)\,(k_2\cdot p_2)\,(p_1\cdot p_2)\,(p_1\cdot p_3)$$

$$+4096\,(k_1\cdot p_3)\,(k_2\cdot p_1)\,(p_1\cdot p_2)\,(p_1\cdot p_4)+4096\,(k_1\cdot p_3)\,(k_2\cdot p_2)\,(p_1\cdot p_2)\,(p_1\cdot p_4)$$

$$+4096\,(k_1\cdot p_4)\,(k_2\cdot p_1)\,(p_1\cdot p_2)\,(p_2\cdot p_3)+4096\,(k_1\cdot p_4)\,(k_2\cdot p_2)\,(p_1\cdot p_2)\,(p_2\cdot p_3)$$

$$+4096\,(k_1\cdot p_3)\,(k_2\cdot p_1)\,(p_1\cdot p_2)\,(p_2\cdot p_4)+4096\,(k_1\cdot p_3)\,(k_2\cdot p_2)\,(p_1\cdot p_2)\,(p_2\cdot p_4)$$

$$-4096\,(k_1\cdot p_1)\,(k_2\cdot p_1)\,(p_1\cdot p_2)\,(p_3\cdot p_4)-4096\,(k_1\cdot p_2)\,(k_2\cdot p_1)\,(p_1\cdot p_2)\,(p_3\cdot p_4)$$

$$-4096\,(k_1\cdot p_1)\,(k_2\cdot p_2)\,(p_1\cdot p_2)\,(p_3\cdot p_4)-4096\,(k_1\cdot p_2)\,(k_2\cdot p_2)\,(p_1\cdot p_2)\,(p_3\cdot p_4)$$

$$+4096\,(k_1\cdot k_2)\,(p_1\cdot p_2)^2\,(p_3\cdot p_4)-4096\,(k_1\cdot p_3)\,(k_2\cdot p_1)\,(p_1\cdot p_2)\,m_\mu^2$$

$$-4096\,(k_1\cdot p_4)\,(k_2\cdot p_1)\,(p_1\cdot p_2)\,m_\mu^2+4096\,(k_1\cdot p_2)\,(k_2\cdot p_2)\,(p_1\cdot p_2)\,m_\mu^2$$

$$-2048\,(k_1\cdot p_3)\,(k_2\cdot p_2)\,(p_1\cdot p_2)\,m_\mu^2-2048\,(k_1\cdot p_4)\,(k_2\cdot p_2)\,(p_1\cdot p_2)\,m_\mu^2$$

$$+2048\,(k_1\cdot p_1)\,(k_2\cdot p_3)\,(p_1\cdot p_2)\,m_\mu^2+2048\,(k_1\cdot p_2)\,(k_2\cdot p_3)\,(p_1\cdot p_2)\,m_\mu^2$$

$$+2048\,(k_1\cdot p_1)\,(k_2\cdot p_4)\,(p_1\cdot p_2)\,m_\mu^2+2048\,(k_1\cdot p_2)\,(k_2\cdot p_4)\,(p_1\cdot p_2)\,m_\mu^2$$

$$-2048\,(k_1\cdot p_2)\,(k_2\cdot p_1)\,(p_1\cdot p_3)\,m_\mu^2-4096\,(k_1\cdot p_2)\,(k_2\cdot p_2)\,(p_1\cdot p_3)\,m_\mu^2$$

$$-2048\,(k_1\cdot p_4)\,(k_2\cdot p_2)\,(p_1\cdot p_3)\,m_\mu^2+2048\,(k_1\cdot p_2)\,(k_2\cdot p_4)\,(p_1\cdot p_3)\,m_\mu^2$$

$$-2048\,(k_1\cdot k_2)\,(p_1\cdot p_2)\,(p_1\cdot p_3)\,m_\mu^2-2048\,(k_1\cdot p_2)\,(k_2\cdot p_1)\,(p_1\cdot p_4)\,m_\mu^2$$

$$-4096\,(k_1\cdot p_2)\,(k_2\cdot p_2)\,(p_1\cdot p_4)\,m_\mu^2-2048\,(k_1\cdot p_3)\,(k_2\cdot p_2)\,(p_1\cdot p_4)\,m_\mu^2$$

$$+2048\,(k_1\cdot p_2)\,(k_2\cdot p_3)\,(p_1\cdot p_4)\,m_\mu^2-2048\,(k_1\cdot k_2)\,(p_1\cdot p_2)\,(p_1\cdot p_4)\,m_\mu^2$$

$$+2048\,(k_1\cdot p_1)\,(k_2\cdot p_1)\,(p_2\cdot p_3)\,m_\mu^2+2048\,(k_1\cdot p_2)\,(k_2\cdot p_1)\,(p_2\cdot p_3)\,m_\mu^2$$

$$+2048\,(k_1\cdot p_1)\,(k_2\cdot p_2)\,(p_2\cdot p_3)\,m_\mu^2-2048\,(k_1\cdot p_4)\,(k_2\cdot p_2)\,(p_2\cdot p_3)\,m_\mu^2$$

$$-2048\,(k_1\cdot p_1)\,(k_2\cdot p_4)\,(p_2\cdot p_3)\,m_\mu^2-2048\,(k_1\cdot p_2)\,(k_2\cdot p_4)\,(p_2\cdot p_3)\,m_\mu^2$$

$$-4096 \left(k_1 \cdot k_2\right) \left(p_1 \cdot p_2\right) \left(p_2 \cdot p_3\right) m_\mu^2 + 2048 \left(k_1 \cdot k_2\right) \left(p_1 \cdot p_4\right) \left(p_2 \cdot p_3\right) m_\mu^2$$

$$+2048 \left(k_1 \cdot p_1\right) \left(k_2 \cdot p_1\right) \left(p_2 \cdot p_4\right) m_\mu^2 + 2048 \left(k_1 \cdot p_2\right) \left(k_2 \cdot p_1\right) \left(p_2 \cdot p_4\right) m_\mu^2$$

$$+2048 \left(k_1 \cdot p_1\right) \left(k_2 \cdot p_2\right) \left(p_2 \cdot p_4\right) m_\mu^2 - 2048 \left(k_1 \cdot p_3\right) \left(k_2 \cdot p_2\right) \left(p_2 \cdot p_4\right) m_\mu^2$$

$$-2048 \left(k_1 \cdot p_1\right) \left(k_2 \cdot p_3\right) \left(p_2 \cdot p_4\right) m_\mu^2 - 2048 \left(k_1 \cdot p_2\right) \left(k_2 \cdot p_3\right) \left(p_2 \cdot p_4\right) m_\mu^2$$

$$-4096 \left(k_1 \cdot k_2\right) \left(p_1 \cdot p_2\right) \left(p_2 \cdot p_4\right) m_\mu^2 + 2048 \left(k_1 \cdot k_2\right) \left(p_1 \cdot p_3\right) \left(p_2 \cdot p_4\right) m_\mu^2$$

$$+4096 \left(k_1 \cdot k_2\right) \left(p_2 \cdot p_3\right) \left(p_2 \cdot p_4\right) m_\mu^2 + 2048 \left(k_1 \cdot p_1\right) \left(k_2 \cdot p_2\right) \left(p_3 \cdot p_4\right) m_\mu^2$$

$$+4096 \left(k_1 \cdot p_2\right) \left(k_2 \cdot p_2\right) \left(p_3 \cdot p_4\right) m_\mu^2 + 4096 \left(k_1 \cdot p_2\right) \left(k_2 \cdot p_1\right) m_\mu^4 - 2048 \left(k_1 \cdot p_1\right) \left(k_2 \cdot p_2\right) m_\mu^4$$

$$+4096 \left(k_1 \cdot p_2\right) \left(k_2 \cdot p_2\right) m_\mu^4 + 2048 \left(k_1 \cdot p_3\right) \left(k_2 \cdot p_2\right) m_\mu^4 + 2048 \left(k_1 \cdot p_4\right) \left(k_2 \cdot p_2\right) m_\mu^4$$

$$-2048 \left(k_1 \cdot p_2\right) \left(k_2 \cdot p_3\right) m_\mu^4 - 2048 \left(k_1 \cdot p_2\right) \left(k_2 \cdot p_4\right) m_\mu^4 + 4096 \left(k_1 \cdot k_2\right) \left(p_1 \cdot p_2\right) m_\mu^4$$

$$\left. -2048 \left(k_1 \cdot k_2\right) \left(p_2 \cdot p_3\right) m_\mu^4 - 2048 \left(k_1 \cdot k_2\right) \left(p_2 \cdot p_4\right) m_\mu^4 \right] \tag{4.72}$$

$$W_{e\mu\to\mu\mu}^{14} = -\frac{e^4 G_F^2}{16\,(q^2-q_s^2)\,(s^2-q_s^2)\,(p_1+p_2-p_3)^2\left[(p_3+p_4-p_1)^2-m_\mu^2\right]} \times$$

$$\left[-4096\,(k_1\cdot p_3)\,(k_2\cdot p_4)\,(p_1\cdot p_2)\,(p_1\cdot p_3)-4096\,(k_1\cdot p_4)\,(k_2\cdot p_4)\,(p_1\cdot p_2)\,(p_1\cdot p_3)\right.$$

$$+4096\,(k_1\cdot p_3)\,(k_2\cdot p_3)\,(p_1\cdot p_2)\,(p_1\cdot p_4)+4096\,(k_1\cdot p_4)\,(k_2\cdot p_3)\,(p_1\cdot p_2)\,(p_1\cdot p_4)$$

$$-4096\,(k_1\cdot p_3)\,(k_2\cdot p_1)\,(p_1\cdot p_4)\,(p_2\cdot p_3)-4096\,(k_1\cdot p_4)\,(k_2\cdot p_1)\,(p_1\cdot p_4)\,(p_2\cdot p_3)$$

$$-4096\,(k_1\cdot p_3)\,(k_2\cdot p_2)\,(p_1\cdot p_4)\,(p_2\cdot p_3)-4096\,(k_1\cdot p_4)\,(k_2\cdot p_2)\,(p_1\cdot p_4)\,(p_2\cdot p_3)$$

$$+4096\,(k_1\cdot p_3)\,(k_2\cdot p_1)\,(p_1\cdot p_3)\,(p_2\cdot p_4)+4096\,(k_1\cdot p_4)\,(k_2\cdot p_1)\,(p_1\cdot p_3)\,(p_2\cdot p_4)$$

$$+4096\,(k_1\cdot p_3)\,(k_2\cdot p_2)\,(p_1\cdot p_3)\,(p_2\cdot p_4)+4096\,(k_1\cdot p_4)\,(k_2\cdot p_2)\,(p_1\cdot p_3)\,(p_2\cdot p_4)$$

$$-4096\,(k_1\cdot p_4)\,(k_2\cdot p_2)\,(p_1\cdot p_2)\,(p_3\cdot p_4)-4096\,(k_1\cdot p_1)\,(k_2\cdot p_3)\,(p_1\cdot p_2)\,(p_3\cdot p_4)$$

$$-4096\,(k_1\cdot p_2)\,(k_2\cdot p_1)\,(p_1\cdot p_3)\,(p_3\cdot p_4)-4096\,(k_1\cdot p_2)\,(k_2\cdot p_2)\,(p_1\cdot p_3)\,(p_3\cdot p_4)$$

$$+4096\,(k_1\cdot k_2)\,(p_1\cdot p_2)\,(p_1\cdot p_3)\,(p_3\cdot p_4)+4096\,(k_1\cdot p_1)\,(k_2\cdot p_1)\,(p_2\cdot p_3)\,(p_3\cdot p_4)$$

$$+4096\,(k_1\cdot p_1)\,(k_2\cdot p_2)\,(p_2\cdot p_3)\,(p_3\cdot p_4)-4096\,(k_1\cdot p_1)\,(k_2\cdot p_2)\,(p_1\cdot p_2)\,m_\mu^2$$

$$+6144\,(k_1\cdot p_3)\,(k_2\cdot p_2)\,(p_1\cdot p_2)\,m_\mu^2+4096\,(k_1\cdot p_4)\,(k_2\cdot p_2)\,(p_1\cdot p_2)\,m_\mu^2$$

$$+2048\,(k_1\cdot p_1)\,(k_2\cdot p_3)\,(p_1\cdot p_2)\,m_\mu^2-4096\,(k_1\cdot p_3)\,(k_2\cdot p_3)\,(p_1\cdot p_2)\,m_\mu^2$$

$$-4096\,(k_1\cdot p_4)\,(k_2\cdot p_3)\,(p_1\cdot p_2)\,m_\mu^2+2048\,(k_1\cdot p_1)\,(k_2\cdot p_4)\,(p_1\cdot p_2)\,m_\mu^2$$

$$+2048\,(k_1\cdot p_3)\,(k_2\cdot p_4)\,(p_1\cdot p_2)\,m_\mu^2+4096\,(k_1\cdot p_4)\,(k_2\cdot p_4)\,(p_1\cdot p_2)\,m_\mu^2$$

$$-2048\,(k_1\cdot p_2)\,(k_2\cdot p_1)\,(p_1\cdot p_3)\,m_\mu^2-2048\,(k_1\cdot p_2)\,(k_2\cdot p_2)\,(p_1\cdot p_3)\,m_\mu^2$$

$$+4096\,(k_1\cdot p_2)\,(k_2\cdot p_4)\,(p_1\cdot p_3)\,m_\mu^2+2048\,(k_1\cdot k_2)\,(p_1\cdot p_2)\,(p_1\cdot p_3)\,m_\mu^2$$

$$+2048\,(k_1\cdot p_2)\,(k_2\cdot p_1)\,(p_1\cdot p_4)\,m_\mu^2-2048\,(k_1\cdot p_2)\,(k_2\cdot p_3)\,(p_1\cdot p_4)\,m_\mu^2$$

$$-2048\,(k_1\cdot k_2)\,(p_1\cdot p_2)\,(p_1\cdot p_4)\,m_\mu^2-2048\,(k_1\cdot p_1)\,(k_2\cdot p_1)\,(p_2\cdot p_3)\,m_\mu^2$$

$$+4096\,(k_1\cdot p_3)\,(k_2\cdot p_1)\,(p_2\cdot p_3)\,m_\mu^2+4096\,(k_1\cdot p_4)\,(k_2\cdot p_1)\,(p_2\cdot p_3)\,m_\mu^2$$

$$-2048\,(k_1\cdot p_1)\,(k_2\cdot p_2)\,(p_2\cdot p_3)\,m_\mu^2+4096\,(k_1\cdot p_3)\,(k_2\cdot p_2)\,(p_2\cdot p_3)\,m_\mu^2$$

$$+4096 \left(k_1 \cdot p_4\right) \left(k_2 \cdot p_2\right) \left(p_2 \cdot p_3\right) m_\mu^2 - 2048 \left(k_1 \cdot p_1\right) \left(k_2 \cdot p_4\right) \left(p_2 \cdot p_3\right) m_\mu^2$$

$$+2048 \left(k_1 \cdot p_3\right) \left(k_2 \cdot p_4\right) \left(p_2 \cdot p_3\right) m_\mu^2 + 2048 \left(k_1 \cdot k_2\right) \left(p_1 \cdot p_4\right) \left(p_2 \cdot p_3\right) m_\mu^2$$

$$-2048 \left(k_1 \cdot p_1\right) \left(k_2 \cdot p_1\right) \left(p_2 \cdot p_4\right) m_\mu^2 - 2048 \left(k_1 \cdot p_3\right) \left(k_2 \cdot p_1\right) \left(p_2 \cdot p_4\right) m_\mu^2$$

$$-4096 \left(k_1 \cdot p_4\right) \left(k_2 \cdot p_1\right) \left(p_2 \cdot p_4\right) m_\mu^2 - 4096 \left(k_1 \cdot p_3\right) \left(k_2 \cdot p_2\right) \left(p_2 \cdot p_4\right) m_\mu^2$$

$$-4096 \left(k_1 \cdot p_4\right) \left(k_2 \cdot p_2\right) \left(p_2 \cdot p_4\right) m_\mu^2 + 2048 \left(k_1 \cdot p_1\right) \left(k_2 \cdot p_3\right) \left(p_2 \cdot p_4\right) m_\mu^2$$

$$-2048 \left(k_1 \cdot p_3\right) \left(k_2 \cdot p_3\right) \left(p_2 \cdot p_4\right) m_\mu^2 - 4096 \left(k_1 \cdot k_2\right) \left(p_1 \cdot p_3\right) \left(p_2 \cdot p_4\right) m_\mu^2$$

$$+2048 \left(k_1 \cdot p_2\right) \left(k_2 \cdot p_1\right) \left(p_3 \cdot p_4\right) m_\mu^2 + 4096 \left(k_1 \cdot p_2\right) \left(k_2 \cdot p_2\right) \left(p_3 \cdot p_4\right) m_\mu^2$$

$$+2048 \left(k_1 \cdot p_2\right) \left(k_2 \cdot p_3\right) \left(p_3 \cdot p_4\right) m_\mu^2 - 2048 \left(k_1 \cdot k_2\right) \left(p_1 \cdot p_2\right) \left(p_3 \cdot p_4\right) m_\mu^2$$

$$-2048 \left(k_1 \cdot k_2\right) \left(p_2 \cdot p_3\right) \left(p_3 \cdot p_4\right) m_\mu^2$$

$$+2048 \left(k_1 \cdot p_2\right) \left(k_2 \cdot p_1\right) m_\mu^4 + 2048 \left(k_1 \cdot p_2\right) \left(k_2 \cdot p_2\right) m_\mu^4 - 4096 \left(k_1 \cdot p_2\right) \left(k_2 \cdot p_4\right) m_\mu^4$$

$$\left. -2048 \left(k_1 \cdot k_2\right) \left(p_1 \cdot p_2\right) m_\mu^4 + 4096 \left(k_1 \cdot k_2\right) \left(p_2 \cdot p_4\right) m_\mu^4 \right] \tag{4.73}$$

$$W^{22}_{e\mu \to \mu\mu} = \frac{e^4 G_F^2}{16\,(q^2 - q_s^2)^2\,\left[(p_3 + p_4 - p_1)^2 - m_\mu^2\right]^2} \times$$

$$\Big[4096\,(k_1 \cdot p_1)\,(k_2 \cdot p_2)\,(p_1 \cdot p_3)\,(p_1 \cdot p_4) - 4096\,(k_1 \cdot p_4)\,(k_2 \cdot p_2)\,(p_1 \cdot p_3)\,(p_1 \cdot p_4)$$

$$+ 4096\,(k_1 \cdot p_3)\,(k_2 \cdot p_2)\,(p_1 \cdot p_4)^2 + 4096\,(k_1 \cdot p_3)\,(k_2 \cdot p_2)\,(p_1 \cdot p_3)\,(p_3 \cdot p_4)$$

$$+ 4096\,(k_1 \cdot p_4)\,(k_2 \cdot p_2)\,(p_1 \cdot p_3)\,(p_3 \cdot p_4) - 4096\,(k_1 \cdot p_1)\,(k_2 \cdot p_2)\,(p_1 \cdot p_4)\,(p_3 \cdot p_4)$$

$$+ 4096\,(k_1 \cdot p_3)\,(k_2 \cdot p_2)\,(p_1 \cdot p_4)\,(p_3 \cdot p_4) + 8192\,(k_1 \cdot p_4)\,(k_2 \cdot p_2)\,(p_1 \cdot p_4)\,(p_3 \cdot p_4)$$

$$- 4096\,(k_1 \cdot p_1)\,(k_2 \cdot p_2)\,(p_3 \cdot p_4)^2 + 4096\,(k_1 \cdot p_1)\,(k_2 \cdot p_2)\,(p_1 \cdot p_3)\,m_\mu^2$$

$$- 4096\,(k_1 \cdot p_3)\,(k_2 \cdot p_2)\,(p_1 \cdot p_3)\,m_\mu^2 - 8192\,(k_1 \cdot p_4)\,(k_2 \cdot p_2)\,(p_1 \cdot p_3)\,m_\mu^2$$

$$- 8192\,(k_1 \cdot p_1)\,(k_2 \cdot p_2)\,(p_1 \cdot p_4)\,m_\mu^2 + 4096\,(k_1 \cdot p_3)\,(k_2 \cdot p_2)\,(p_1 \cdot p_4)\,m_\mu^2$$

$$+ 4096\,(k_1 \cdot p_4)\,(k_2 \cdot p_2)\,(p_1 \cdot p_4)\,m_\mu^2 + 4096\,(k_1 \cdot p_1)\,(k_2 \cdot p_2)\,(p_3 \cdot p_4)\,m_\mu^2$$

$$- 8192\,(k_1 \cdot p_3)\,(k_2 \cdot p_2)\,(p_3 \cdot p_4)\,m_\mu^2 - 4096\,(k_1 \cdot p_4)\,(k_2 \cdot p_2)\,(p_3 \cdot p_4)\,m_\mu^2$$

$$- 4096\,(k_1 \cdot p_1)\,(k_2 \cdot p_2)\,m_\mu^4 + 4096\,(k_1 \cdot p_3)\,(k_2 \cdot p_2)\,m_\mu^4$$

$$+ 8192\,(k_1 \cdot p_4)\,(k_2 \cdot p_2)\,m_\mu^4 \Big] \tag{4.74}$$

$$W^{23}_{e\mu \to \mu\mu} = -\frac{e^4 G_F^2}{16\left(q^2-q_s^2\right)\left(s^2-q_s^2\right)\left[(p_3+p_4-p_1)^2-m_\mu^2\right]\left(p_1+p_2-p_4\right)^2} \times$$

$$\Big[4096\,(k_1\cdot p_3)(k_2\cdot p_4)(p_1\cdot p_2)(p_1\cdot p_3) + 4096\,(k_1\cdot p_4)(k_2\cdot p_4)(p_1\cdot p_2)(p_1\cdot p_3)$$

$$-4096\,(k_1\cdot p_3)(k_2\cdot p_3)(p_1\cdot p_2)(p_1\cdot p_4) - 4096\,(k_1\cdot p_4)(k_2\cdot p_3)(p_1\cdot p_2)(p_1\cdot p_4)$$

$$+4096\,(k_1\cdot p_3)(k_2\cdot p_1)(p_1\cdot p_4)(p_2\cdot p_3) + 4096\,(k_1\cdot p_4)(k_2\cdot p_1)(p_1\cdot p_4)(p_2\cdot p_3)$$

$$+4096\,(k_1\cdot p_3)(k_2\cdot p_2)(p_1\cdot p_4)(p_2\cdot p_3) + 4096\,(k_1\cdot p_4)(k_2\cdot p_2)(p_1\cdot p_4)(p_2\cdot p_3)$$

$$-4096\,(k_1\cdot p_3)(k_2\cdot p_1)(p_1\cdot p_3)(p_2\cdot p_4) - 4096\,(k_1\cdot p_4)(k_2\cdot p_1)(p_1\cdot p_3)(p_2\cdot p_4)$$

$$-4096\,(k_1\cdot p_3)(k_2\cdot p_2)(p_1\cdot p_3)(p_2\cdot p_4) - 4096\,(k_1\cdot p_4)(k_2\cdot p_2)(p_1\cdot p_3)(p_2\cdot p_4)$$

$$-4096\,(k_1\cdot p_3)(k_2\cdot p_2)(p_1\cdot p_2)(p_3\cdot p_4) - 4096\,(k_1\cdot p_1)(k_2\cdot p_4)(p_1\cdot p_2)(p_3\cdot p_4)$$

$$-4096\,(k_1\cdot p_2)(k_2\cdot p_1)(p_1\cdot p_4)(p_3\cdot p_4) - 4096\,(k_1\cdot p_2)(k_2\cdot p_2)(p_1\cdot p_4)(p_3\cdot p_4)$$

$$+4096\,(k_1\cdot k_2)(p_1\cdot p_2)(p_1\cdot p_4)(p_3\cdot p_4) + 4096\,(k_1\cdot p_1)(k_2\cdot p_1)(p_2\cdot p_4)(p_3\cdot p_4)$$

$$+4096\,(k_1\cdot p_1)(k_2\cdot p_2)(p_2\cdot p_4)(p_3\cdot p_4) - 4096\,(k_1\cdot p_1)(k_2\cdot p_2)(p_1\cdot p_2)\,m_\mu^2$$

$$+8192\,(k_1\cdot p_3)(k_2\cdot p_2)(p_1\cdot p_2)\,m_\mu^2 + 4096\,(k_1\cdot p_4)(k_2\cdot p_2)(p_1\cdot p_2)\,m_\mu^2$$

$$+2048\,(k_1\cdot p_1)(k_2\cdot p_3)(p_1\cdot p_2)\,m_\mu^2 + 4096\,(k_1\cdot p_3)(k_2\cdot p_3)(p_1\cdot p_2)\,m_\mu^2$$

$$+2048\,(k_1\cdot p_4)(k_2\cdot p_3)(p_1\cdot p_2)\,m_\mu^2 + 2048\,(k_1\cdot p_1)(k_2\cdot p_4)(p_1\cdot p_2)\,m_\mu^2$$

$$-8192\,(k_1\cdot p_3)(k_2\cdot p_4)(p_1\cdot p_2)\,m_\mu^2 - 2048\,(k_1\cdot p_4)(k_2\cdot p_4)(p_1\cdot p_2)\,m_\mu^2$$

$$+2048\,(k_1\cdot p_2)(k_2\cdot p_1)(p_1\cdot p_3)\,m_\mu^2 - 2048\,(k_1\cdot p_2)(k_2\cdot p_4)(p_1\cdot p_3)\,m_\mu^2$$

$$-2048\,(k_1\cdot k_2)(p_1\cdot p_2)(p_1\cdot p_3)\,m_\mu^2 - 2048\,(k_1\cdot p_2)(k_2\cdot p_1)(p_1\cdot p_4)\,m_\mu^2$$

$$+4096\,(k_1\cdot p_2)(k_2\cdot p_3)(p_1\cdot p_4)\,m_\mu^2 - 2048\,(k_1\cdot p_2)(k_2\cdot p_4)(p_1\cdot p_4)\,m_\mu^2$$

$$+2048\,(k_1\cdot k_2)(p_1\cdot p_2)(p_1\cdot p_4)\,m_\mu^2 - 2048\,(k_1\cdot p_1)(k_2\cdot p_1)(p_2\cdot p_3)\,m_\mu^2$$

$$-4096\,(k_1\cdot p_3)(k_2\cdot p_1)(p_2\cdot p_3)\,m_\mu^2 - 2048\,(k_1\cdot p_4)(k_2\cdot p_1)(p_2\cdot p_3)\,m_\mu^2$$

$$-4096\,(k_1\cdot p_3)(k_2\cdot p_2)(p_2\cdot p_3)\,m_\mu^2 - 4096\,(k_1\cdot p_4)(k_2\cdot p_2)(p_2\cdot p_3)\,m_\mu^2$$

$$+ 2048 \left(k_1 \cdot p_1\right)\left(k_2 \cdot p_4\right)\left(p_2 \cdot p_3\right) m_\mu^2 - 2048 \left(k_1 \cdot p_4\right)\left(k_2 \cdot p_4\right)\left(p_2 \cdot p_3\right) m_\mu^2$$

$$- 4096 \left(k_1 \cdot k_2\right)\left(p_1 \cdot p_4\right)\left(p_2 \cdot p_3\right) m_\mu^2 - 2048 \left(k_1 \cdot p_1\right)\left(k_2 \cdot p_1\right)\left(p_2 \cdot p_4\right) m_\mu^2$$

$$+ 8192 \left(k_1 \cdot p_3\right)\left(k_2 \cdot p_1\right)\left(p_2 \cdot p_4\right) m_\mu^2 + 2048 \left(k_1 \cdot p_4\right)\left(k_2 \cdot p_1\right)\left(p_2 \cdot p_4\right) m_\mu^2$$

$$- 4096 \left(k_1 \cdot p_1\right)\left(k_2 \cdot p_2\right)\left(p_2 \cdot p_4\right) m_\mu^2 + 8192 \left(k_1 \cdot p_3\right)\left(k_2 \cdot p_2\right)\left(p_2 \cdot p_4\right) m_\mu^2$$

$$+ 4096 \left(k_1 \cdot p_4\right)\left(k_2 \cdot p_2\right)\left(p_2 \cdot p_4\right) m_\mu^2 - 2048 \left(k_1 \cdot p_1\right)\left(k_2 \cdot p_3\right)\left(p_2 \cdot p_4\right) m_\mu^2$$

$$+ 2048 \left(k_1 \cdot p_4\right)\left(k_2 \cdot p_3\right)\left(p_2 \cdot p_4\right) m_\mu^2 + 2048 \left(k_1 \cdot k_2\right)\left(p_1 \cdot p_3\right)\left(p_2 \cdot p_4\right) m_\mu^2$$

$$+ 2048 \left(k_1 \cdot k_2\right)\left(p_1 \cdot p_4\right)\left(p_2 \cdot p_4\right) m_\mu^2 + 2048 \left(k_1 \cdot p_2\right)\left(k_2 \cdot p_1\right)\left(p_3 \cdot p_4\right) m_\mu^2$$

$$+ 4096 \left(k_1 \cdot p_2\right)\left(k_2 \cdot p_2\right)\left(p_3 \cdot p_4\right) m_\mu^2 + 2048 \left(k_1 \cdot p_2\right)\left(k_2 \cdot p_4\right)\left(p_3 \cdot p_4\right) m_\mu^2$$

$$- 2048 \left(k_1 \cdot k_2\right)\left(p_1 \cdot p_2\right)\left(p_3 \cdot p_4\right) m_\mu^2 - 2048 \left(k_1 \cdot k_2\right)\left(p_2 \cdot p_4\right)\left(p_3 \cdot p_4\right) m_\mu^2$$

$$+ 2048 \left(k_1 \cdot p_2\right)\left(k_2 \cdot p_1\right) m_\mu^4 - 4096 \left(k_1 \cdot p_2\right)\left(k_2 \cdot p_3\right) m_\mu^4 + 2048 \left(k_1 \cdot p_2\right)\left(k_2 \cdot p_4\right) m_\mu^4$$

$$\left. - 2048 \left(k_1 \cdot k_2\right)\left(p_1 \cdot p_2\right) m_\mu^4 + 4096 \left(k_1 \cdot k_2\right)\left(p_2 \cdot p_3\right) m_\mu^4 - 2048 \left(k_1 \cdot k_2\right)\left(p_2 \cdot p_4\right) m_\mu^4 \right]$$

$$(4.75)$$

$$
\begin{aligned}
W_{e\mu \to \mu\mu}^{24} \;=\; & -\frac{e^4 G_F^2}{16 \left(q^2 - q_s^2\right)\left(s^2 - q_s^2\right)\left[\left(p_3 + p_4 - p_1\right)^2 - m_\mu^2\right]^2} \times \\
& \Big[-8192 \left(k_1 \cdot p_3\right)\left(k_2 \cdot p_2\right)\left(p_1 \cdot p_3\right)\left(p_3 \cdot p_4\right) - 8192 \left(k_1 \cdot p_4\right)\left(k_2 \cdot p_2\right)\left(p_1 \cdot p_3\right)\left(p_3 \cdot p_4\right) \\
& - 8192 \left(k_1 \cdot p_3\right)\left(k_2 \cdot p_2\right)\left(p_1 \cdot p_4\right)\left(p_3 \cdot p_4\right) - 8192 \left(k_1 \cdot p_4\right)\left(k_2 \cdot p_2\right)\left(p_1 \cdot p_4\right)\left(p_3 \cdot p_4\right) \\
& + 8192 \left(k_1 \cdot p_1\right)\left(k_2 \cdot p_2\right)\left(p_3 \cdot p_4\right)^2 + 8192 \left(k_1 \cdot p_3\right)\left(k_2 \cdot p_2\right)\left(p_1 \cdot p_3\right) m_\mu^2 \\
& + 8192 \left(k_1 \cdot p_4\right)\left(k_2 \cdot p_2\right)\left(p_1 \cdot p_3\right) m_\mu^2 + 8192 \left(k_1 \cdot p_3\right)\left(k_2 \cdot p_2\right)\left(p_1 \cdot p_4\right) m_\mu^2 \\
& + 8192 \left(k_1 \cdot p_4\right)\left(k_2 \cdot p_2\right)\left(p_1 \cdot p_4\right) m_\mu^2 - 16384 \left(k_1 \cdot p_1\right)\left(k_2 \cdot p_2\right)\left(p_3 \cdot p_4\right) m_\mu^2 \\
& + 16384 \left(k_1 \cdot p_3\right)\left(k_2 \cdot p_2\right)\left(p_3 \cdot p_4\right) m_\mu^2 + 16384 \left(k_1 \cdot p_4\right)\left(k_2 \cdot p_2\right)\left(p_3 \cdot p_4\right) m_\mu^2 \\
& - 8192 \left(k_1 \cdot p_3\right)\left(k_2 \cdot p_2\right) m_\mu^4 - 8192 \left(k_1 \cdot p_4\right)\left(k_2 \cdot p_2\right) m_\mu^4 \Big] \qquad (4.76)
\end{aligned}
$$

$$W^{33}_{e\mu \to \mu\mu} = \frac{e^4 G_F^2}{16 \left(s^2 - q_s^2\right)^2 \left(p_1 + p_2 - p_4\right)^4} \times$$

$$\Big[-4096 \, (k_1 \cdot p_3) \, (k_2 \cdot p_4) \, (p_1 \cdot p_2)^2 + 4096 \, (k_1 \cdot p_3) \, (k_2 \cdot p_4) \, (p_1 \cdot p_2) \, (p_1 \cdot p_3)$$

$$+ 4096 \, (k_1 \cdot p_3) \, (k_2 \cdot p_1) \, (p_1 \cdot p_2) \, (p_1 \cdot p_4) + 4096 \, (k_1 \cdot p_3) \, (k_2 \cdot p_2) \, (p_1 \cdot p_2) \, (p_1 \cdot p_4)$$

$$- 4096 \, (k_1 \cdot p_3) \, (k_2 \cdot p_3) \, (p_1 \cdot p_2) \, (p_1 \cdot p_4) + 4096 \, (k_1 \cdot p_3) \, (k_2 \cdot p_4) \, (p_1 \cdot p_2) \, (p_2 \cdot p_3)$$

$$+ 4096 \, (k_1 \cdot p_3) \, (k_2 \cdot p_1) \, (p_1 \cdot p_2) \, (p_2 \cdot p_4) + 8192 \, (k_1 \cdot p_3) \, (k_2 \cdot p_2) \, (p_1 \cdot p_2) \, (p_2 \cdot p_4)$$

$$- 8192 \, (k_1 \cdot p_3) \, (k_2 \cdot p_3) \, (p_1 \cdot p_2) \, (p_2 \cdot p_4) - 4096 \, (k_1 \cdot p_3) \, (k_2 \cdot p_2) \, (p_1 \cdot p_3) \, (p_2 \cdot p_4)$$

$$+ 4096 \, (k_1 \cdot p_3) \, (k_2 \cdot p_3) \, (p_1 \cdot p_3) \, (p_2 \cdot p_4) + 4096 \, (k_1 \cdot p_3) \, (k_2 \cdot p_1) \, (p_2 \cdot p_3) \, (p_2 \cdot p_4)$$

$$- 4096 \, (k_1 \cdot p_3) \, (k_2 \cdot p_1) \, (p_1 \cdot p_2) \, (p_3 \cdot p_4) - 4096 \, (k_1 \cdot p_3) \, (k_2 \cdot p_2) \, (p_1 \cdot p_2) \, (p_3 \cdot p_4)$$

$$+ 4096 \, (k_1 \cdot p_3) \, (k_2 \cdot p_3) \, (p_1 \cdot p_2) \, (p_3 \cdot p_4) - 4096 \, (k_1 \cdot p_3) \, (k_2 \cdot p_1) \, (p_1 \cdot p_2) \, m_\mu^2$$

$$+ 4096 \, (k_1 \cdot p_3) \, (k_2 \cdot p_3) \, (p_1 \cdot p_2) \, m_\mu^2 - 4096 \, (k_1 \cdot p_3) \, (k_2 \cdot p_4) \, (p_1 \cdot p_2) \, m_\mu^2$$

$$- 4096 \, (k_1 \cdot p_3) \, (k_2 \cdot p_2) \, (p_1 \cdot p_3) \, m_\mu^2 + 4096 \, (k_1 \cdot p_3) \, (k_2 \cdot p_1) \, (p_2 \cdot p_3) \, m_\mu^2$$

$$- 4096 \, (k_1 \cdot p_3) \, (k_2 \cdot p_3) \, (p_2 \cdot p_3) \, m_\mu^2 + 4096 \, (k_1 \cdot p_3) \, (k_2 \cdot p_2) \, (p_2 \cdot p_4) \, m_\mu^2$$

$$- 4096 \, (k_1 \cdot p_3) \, (k_2 \cdot p_3) \, (p_2 \cdot p_4) \, m_\mu^2 + 4096 \, (k_1 \cdot p_3) \, (k_2 \cdot p_2) \, m_\mu^4 \Big] \qquad (4.77)$$

$$W^{34}_{e\mu \to \mu\mu} = \frac{e^4 G_F^2}{16\,(s^2-q_s^2)^2\,(p_1+p_2-p_4)^2\,\left[(p_3+p_4-p_1)^2-m_\mu^2\right]} \times$$

$$\Big[4096\,(k_1 \cdot p_4)\,(k_2 \cdot p_2)\,(p_1 \cdot p_2)\,(p_1 \cdot p_3) - 2048\,(k_1 \cdot p_4)\,(k_2 \cdot p_3)\,(p_1 \cdot p_2)\,(p_1 \cdot p_3)$$

$$-\,6144\,(k_1 \cdot p_3)\,(k_2 \cdot p_4)\,(p_1 \cdot p_2)\,(p_1 \cdot p_3) - 4096\,(k_1 \cdot p_4)\,(k_2 \cdot p_4)\,(p_1 \cdot p_2)\,(p_1 \cdot p_3)$$

$$-\,2048\,(k_1 \cdot p_4)\,(k_2 \cdot p_2)\,(p_1 \cdot p_3)^2 + 2048\,(k_1 \cdot p_2)\,(k_2 \cdot p_4)\,(p_1 \cdot p_3)^2$$

$$+\,4096\,(k_1 \cdot p_3)\,(k_2 \cdot p_3)\,(p_1 \cdot p_2)\,(p_1 \cdot p_4) + 4096\,(k_1 \cdot p_4)\,(k_2 \cdot p_3)\,(p_1 \cdot p_2)\,(p_1 \cdot p_4)$$

$$-\,4096\,(k_1 \cdot p_2)\,(k_2 \cdot p_2)\,(p_1 \cdot p_3)\,(p_1 \cdot p_4) + 2048\,(k_1 \cdot p_3)\,(k_2 \cdot p_2)\,(p_1 \cdot p_3)\,(p_1 \cdot p_4)$$

$$+\,2048\,(k_1 \cdot p_2)\,(k_2 \cdot p_3)\,(p_1 \cdot p_3)\,(p_1 \cdot p_4) + 2048\,(k_1 \cdot p_4)\,(k_2 \cdot p_1)\,(p_1 \cdot p_3)\,(p_2 \cdot p_3)$$

$$-\,2048\,(k_1 \cdot p_1)\,(k_2 \cdot p_4)\,(p_1 \cdot p_3)\,(p_2 \cdot p_3) + 4096\,(k_1 \cdot p_3)\,(k_2 \cdot p_4)\,(p_1 \cdot p_3)\,(p_2 \cdot p_3)$$

$$-\,4096\,(k_1 \cdot p_3)\,(k_2 \cdot p_1)\,(p_1 \cdot p_4)\,(p_2 \cdot p_3) - 4096\,(k_1 \cdot p_4)\,(k_2 \cdot p_1)\,(p_1 \cdot p_4)\,(p_2 \cdot p_3)$$

$$+\,4096\,(k_1 \cdot p_1)\,(k_2 \cdot p_2)\,(p_1 \cdot p_4)\,(p_2 \cdot p_3) - 8192\,(k_1 \cdot p_3)\,(k_2 \cdot p_2)\,(p_1 \cdot p_4)\,(p_2 \cdot p_3)$$

$$-\,4096\,(k_1 \cdot p_4)\,(k_2 \cdot p_2)\,(p_1 \cdot p_4)\,(p_2 \cdot p_3) - 2048\,(k_1 \cdot k_2)\,(p_1 \cdot p_3)\,(p_1 \cdot p_4)\,(p_2 \cdot p_3)$$

$$+\,6144\,(k_1 \cdot p_3)\,(k_2 \cdot p_1)\,(p_1 \cdot p_3)\,(p_2 \cdot p_4) + 4096\,(k_1 \cdot p_4)\,(k_2 \cdot p_1)\,(p_1 \cdot p_3)\,(p_2 \cdot p_4)$$

$$+\,8192\,(k_1 \cdot p_3)\,(k_2 \cdot p_2)\,(p_1 \cdot p_3)\,(p_2 \cdot p_4) + 4096\,(k_1 \cdot p_4)\,(k_2 \cdot p_2)\,(p_1 \cdot p_3)\,(p_2 \cdot p_4)$$

$$+\,2048\,(k_1 \cdot p_1)\,(k_2 \cdot p_3)\,(p_1 \cdot p_3)\,(p_2 \cdot p_4) - 4096\,(k_1 \cdot p_3)\,(k_2 \cdot p_3)\,(p_1 \cdot p_3)\,(p_2 \cdot p_4)$$

$$-\,2048\,(k_1 \cdot k_2)\,(p_1 \cdot p_3)^2\,(p_2 \cdot p_4) - 4096\,(k_1 \cdot p_1)\,(k_2 \cdot p_2)\,(p_1 \cdot p_2)\,(p_3 \cdot p_4)$$

$$+\,8192\,(k_1 \cdot p_3)\,(k_2 \cdot p_2)\,(p_1 \cdot p_2)\,(p_3 \cdot p_4) - 4096\,(k_1 \cdot p_3)\,(k_2 \cdot p_3)\,(p_1 \cdot p_2)\,(p_3 \cdot p_4)$$

$$-\,2048\,(k_1 \cdot p_4)\,(k_2 \cdot p_3)\,(p_1 \cdot p_2)\,(p_3 \cdot p_4) + 4096\,(k_1 \cdot p_1)\,(k_2 \cdot p_4)\,(p_1 \cdot p_2)\,(p_3 \cdot p_4)$$

$$-\,2048\,(k_1 \cdot p_3)\,(k_2 \cdot p_4)\,(p_1 \cdot p_2)\,(p_3 \cdot p_4) - 2048\,(k_1 \cdot p_2)\,(k_2 \cdot p_1)\,(p_1 \cdot p_3)\,(p_3 \cdot p_4)$$

$$+\,2048\,(k_1 \cdot p_1)\,(k_2 \cdot p_2)\,(p_1 \cdot p_3)\,(p_3 \cdot p_4) - 8192\,(k_1 \cdot p_3)\,(k_2 \cdot p_2)\,(p_1 \cdot p_3)\,(p_3 \cdot p_4)$$

$$-\,2048\,(k_1 \cdot p_4)\,(k_2 \cdot p_2)\,(p_1 \cdot p_3)\,(p_3 \cdot p_4) + 2048\,(k_1 \cdot p_2)\,(k_2 \cdot p_4)\,(p_1 \cdot p_3)\,(p_3 \cdot p_4)$$

$$+\,2048\,(k_1 \cdot k_2)\,(p_1 \cdot p_2)\,(p_1 \cdot p_3)\,(p_3 \cdot p_4) + 4096\,(k_1 \cdot p_2)\,(k_2 \cdot p_1)\,(p_1 \cdot p_4)\,(p_3 \cdot p_4)$$

$$+4096\,(k_1 \cdot p_2)\,(k_2 \cdot p_2)\,(p_1 \cdot p_4)\,(p_3 \cdot p_4)-2048\,(k_1 \cdot p_3)\,(k_2 \cdot p_2)\,(p_1 \cdot p_4)\,(p_3 \cdot p_4)$$

$$-2048\,(k_1 \cdot p_2)\,(k_2 \cdot p_3)\,(p_1 \cdot p_4)\,(p_3 \cdot p_4)-4096\,(k_1 \cdot k_2)\,(p_1 \cdot p_2)\,(p_1 \cdot p_4)\,(p_3 \cdot p_4)$$

$$+4096\,(k_1 \cdot p_3)\,(k_2 \cdot p_1)\,(p_2 \cdot p_3)\,(p_3 \cdot p_4)+2048\,(k_1 \cdot p_4)\,(k_2 \cdot p_1)\,(p_2 \cdot p_3)\,(p_3 \cdot p_4)$$

$$-2048\,(k_1 \cdot p_1)\,(k_2 \cdot p_4)\,(p_2 \cdot p_3)\,(p_3 \cdot p_4)+2048\,(k_1 \cdot k_2)\,(p_1 \cdot p_4)\,(p_2 \cdot p_3)\,(p_3 \cdot p_4)$$

$$-4096\,(k_1 \cdot p_1)\,(k_2 \cdot p_1)\,(p_2 \cdot p_4)\,(p_3 \cdot p_4)+2048\,(k_1 \cdot p_3)\,(k_2 \cdot p_1)\,(p_2 \cdot p_4)\,(p_3 \cdot p_4)$$

$$-4096\,(k_1 \cdot p_1)\,(k_2 \cdot p_2)\,(p_2 \cdot p_4)\,(p_3 \cdot p_4)+2048\,(k_1 \cdot p_1)\,(k_2 \cdot p_3)\,(p_2 \cdot p_4)\,(p_3 \cdot p_4)$$

$$-2048\,(k_1 \cdot k_2)\,(p_1 \cdot p_3)\,(p_2 \cdot p_4)\,(p_3 \cdot p_4)-2048\,(k_1 \cdot p_2)\,(k_2 \cdot p_1)\,(p_3 \cdot p_4)^2$$

$$+2048\,(k_1 \cdot p_1)\,(k_2 \cdot p_2)\,(p_3 \cdot p_4)^2+2048\,(k_1 \cdot k_2)\,(p_1 \cdot p_2)\,(p_3 \cdot p_4)^2$$

$$-2048\,(k_1 \cdot p_1)\,(k_2 \cdot p_3)\,(p_1 \cdot p_2)\,m_\mu^2-2048\,(k_1 \cdot p_4)\,(k_2 \cdot p_3)\,(p_1 \cdot p_2)\,m_\mu^2$$

$$+2048\,(k_1 \cdot p_1)\,(k_2 \cdot p_4)\,(p_1 \cdot p_2)\,m_\mu^2+2048\,(k_1 \cdot p_4)\,(k_2 \cdot p_4)\,(p_1 \cdot p_2)\,m_\mu^2$$

$$-2048\,(k_1 \cdot p_2)\,(k_2 \cdot p_1)\,(p_1 \cdot p_3)\,m_\mu^2+4096\,(k_1 \cdot p_2)\,(k_2 \cdot p_2)\,(p_1 \cdot p_3)\,m_\mu^2$$

$$+2048\,(k_1 \cdot p_3)\,(k_2 \cdot p_2)\,(p_1 \cdot p_3)\,m_\mu^2+4096\,(k_1 \cdot p_4)\,(k_2 \cdot p_2)\,(p_1 \cdot p_3)\,m_\mu^2$$

$$-6144\,(k_1 \cdot p_2)\,(k_2 \cdot p_3)\,(p_1 \cdot p_3)\,m_\mu^2+2048\,(k_1 \cdot p_2)\,(k_2 \cdot p_4)\,(p_1 \cdot p_3)\,m_\mu^2$$

$$+2048\,(k_1 \cdot k_2)\,(p_1 \cdot p_2)\,(p_1 \cdot p_3)\,m_\mu^2-2048\,(k_1 \cdot p_1)\,(k_2 \cdot p_2)\,(p_1 \cdot p_4)\,m_\mu^2$$

$$+4096\,(k_1 \cdot p_3)\,(k_2 \cdot p_2)\,(p_1 \cdot p_4)\,m_\mu^2+2048\,(k_1 \cdot p_4)\,(k_2 \cdot p_2)\,(p_1 \cdot p_4)\,m_\mu^2$$

$$-4096\,(k_1 \cdot p_2)\,(k_2 \cdot p_3)\,(p_1 \cdot p_4)\,m_\mu^2+2048\,(k_1 \cdot p_1)\,(k_2 \cdot p_1)\,(p_2 \cdot p_3)\,m_\mu^2$$

$$+2048\,(k_1 \cdot p_4)\,(k_2 \cdot p_1)\,(p_2 \cdot p_3)\,m_\mu^2-4096\,(k_1 \cdot p_1)\,(k_2 \cdot p_2)\,(p_2 \cdot p_3)\,m_\mu^2$$

$$+8192\,(k_1 \cdot p_3)\,(k_2 \cdot p_2)\,(p_2 \cdot p_3)\,m_\mu^2+4096\,(k_1 \cdot p_4)\,(k_2 \cdot p_2)\,(p_2 \cdot p_3)\,m_\mu^2$$

$$-2048\,(k_1 \cdot p_1)\,(k_2 \cdot p_4)\,(p_2 \cdot p_3)\,m_\mu^2+4096\,(k_1 \cdot p_3)\,(k_2 \cdot p_4)\,(p_2 \cdot p_3)\,m_\mu^2$$

$$+2048\,(k_1 \cdot p_4)\,(k_2 \cdot p_4)\,(p_2 \cdot p_3)\,m_\mu^2+6144\,(k_1 \cdot k_2)\,(p_1 \cdot p_3)\,(p_2 \cdot p_3)\,m_\mu^2$$

$$+4096 \left(k_1 \cdot k_2\right) \left(p_1 \cdot p_4\right) \left(p_2 \cdot p_3\right) m_\mu^2 - 2048 \left(k_1 \cdot p_1\right) \left(k_2 \cdot p_1\right) \left(p_2 \cdot p_4\right) m_\mu^2$$

$$-2048 \left(k_1 \cdot p_4\right) \left(k_2 \cdot p_1\right) \left(p_2 \cdot p_4\right) m_\mu^2 + 2048 \left(k_1 \cdot p_1\right) \left(k_2 \cdot p_3\right) \left(p_2 \cdot p_4\right) m_\mu^2$$

$$-4096 \left(k_1 \cdot p_3\right) \left(k_2 \cdot p_3\right) \left(p_2 \cdot p_4\right) m_\mu^2 - 2048 \left(k_1 \cdot p_4\right) \left(k_2 \cdot p_3\right) \left(p_2 \cdot p_4\right) m_\mu^2$$

$$-2048 \left(k_1 \cdot k_2\right) \left(p_1 \cdot p_3\right) \left(p_2 \cdot p_4\right) m_\mu^2 - 2048 \left(k_1 \cdot p_2\right) \left(k_2 \cdot p_1\right) \left(p_3 \cdot p_4\right) m_\mu^2$$

$$-4096 \left(k_1 \cdot p_1\right) \left(k_2 \cdot p_2\right) \left(p_3 \cdot p_4\right) m_\mu^2 - 4096 \left(k_1 \cdot p_2\right) \left(k_2 \cdot p_2\right) \left(p_3 \cdot p_4\right) m_\mu^2$$

$$+6144 \left(k_1 \cdot p_3\right) \left(k_2 \cdot p_2\right) \left(p_3 \cdot p_4\right) m_\mu^2 + 6144 \left(k_1 \cdot p_2\right) \left(k_2 \cdot p_3\right) \left(p_3 \cdot p_4\right) m_\mu^2$$

$$-2048 \left(k_1 \cdot p_2\right) \left(k_2 \cdot p_4\right) \left(p_3 \cdot p_4\right) m_\mu^2 + 2048 \left(k_1 \cdot k_2\right) \left(p_1 \cdot p_2\right) \left(p_3 \cdot p_4\right) m_\mu^2$$

$$-6144 \left(k_1 \cdot k_2\right) \left(p_2 \cdot p_3\right) \left(p_3 \cdot p_4\right) m_\mu^2 + 2048 \left(k_1 \cdot k_2\right) \left(p_2 \cdot p_4\right) \left(p_3 \cdot p_4\right) m_\mu^2$$

$$+4096 \left(k_1 \cdot p_2\right) \left(k_2 \cdot p_1\right) m_\mu^4 + 2048 \left(k_1 \cdot p_1\right) \left(k_2 \cdot p_2\right) m_\mu^4 - 4096 \left(k_1 \cdot p_3\right) \left(k_2 \cdot p_2\right) m_\mu^4$$

$$-2048 \left(k_1 \cdot p_4\right) \left(k_2 \cdot p_2\right) m_\mu^4 + 4096 \left(k_1 \cdot p_2\right) \left(k_2 \cdot p_3\right) m_\mu^4 - 4096 \left(k_1 \cdot p_2\right) \left(k_2 \cdot p_4\right) m_\mu^4$$

$$\left. -4096 \left(k_1 \cdot k_2\right) \left(p_1 \cdot p_2\right) m_\mu^4 - 4096 \left(k_1 \cdot k_2\right) \left(p_2 \cdot p_3\right) m_\mu^4 + 4096 \left(k_1 \cdot k_2\right) \left(p_2 \cdot p_4\right) m_\mu^4 \right]$$

$$\tag{4.78}$$

$$
\begin{aligned}
W_{e\mu\to\mu\mu}^{44} \;=\; & \frac{e^4 G_F^2}{16\,(s^2 - q_s^2)^2 \left[(p_3 + p_4 - p_1)^2 - m_\mu^2\right]^2} \\[2mm]
& \Big[4096\,(k_1 \cdot p_4)\,(k_2 \cdot p_2)\,(p_1 \cdot p_3)^2 + 4096\,(k_1 \cdot p_1)\,(k_2 \cdot p_2)\,(p_1 \cdot p_3)\,(p_1 \cdot p_4) \\[2mm]
& -4096\,(k_1 \cdot p_3)\,(k_2 \cdot p_2)\,(p_1 \cdot p_3)\,(p_1 \cdot p_4) - 4096\,(k_1 \cdot p_1)\,(k_2 \cdot p_2)\,(p_1 \cdot p_3)\,(p_3 \cdot p_4) \\[2mm]
& +8192\,(k_1 \cdot p_3)\,(k_2 \cdot p_2)\,(p_1 \cdot p_3)\,(p_3 \cdot p_4) + 4096\,(k_1 \cdot p_4)\,(k_2 \cdot p_2)\,(p_1 \cdot p_3)\,(p_3 \cdot p_4) \\[2mm]
& +4096\,(k_1 \cdot p_3)\,(k_2 \cdot p_2)\,(p_1 \cdot p_4)\,(p_3 \cdot p_4) + 4096\,(k_1 \cdot p_4)\,(k_2 \cdot p_2)\,(p_1 \cdot p_4)\,(p_3 \cdot p_4) \\[2mm]
& -4096\,(k_1 \cdot p_1)\,(k_2 \cdot p_2)\,(p_3 \cdot p_4)^2 - 8192\,(k_1 \cdot p_1)\,(k_2 \cdot p_2)\,(p_1 \cdot p_3)\,m_\mu^2 \\[2mm]
& +4096\,(k_1 \cdot p_3)\,(k_2 \cdot p_2)\,(p_1 \cdot p_3)\,m_\mu^2 + 4096\,(k_1 \cdot p_4)\,(k_2 \cdot p_2)\,(p_1 \cdot p_3)\,m_\mu^2 \\[2mm]
& +4096\,(k_1 \cdot p_1)\,(k_2 \cdot p_2)\,(p_1 \cdot p_4)\,m_\mu^2 - 8192\,(k_1 \cdot p_3)\,(k_2 \cdot p_2)\,(p_1 \cdot p_4)\,m_\mu^2 \\[2mm]
& -4096\,(k_1 \cdot p_4)\,(k_2 \cdot p_2)\,(p_1 \cdot p_4)\,m_\mu^2 + 4096\,(k_1 \cdot p_1)\,(k_2 \cdot p_2)\,(p_3 \cdot p_4)\,m_\mu^2 \\[2mm]
& -4096\,(k_1 \cdot p_3)\,(k_2 \cdot p_2)\,(p_3 \cdot p_4)\,m_\mu^2 - 8192\,(k_1 \cdot p_4)\,(k_2 \cdot p_2)\,(p_3 \cdot p_4)\,m_\mu^2 \\[2mm]
& -4096\,(k_1 \cdot p_1)\,(k_2 \cdot p_2)\,m_\mu^4 + 8192\,(k_1 \cdot p_3)\,(k_2 \cdot p_2)\,m_\mu^4 + 4096\,(k_1 \cdot p_4)\,(k_2 \cdot p_2)\,m_\mu^4 \Big]
\end{aligned}
$$

$$(4.79)$$

Chapter 5

Illuminating interfaces between phases of a U(1)×U(1) gauge theory

We study boundaries between phases in which different linear combinations of gauge generators are free. Mixing of gauge generators is familiar from the standard model of particle physics, and the possibility of creating neighboring domains in which different linear combinations of gauge generators are free is now receiving serious attention. To set the stage for this work we first briefly review a concrete example.

In the standard model, the propagating $U(1)$ gauge boson (the photon) is associated with a particular Abelian $U(1)_Q$ subgroup of the full standard model gauge group. This subgroup emerged unbroken from the electroweak Higgs symmetry breaking $SU(2) \otimes U(1)_Y \rightarrow U(1)_Q$ at the TeV scale, and is generated by some linear com-

bination of the "W_3" generator of the $SU(2)$ weak interaction and the "Y" generator of the $U(1)$ hypercharge interaction.

We now know that in quark matter the gauge group for the propagating $U(1)$ gauge boson will be rotated into a different direction by a further layer of symmetry breaking at the MeV scale. At sufficiently high density, quark matter will develop a condensate of quark Cooper pairs that plays the role of a Higgs field [48, 49]. (For reviews of this phenomenon of "color superconductivity" see Ref. [50]). In the real world, quark matter is expected to contain the three lightest flavors, and in this case the condensate forms a "color-flavor-locked" (CFL) phase [51], in which a linear combination of the photon and one of the gluons remains massless, while the orthogonal linear combination and the remainder of the gluons become massive by the Higgs mechanism. The gauge symmetry breaking is $SU(3)_{\text{color}} \otimes U(1)_Q \to U(1)_{\tilde{Q}}$. Thus a "rotated" electromagnetism is present in the CFL color superconducting phase of quark matter. This raises the interesting possibility of having an interface between a vacuum region in which the propagating gauge boson is the usual Q-photon, and a quark matter region in which it is a different particle, the $\tilde{Q}$-photon, which is a mixture of the photon and a gluon. What will happen to electromagnetic fields, including light beams, that encounter such an interface?

The $U(1) \otimes U(1)$ gauge system arises in various other physical contexts. Electroweak symmetry breaking can be simplified to a $U(1) \otimes U(1)$ system by focussing on the hypercharge and W_3 bosons, which mix to form the photon and Z^0. The $U(1) \otimes U(1)$ gauge system also arises in extensions of the standard model, where an

extra $U(1)$ gauge symmetry with a corresponding Z' gauge boson is added. Natural contexts for this include Grand Unified Theories with gauge groups such as $SO(10)$ and E_6, and some string models [52, 53].

In chapter 5 we study the light reflection and transmission properties of a boundary between phases in a $U(1) \otimes U(1)$ gauge theory. There have been previous studies of the behavior of magnetic fields [54] and light beams [55] in the specific case of the interface between the vacuum and CFL quark matter. However, we consider the most general realization of the gauge symmetries that supports propagating gauge bosons. On one side of the boundary both $U(1)$ gauge symmetries may be free, or some linear combination may be Higgsed or confined. On the other side, both $U(1)$ gauge symmetries may be free, or a *different* linear combination may be Higgsed or confined, where the difference is parameterized by a "mismatch angle" α. We calculate the nature and intensity of the reflected and transmitted gauge bosons in each case.

We introduce the $U(1) \otimes U(1)$ model and show how Higgsing or confinement of a gauge field can be implemented by appropriate boundary conditions at the interface and describe the calculation of the reflection and transmission coefficients for the various types of boundary. We then discuss how they compare with previous calculations, explain some mysterious features, and analyze their compatibility with expectations based on the complementarity principle. We also analyze subleties of the low-frequency limit and a detailed example of complementarity.

5.1 Confinement and Higgsing via Boundary Conditions in the $U(1) \otimes U(1)$ model

We place the interface at the $z = 0$ plane. On the $z > 0$ side of the interface we work in the $U(1)_Q \otimes U(1)_{T_8}$ basis. $U(1)_Q$ is free, so that photons can propagate, and $U(1)_{T_8}$ may be confined, Higgsed, or free. On the $z < 0$ side of the interface we work in the $U(1)_{\tilde{Q}} \otimes U(1)_X$ basis. $U(1)_{\tilde{Q}}$ is free, so that $\tilde{Q}$-photons can propagate, and $U(1)_X$ may be confined, Higgsed, or free [1]. The $\tilde{Q}$-photon

$$A_\mu^{\tilde{Q}} = \cos \alpha A_\mu + \sin \alpha G_\mu^8 \tag{5.1}$$

remains free, while the orthogonal "X" gauge boson

$$A_\mu^X = -\sin \alpha A_\mu + \cos \alpha G_\mu^8 \tag{5.2}$$

may be free, Higgsed, or confined. In the case of CFL matter, electromagnetism (Q) is much more weakly coupled than the strong interaction (T_8) at the relevant energy scale, so the mixing angle α (analogous to the Weinberg angle in the standard model) is small, and the $\tilde{Q}$ photon is mostly the ordinary Q-photon, with a small admixture of the T_8 gluon. However, in our general treatment, we will keep α as an arbitrary parameter.

---

[1] These names for the generators are taken over from earlier treatments of the interface between a vacuum and CFL quark matter [54, 55], where one only considers the electromagnetic generator Q and the color generator T_8 with which it mixes. In the CFL quark matter, a quark-quark condensate acts as a Higgs field, breaking a linear combination X and leaving the orthogonal linear combination $\tilde{Q}$ unbroken.
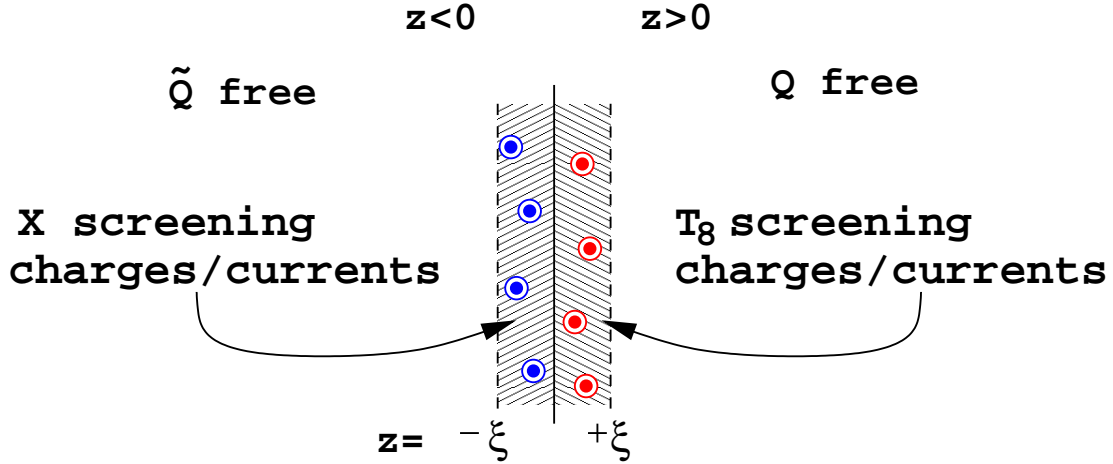
Figure 5.1: The phase boundary that we study. In the $z > 0$ region, the Q gauge boson is free, and the orthogonal T_8 gauge boson may be free, or it may be Higgsed or confined. In the $z < 0$ region, the $\tilde{Q}$ gauge boson is free, and the orthogonal X gauge boson may be free, or it may be Higgsed or confined. Higgsing and confinement are implemented by currents or charges in the boundary region of thickness ξ. The condensates that cause Higgsing/confinement are assumed to change over a much shorter distance.

We study the behavior of Q-photons coming in from $z = +\infty$, and reflecting off or transmitting through the interface. As in Ref. [54], we use free Maxwell equations to describe all the gauge fields, with confinement and Higgsing implemented via boundary conditions at the interface (Fig. 5.1), as we now describe.

At the boundary of a free phase, there are no limitations on the electric and magnetic fields of both $U(1)$ generators: both types of gauge boson can propagate, and there are no charges or currents present.

At the boundary of a Higgsed phase, there is a layer of thickness ξ in which there are electric charges and super-currents associated with the Higgsed generator. This corresponds to the real physics of a Higgs phase, in which a condensate of a charged

field supplies mobile electric charges that screen out electric flux and repel magnetic flux (the Meissner effect). For a confined phase, there is a boundary layer of thickness ξ in which there are magnetic charges and super-currents associated with the confined generator. This corresponds to the dual superconductor picture of confinement [85], in which there are mobile magnetic charges that screen out magnetic flux and repel electric flux.

Note that we assume the "sharp interface" scenario of Ref. [54], in which the wavelength λ of the light shining on the boundary is much larger than the penetration depth ξ for the gauge fields. This assumption seems straightforward but actually under some circumstances there are subtle order-of-limits issues. We will discuss them in section 5.3 when we address the paradoxical nature of the $\alpha \to 0$ limit for certain interfaces.

To proceed, we write all fields as two-component objects in the two-dimensional space of gauge symmetry generators spanned by Q and T_8. The $(\tilde{Q}, X)$ basis is rotated by the angle α:

$$
Q = \begin{pmatrix} 1 \\ 0 \end{pmatrix}, \qquad T_8 = \begin{pmatrix} 0 \\ 1 \end{pmatrix},
$$
$$
\tilde{Q} = \begin{pmatrix} \cos\alpha \\ \sin\alpha \end{pmatrix}, \quad X = \begin{pmatrix} -\sin\alpha \\ \cos\alpha \end{pmatrix}.
$$

(5.3)

so a general magnetic field takes the form

$$
\vec{B} = \begin{pmatrix} \vec{B}^Q \\ \vec{B}^{T_8} \end{pmatrix} = \begin{pmatrix} \cos\alpha\,\vec{B}^{\tilde{Q}} - \sin\alpha\,\vec{B}^X \\ \sin\alpha\,\vec{B}^{\tilde{Q}} + \cos\alpha\,\vec{B}^X \end{pmatrix}
$$

(5.4)

and similarly for $\vec{E}$. The generalized Maxwell equations are

$$\nabla \cdot \vec{D} = \rho \quad , \quad \nabla \times \vec{E} = \vec{J}_M - \frac{\partial \vec{B}}{\partial t}, \tag{5.5}$$

$$\nabla \cdot \vec{B} = \rho_M \quad , \quad \nabla \times \vec{H} = \vec{J} + \frac{\partial \vec{D}}{\partial t} \tag{5.6}$$

where ρ_M and J_M are magnetic charge and current densities, and we assume the usual linear relationship between $\vec{E}$ and $\vec{D}$, and between $\vec{B}$ and $\vec{H}$,

$$Q\text{-photons:} \qquad \tilde{Q}\text{-photons:}$$

$$\vec{D}^Q = \varepsilon \vec{E}^Q, \qquad \vec{D}^{\tilde{Q}} = \tilde{\varepsilon} \vec{E}^{\tilde{Q}}, \tag{5.7}$$

$$\vec{H}^Q = \frac{1}{\mu} \vec{B}^Q, \qquad \vec{H}^{\tilde{Q}} = \frac{1}{\tilde{\mu}} \vec{B}^{\tilde{Q}}.$$

We assume that the wavelength of the gauge bosons incident on the surface is much greater than the penetration depth ξ so we can integrate the Maxwell equations over $-\xi < z < \xi$, and obtain boundary conditions that relate the fields at $z = -\xi$ to those at $z = +\xi$ (Ref. [86], sect. I.5). For the fields with divergence equations (D and B) the boundary conditions relate the components perpendicular to the surface; for the fields with curl equations (E and H) boundary conditions relate the components parallel to the surface.

$$D_\perp^Q(\xi)\begin{pmatrix}1\\0\end{pmatrix} + D_\perp^{T_8}(\xi)\begin{pmatrix}0\\1\end{pmatrix} - D_\perp^{\tilde{Q}}(-\xi)\begin{pmatrix}\cos\alpha\\\sin\alpha\end{pmatrix} - D_\perp^X(-\xi)\begin{pmatrix}-\sin\alpha\\\cos\alpha\end{pmatrix} = \sigma^{T_8}\begin{pmatrix}0\\1\end{pmatrix} + \sigma^X\begin{pmatrix}-\sin\alpha\\\cos\alpha\end{pmatrix} \tag{5.8}$$

$$E_\parallel^Q(\xi)\begin{pmatrix}1\\0\end{pmatrix} + E_\parallel^{T_8}(\xi)\begin{pmatrix}0\\1\end{pmatrix} - E_\parallel^{\tilde{Q}}(-\xi)\begin{pmatrix}\cos\alpha\\\sin\alpha\end{pmatrix} - E_\parallel^X(-\xi)\begin{pmatrix}-\sin\alpha\\\cos\alpha\end{pmatrix} = K_M^{T_8}\begin{pmatrix}0\\1\end{pmatrix} + K_M^X\begin{pmatrix}-\sin\alpha\\\cos\alpha\end{pmatrix} \tag{5.9}$$

$$B_\perp^Q(\xi)\begin{pmatrix}1\\0\end{pmatrix} + B_\perp^{T_8}(\xi)\begin{pmatrix}0\\1\end{pmatrix} - B_\perp^{\tilde{Q}}(-\xi)\begin{pmatrix}\cos\alpha\\\sin\alpha\end{pmatrix} - B_\perp^X(-\xi)\begin{pmatrix}-\sin\alpha\\\cos\alpha\end{pmatrix} = \sigma_M^{T_8}\begin{pmatrix}0\\1\end{pmatrix} + \sigma_M^X\begin{pmatrix}-\sin\alpha\\\cos\alpha\end{pmatrix} \tag{5.10}$$

$$H_\parallel^Q(\xi)\begin{pmatrix}1\\0\end{pmatrix} + H_\parallel^{T_8}(\xi)\begin{pmatrix}0\\1\end{pmatrix} - H_\parallel^{\tilde{Q}}(-\xi)\begin{pmatrix}\cos\alpha\\\sin\alpha\end{pmatrix} - H_\parallel^X(-\xi)\begin{pmatrix}-\sin\alpha\\\cos\alpha\end{pmatrix} = K^{T_8}\begin{pmatrix}0\\1\end{pmatrix} + K^X\begin{pmatrix}-\sin\alpha\\\cos\alpha\end{pmatrix} \tag{5.11}$$

The σ's and K's are the effective surface charge and current densities, and their presence varies depending on the physical situation being addressed. For Higgsed

generators there are electric surface current and charge densities, for confined gener-

ators there are magnetic surface current and charge densities, and for free generators

there are no surface current or charge densities.
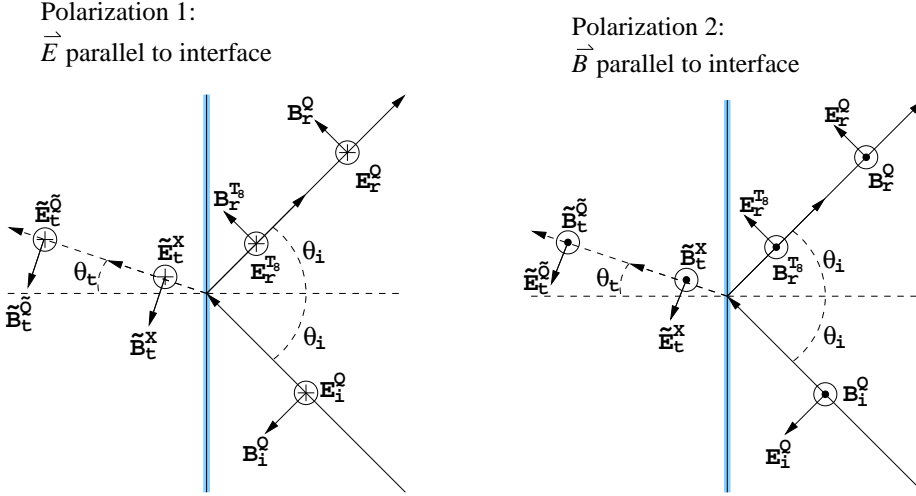
Figure 5.2: Polarizations of the incident photon beam

5.2   Reflection and Transmission at the Interface

In our analysis we treated both possible polarizations, as illustrated in Fig. 5.2. With-

out loss of generality, we assume that the waves incident from $z = +\infty$ will be purely

Q gauge bosons. For free phases, two different types of gauge boson may be reflected

and/or transmitted. It is also assumed that in a phase where both types of gauge

boson are massless, the index of refraction (and hence the ε and μ) is the same for

both.

In addition, the usual rules of optics apply, since they are purely kinematic in

nature [86]. Therefore the angle of reflection equals the angle of incidence, and Snell's

Law applies to the transmitted waves.

To find the transmission and reflection coefficients, we applied the boundary conditions of section 5.1 to the kinematic situations shown in Fig. 5.2. Tables 5.1 and 5.2 show the results of these calculations for the eight non-trivial phase combinations. (Some intermediate results, the transmission/reflection *amplitudes*, are shown and discussed in 5.5).

The shorthand parameters used throughout the calculations are defined as follows:

$$r \equiv \frac{\mu}{\tilde{\mu}}\frac{\tilde{n}}{n} = \sqrt{\frac{\tilde{\varepsilon}\mu}{\varepsilon\tilde{\mu}}}, \tag{5.12}$$

$$c_i \equiv \cos\theta_i, s_i \equiv \sin\theta_i, \tag{5.13}$$

$$c_t \equiv \cos\theta_t, s_t \equiv \sin\theta_t. \tag{5.14}$$

We can eliminate $\cos\theta_t$ from the amplitudes by making use of Snell's Law,

$$n\sin\theta_i = \tilde{n}\sin\theta_t \tag{5.15}$$

$$\rightarrow \cos\theta_t = \sqrt{1 - \frac{n^2}{\tilde{n}^2}\sin^2\theta_i}. \tag{5.16}$$

Reflection and transmission coefficients are defined by

$$R = \frac{I_r}{I_i} \equiv \frac{\vec{S}_{r\perp}}{\vec{S}_{i\perp}} \tag{5.17}$$

$$T = \frac{I_t}{I_i} \equiv \frac{\vec{S}_{t\perp}}{\vec{S}_{i\perp}} \tag{5.18}$$

where I_i, I_r, I_t refer to the incident, reflected, and transmitted intensities, respectively, and $\vec{S}_i, \vec{S}_r, \vec{S}_t$ refer to the incident, reflected, and transmitted Poynting vectors; specif-

ically,

$$
\begin{aligned}
R^Q &= \frac{\hat{z} \cdot \vec{E}_r^Q \times \vec{H}_r^Q}{\hat{z} \cdot \vec{E}_i^Q \times \vec{H}_i^Q} &= \frac{c_r \mathcal{E}_r^{Q2}}{c_i \mathcal{E}_i^{Q2}}, \\[2mm]
R^{T_8} &= \frac{\hat{z} \cdot \vec{E}_r^{T_8} \times \vec{H}_r^{T_8}}{\hat{z} \cdot \vec{E}_i^Q \times \vec{H}_i^Q} &= \frac{c_r \mathcal{E}_r^{T_8\,2}}{c_i \mathcal{E}_i^{T_8\,2}}, \\[2mm]
T^{\tilde{Q}} &= \frac{\hat{z} \cdot \vec{E}_t^{\tilde{Q}} \times \vec{H}_t^{\tilde{Q}}}{\hat{z} \cdot \vec{E}_i^Q \times \vec{H}_i^Q} &= \sqrt{\frac{\tilde{\epsilon}\mu}{\epsilon\tilde{\mu}}} \frac{c_t \mathcal{E}_t^{\tilde{Q}2}}{c_i \mathcal{E}_i^{Q2}}.
\end{aligned}
\tag{5.19}
$$

For clarity, we will illustrate how the calculations leading to tables 5.1 and 5.2 are done by looking at two of the cases in detail. The amplitudes $\mathcal{E}$ give the electric fields associated with the incident, reflected, and transmitted photons,

$$
\begin{aligned}
\vec{E}_i^Q &= \mathcal{E}_i^Q \vec{n}_i \exp(i(\vec{k}_i \cdot \vec{x} - \omega t)) \,, \\[2mm]
\vec{E}_r^{(Q,T_8)} &= \mathcal{E}_r^{(Q,T_8)} \vec{n}_r \exp(i(\vec{k}_r \cdot \vec{x} - \omega t)) \,, \\[2mm]
\vec{E}_t^{\tilde{Q}} &= \mathcal{E}_t^{\tilde{Q}} \vec{n}_t \exp(i(\vec{k}_t \cdot \vec{x} - \omega t)) \,,
\end{aligned}
\tag{5.20}
$$

where $\vec{n}$ is the unit polarization vector for each wave.

5.2.1 T_8 **Free,** X **Confined**

For this combination of phases, the boundary condition equations (5.8), (5.9), (5.10), (5.11) become

$$D_\perp^Q(\xi)\begin{pmatrix}1\\0\end{pmatrix} + D_\perp^{T_8}(\xi)\begin{pmatrix}0\\1\end{pmatrix} - D_\perp^{\tilde{Q}}(-\xi)\begin{pmatrix}\cos\alpha\\\sin\alpha\end{pmatrix} = 0 \tag{5.21}$$

$$E_\parallel^Q(\xi)\begin{pmatrix}1\\0\end{pmatrix} + E_\parallel^{T_8}(\xi)\begin{pmatrix}0\\1\end{pmatrix} - E_\parallel^{\tilde{Q}}(-\xi)\begin{pmatrix}\cos\alpha\\\sin\alpha\end{pmatrix} = K_M^X\begin{pmatrix}-\sin\alpha\\\cos\alpha\end{pmatrix} \tag{5.22}$$

$$B_\perp^Q(\xi)\begin{pmatrix}1\\0\end{pmatrix} + B_\perp^{T_8}(\xi)\begin{pmatrix}0\\1\end{pmatrix} - B_\perp^{\tilde{Q}}(-\xi)\begin{pmatrix}\cos\alpha\\\sin\alpha\end{pmatrix} = \sigma_M^X\begin{pmatrix}-\sin\alpha\\\cos\alpha\end{pmatrix} \tag{5.23}$$

$$H_\parallel^Q(\xi)\begin{pmatrix}1\\0\end{pmatrix} + H_\parallel^{T_8}(\xi)\begin{pmatrix}0\\1\end{pmatrix} - H_\parallel^{\tilde{Q}}(-\xi)\begin{pmatrix}\cos\alpha\\\sin\alpha\end{pmatrix} = 0 \tag{5.24}$$

Dotting the equations with either $\begin{pmatrix}\cos\alpha\\-\sin\alpha\end{pmatrix}$, $\begin{pmatrix}1\\0\end{pmatrix}$, or $\begin{pmatrix}0\\1\end{pmatrix}$ as appropriate yields equations that do not depend on the charge or current densities. In this case, we obtain

$$H_\parallel^Q(\xi) = \cos\alpha H_\parallel^{\tilde{Q}}(-\xi) \tag{5.25}$$

$$H_\parallel^{T_8}(\xi) = \sin\alpha H_\parallel^{\tilde{Q}}(-\xi) \tag{5.26}$$

$$\cos\alpha E_\parallel^Q(\xi) + \sin\alpha E_\parallel^{T_8}(\xi) = E_\parallel^{\tilde{Q}}(-\xi) \tag{5.27}$$

$$\cos\alpha B_\perp^Q(\xi) + \sin\alpha B_\perp^{T_8}(\xi) = B_\perp^{\tilde{Q}}(-\xi) \tag{5.28}$$

For polarization 1 of Fig. 5.2, equations (5.25), (5.26) and (5.28) lead to

$$rc_i(\mathcal{E}_i^Q - \mathcal{E}_r^Q) = \cos\alpha c_t \mathcal{E}_t^{\tilde{Q}} \tag{5.29}$$

$$-rc_i\mathcal{E}_r^{T_8} = \sin\alpha c_t \mathcal{E}_t^{\tilde{Q}} \tag{5.30}$$

$$\cos\alpha(\mathcal{E}_i^Q + \mathcal{E}_r^Q) + \sin\alpha\mathcal{E}_r^{T_8} = \mathcal{E}_t^{\tilde{Q}} \tag{5.31}$$

which can be solved for the amplitudes in Table 5.4, row 5. Using (5.17) and (5.19) we obtain the reflection/transmission coefficients of Table 5.1, row 5.

For polarization 2 of Fig. 5.2, equations (5.25), (5.26) and (5.27) lead to

$$r(\mathcal{E}_i^Q + \mathcal{E}_r^Q) = \cos\alpha\mathcal{E}_t^{\tilde{Q}} \tag{5.32}$$

$$r\mathcal{E}_r^{T_8} = \sin\alpha\mathcal{E}_t^{\tilde{Q}} \tag{5.33}$$

$$c_i(\cos\alpha(\mathcal{E}_i^Q - \mathcal{E}_r^Q) - \sin\alpha\mathcal{E}_r^{T_8}) = c_t\mathcal{E}_t^{\tilde{Q}} \tag{5.34}$$

which can similarly be solved for the amplitudes in Table 5.5, row 5, and reflection/transmission coefficients in Table 5.2, row 5.

5.2.2 T_8 Higgsed, X Higgsed

When there is Higgsing in both regions, the boundary condition equations (5.8)-(5.11)

become

$$D_\perp^Q(\xi) \begin{pmatrix} 1 \\ 0 \end{pmatrix} - D_\perp^{\tilde{Q}}(-\xi) \begin{pmatrix} \cos\alpha \\ \sin\alpha \end{pmatrix} = \sigma^{T_8} \begin{pmatrix} 0 \\ 1 \end{pmatrix} + \sigma^X \begin{pmatrix} -\sin\alpha \\ \cos\alpha \end{pmatrix} \tag{5.35}$$

$$E_\parallel^Q(\xi) \begin{pmatrix} 1 \\ 0 \end{pmatrix} - E_\parallel^{\tilde{Q}}(-\xi) \begin{pmatrix} \cos\alpha \\ \sin\alpha \end{pmatrix} = 0 \tag{5.36}$$

$$B_\perp^Q(\xi) \begin{pmatrix} 1 \\ 0 \end{pmatrix} - B_\perp^{\tilde{Q}}(-\xi) \begin{pmatrix} \cos\alpha \\ \sin\alpha \end{pmatrix} = 0 \tag{5.37}$$

$$H_\parallel^Q(\xi) \begin{pmatrix} 1 \\ 0 \end{pmatrix} - H_\parallel^{\tilde{Q}}(-\xi) \begin{pmatrix} \cos\alpha \\ \sin\alpha \end{pmatrix} = K^{T_8} \begin{pmatrix} 0 \\ 1 \end{pmatrix} + K^X \begin{pmatrix} -\sin\alpha \\ \cos\alpha \end{pmatrix} \tag{5.38}$$

In this case, we find

$$E_\parallel^Q(\xi) = E_\parallel^{\tilde{Q}}(-\xi) = 0 \tag{5.39}$$

$$B_\perp^Q(\xi) = B_\perp^{\tilde{Q}}(-\xi) = 0 \tag{5.40}$$

For polarization 1 of Fig. 5.2, either equation (5.39) or (5.40) leads to the simple

equations

$$\mathcal{E}_i^Q + \mathcal{E}_r^Q = 0 \tag{5.41}$$

$$\mathcal{E}_t^{\tilde{Q}} = 0 \tag{5.42}$$

which shows that waves of this polarization are completely reflected with a 180 degree

phase shift.

119

Table 5.1: Reflection and Transmission Coefficients for Polarization 1. For definitions see (5.12): c_i and c_t are the cosines of the incident and transmitted beams; α is the mismatch between the generators of the free $U(1)$'s in the outside region (Q) and the inside region $(\tilde{Q})$; r is a function of the permittivities and permeabilities of the two regions.

Outer region (T_8)	Inner region (X)	R^Q	R^{T_8}	$T^{\tilde{Q}}$	T^X
Higgsed	Higgsed	1	0	0	0
Confined	Confined	1	0	0	0
Free	Higgsed	$\left(\dfrac{c_i\cos 2\alpha - rc_t}{c_i+rc_t}\right)^2$	$\left(\dfrac{c_i\sin 2\alpha}{c_i+rc_t}\right)^2$	$\dfrac{4rc_ic_t\cos^2\alpha}{(c_i+rc_t)^2}$	0
Higgsed	Free	$\left(\dfrac{c_i-rc_t}{c_i+rc_t}\right)^2$	0	$\dfrac{4rc_ic_t\cos^2\alpha}{(c_i+rc_t)^2}$	$\dfrac{4rc_ic_t\sin^2\alpha}{(c_i+rc_t)^2}$
Free	Confined	$\left(\dfrac{c_i-rc_t\cos 2\alpha}{c_i+rc_t}\right)^2$	$\left(\dfrac{rc_t\sin 2\alpha}{c_i+rc_t}\right)^2$	$\dfrac{4rc_ic_t\cos^2\alpha}{(c_i+rc_t)^2}$	0
Confined	Free	$\left(\dfrac{c_i-rc_t}{c_i+rc_t}\right)^2$	0	$\dfrac{4rc_ic_t\cos^2\alpha}{(c_i+rc_t)^2}$	$\dfrac{4rc_ic_t\sin^2\alpha}{(c_i+rc_t)^2}$
Higgsed	Confined	$\left(\dfrac{c_i-rc_t\cos^2\alpha}{c_i+rc_t\cos^2\alpha}\right)^2$	0	$\dfrac{4rc_ic_t\cos^2\alpha}{(c_i+rc_t\cos^2\alpha)^2}$	0
Confined	Higgsed	$\left(\dfrac{c_i\cos^2\alpha-rc_t}{c_i\cos^2\alpha+rc_t}\right)^2$	0	$\dfrac{4rc_ic_t\cos^2\alpha}{(c_i\cos^2\alpha+rc_t)^2}$	0

For polarization 2 of Fig. 5.2, either equation (5.39) or (5.40) leads to the equally simple equations

$$\mathcal{E}_r^Q - \mathcal{E}_i^Q \;=\; 0 \tag{5.43}$$

$$\mathcal{E}_t^{\tilde{Q}} \;=\; 0 \tag{5.44}$$

which shows that waves of this polarization are completely reflected with no phase shift.

Table 5.2: Reflection and Transmission Coefficients for Polarization 2

Outer region (T_8)	Inner region (X)	R^Q	R^{T_8}	$T^{\tilde{Q}}$	T^X
Higgsed	Higgsed	1	0	0	0
Confined	Confined	1	0	0	0
Free	Higgsed	$\left(\dfrac{rc_i - c_t\cos 2\alpha}{rc_i + c_t}\right)^2$	$\left(\dfrac{c_t\sin 2\alpha}{rc_i + c_t}\right)^2$	$\dfrac{4rc_ic_t\cos^2\alpha}{(rc_i + c_t)^2}$	0
Higgsed	Free	$\left(\dfrac{rc_i - c_t}{rc_i + c_t}\right)^2$	0	$\dfrac{4rc_ic_t\cos^2\alpha}{(rc_i + c_t)^2}$	$\dfrac{4rc_ic_t\sin^2\alpha}{(rc_i + c_t)^2}$
Free	Confined	$\left(\dfrac{rc_i\cos 2\alpha - c_t}{rc_i + c_t}\right)^2$	$\left(\dfrac{rc_i\sin 2\alpha}{rc_i + c_t}\right)^2$	$\dfrac{4rc_ic_t\cos^2\alpha}{(rc_i + c_t)^2}$	0
Confined	Free	$\left(\dfrac{rc_i - c_t}{rc_i + c_t}\right)^2$	0	$\dfrac{4rc_ic_t\cos^2\alpha}{(rc_i + c_t)^2}$	$\dfrac{4rc_ic_t\sin^2\alpha}{(rc_i + c_t)^2}$
Higgsed	Confined	$\left(\dfrac{rc_i\cos^2\alpha - c_t}{rc_i\cos^2\alpha + c_t}\right)^2$	0	$\dfrac{4rc_ic_t\cos^2\alpha}{(rc_i\cos^2\alpha + c_t)^2}$	0
Confined	Higgsed	$\left(\dfrac{rc_i - c_t\cos^2\alpha}{rc_i + c_t\cos^2\alpha}\right)^2$	0	$\dfrac{4rc_ic_t\cos^2\alpha}{(rc_i + c_t\cos^2\alpha)^2}$	0

5.3   Summary and Discussion

We have studied reflection and transmission of gauge bosons at the interface between differently realized phases of a $U(1) \otimes U(1)$ gauge theory. In order to allow gauge bosons to propagate, at least one linear combination of the gauge generators must be free on each side of the interface: this is taken to be Q in the outer region ($z > 0$) and $\tilde{Q}$ in the inner region ($z < 0$). The other generator is T_8 in the outer region and X in the inner region. The possibilities for this other generator are that it can be also free, Higgsed, or confined. The (Q, T_8) basis may in general be rotated by an angle α relative to the $(\tilde{Q}, X)$ basis. Since the Free/Free boundary (T_8 free outside, X free inside) is trivial for any α, this means that there are 8 possible types of boundary. The transmission and reflection coefficients for light arriving at these different types of boundary are given in Tables 5.1 and 5.2. These are complicated so we give a qualitative summary in table 5.3, and we will now discuss the entries in that table.

Table 5.3: Behavior of gauge bosons at an interface in $U(1) \otimes U(1)$ gauge theory for various realizations of the gauge symmetries on each side. The gauge bosons are assumed to arrive as Q-photons from the "outer" phase.

		Inner $(z < 0)$, $\tilde{Q}$ free		
		X Free	X Higgsed	X Confined
	T_8 Free	transmission	Q, T_8 reflection $\tilde{Q}$ transmission	Q, T_8 reflection $\tilde{Q}$ transmission
Outer $(z > 0)$ Q free	T_8 Higgsed	Q reflection $\tilde{Q}, X$ transmission	total reflection	Q reflection $\tilde{Q}$ transmission
	T_8 Confined	Q reflection $\tilde{Q}, X$ transmission	Q reflection $\tilde{Q}$ transmission	total reflection

5.3.1   How the different boundaries behave

If all generators everywhere are free (T_8 and X both free, row 1 column 1 of table 5.3), then there is no distinction between the inner and outer regions other than a possible difference in refractive index, so there will be transmission and reflection as at a dielectric boundary like a glass-air boundary.

If both generators in the outer region are free (T_8 free) but in the inner region X is Higgsed or confined (row 1 columns 2 and 3 of table 5.3), then the gauge bosons are partially reflected and partially transmitted, depending on the angle between $\tilde{Q}$ and Q. However, even though the incident wave is pure Q gauge bosons, there will

be some additional T_8 bosons created and reflected back. The transmitted wave will be pure $\tilde{Q}$ gauge bosons. Similarly, if both generators in the inner region are free (X is free) and in the outer region T_8 is Higgsed or confined (column 1 rows 2 and 3 of table 5.3) then there will be transmission of both $\tilde{Q}$ and X, adding up to make a Q-photon.

If there is only one free generator in each region, Q on the outside and $\tilde{Q}$ on the inside, then the reflected wave must be pure Q-photons and the transmitted wave must be pure $\tilde{Q}$ photons. If the broken generator is Higgsed on one side and confined on the other then there is partial reflection and partial transmission (row 2 column 3 and column 3 row 2 of table 5.3). This was the case studied in [55].

If the broken generators on the inside and outside are both Higgsed, or both confined then the behavior is very different. Electromagnetic waves are *completely reflected* at an interface between two Higgsed phases with different values of α (row 2 column 2 of table 5.3) or between two confined phases where the confined gauge fields are different linear combinations of Q and T_8 (row 3 column 3 of table 5.3). In addition, since one polarization is flipped in each case while the other stays the same, left circularly polarized waves are reflected as right circularly polarized waves, and vice versa. This raises an interesting puzzle: the Higgs/Higgs and confined/confined boundaries both show total reflection independent of the value of α. But when $\alpha = 0$ both phases have identical unbroken gauge generators, so the interface is just a boundary between two media with different dielectric constants, and there should be some transmission. In fact, in the limit $(\tilde{\epsilon}, \tilde{\mu}) \rightarrow (\epsilon, \mu)$ there is no boundary, and there

must be total transmission. This paradox is analyzed below.

5.3.2   Compatibility with previous results

In Ref. [55], Manuel and Rajagopal studied the case where X is Higgsed on the inside and T_8 is confined on the outside, and our results for that case agree with theirs. One of their main conclusions was that it is possible to use light reflection calculations to show that there are magnetic monopoles in the QCD vacuum. Their argument was that the situation they studied corresponds to the boundary between the confining QCD vacuum and color-superconducting quark matter, and for that situation they derived the confining boundary condition for T_8 color-magnetic flux, which tells us there are T_8 magnetic monopoles in the boundary region, from a few basic assumptions, namely: (1) color is not Higgsed, so there are no color (T_8) supercurrents in the boundary layer; (2) no gluons (ie T_8 gauge bosons) propagate in the confined phase; (3) conservation of energy; (4) Snell's law for the angles of reflection and transmission.

This result can be obtained more directly, without using light reflection calculations, from considerations of static electromagnetic fields at an interface using assumptions (1) and (2) alone. Consider what must happen to $\tilde{Q}$ magnetic flux lines that arrive at the boundary from the quark matter side. Their T_8 component cannot penetrate into the QCD vacuum region, since color is confined there (assumption (2)), and they cannot be turned back into the quark matter region by the Meissner effect because there are no T_8 supercurrents in the boundary layer (assumption (1)). So the flux lines have to end. This means that at the edge of a color-confined phase there

must be a boundary layer of color magnetic monopoles that eat up any unwanted color magnetic flux that might try to enter the confined region.

5.3.3 The singular $\alpha \to 0$ limit

We now turn to the paradoxical behavior of the Higgsed/Higgsed and confined/confined interfaces, which seem to always reflect all light even in the limit $\alpha \to 0$, where the interface becomes a typical dielectric boundary which ought to transmit at least some light. To understand this we have to be careful about specifying the wavelength of the light that is incident on the boundary.

As mentioned in section 5.1, throughout our calculations we have worked in the limit of long wavelength relative to the penetration depth, $\lambda \gg \xi$. This corresponds to the low frequency limit, $\omega \ll c/\xi$. It turns out that, for the Higgsed/Higgsed and confined/confined interfaces, the limit of low frequency does not commute with the limit $\alpha \to 0$ in which the unbroken $U(1)$'s on either side of the boundary become the same. An explicit calculation for the Higgs-Higgs boundary at finite α and ω is given in section 5.4.

We can summarize the result as follows. For polarization 1 (the argument for polarization 2 is analogous) the transmission amplitude at low frequency ($\omega\xi \ll c$) and small α is of the form

$$\frac{\omega\xi}{\omega\xi + i\alpha^2 c} \tag{5.45}$$

where ξ is the penetration depth, and dimensionless factors of order one (cosines of angles, etc) have been omitted. In the limit where $\omega \to 0$ first, $\omega\xi \ll \alpha^2 c \ll c$,

the transmission amplitude is zero: this is the total reflection expressed in the first two rows of tables 5.1 and 5.2. In the limit where $\alpha \to 0$ first, $\alpha^2 c \ll \omega \xi \ll c$, the transmission amplitude is of order 1: this is what we expect when there is no mismatch between the unbroken $U(1)$'s at the boundary. We conclude that the paradox is resolved in this way: at small α there is total reflection for frequencies below $\alpha^2 c / \xi$, but higher frequencies are transmitted. As $\alpha \to 0$ the range of reflected frequencies becomes smaller and smaller, and finally disappears.

For most of the boundaries we studied, the two limits commute, and we can, without ambiguity, work at arbitrarily low frequency, and discuss how the reflection and transmission depend on α. But for the Higgs/Higgs and confined/confined boundaries the order of the limits must be specified.

5.3.4   Complementarity

The complementarity principle [87] states that for any Higgsed description of a gauge theory there should be a corresponding confined description, so that there is no way to distinguish a confined phase from a Higgs phase. Since the Higgs phase involves condensation of electrically charged fields, while the confined phase involves condensation of magnetically charged fields, we expect that the confined $\rightleftharpoons$ Higgs mapping will involve a magnetic $\rightleftharpoons$ electric duality transformation. Exchanging magnetic and electric fields converts polarization 1 into polarization 2 (see Fig. 5.2), so the confined $\rightleftharpoons$ Higgs mapping will be

$$
\begin{aligned}
\vec{E} &\rightarrow \vec{H}, & \vec{H} &\rightarrow -\vec{E}, \\
\vec{D} &\rightarrow \vec{B}, & \vec{B} &\rightarrow -\vec{D}, \\
q_e &\rightarrow q_m, & q_m &\rightarrow -q_e, \\
\vec{J}_e &\rightarrow \vec{J}_m, & \vec{J}_m &\rightarrow -\vec{J}_e,
\end{aligned}
$$

$$\tilde{\epsilon} \rightleftharpoons \tilde{\mu},$$

$$r \rightleftharpoons 1/r$$

(5.46)

$$\text{polarization } 1 \rightleftharpoons \text{polarization } 2$$

$$\text{Higgsed} \rightleftharpoons \text{Confined}$$

Since the reflection and transmission coefficients are related to the energy and momentum flow in the scattering process, they are directly observable, and should be invariant under the duality transformation (5.46). Inspecting tables 5.1 and 5.2 we see that this is indeed the case. For example, the reflection and transmission coefficients for the Higgsed-Free boundary (third line of table 5.1) are transformed into those for the Confined-Free boundary (fifth line in table 5.2). In other words, if we shine light on a boundary and obtain the results of table 5.1 line 3, then we could not distinguish whether the outside phase is Higgsed or confined.

This means that by measuring only the reflected and transmitted indensities, we can only distinguish 4 of the 8 types of non-trivial boundary. What is clear from tables 5.1 and 5.2 is that this ambiguity only exists as a single global choice. There is not a separate confined vs. Higgs choice for each phase independently. This is exactly what we expect from the principle of complementarity.

One might naively think that it should be possible to overcome this ambiguity

by measuring the electric and magnetic fields (which are also gauge-invariant and physically measureable) directly. Carefully constructing the corresponding thought-experiment shows that this does not in fact overcome the ambiguity: we discuss this in section 5.5.

5.3.5   Future directions

As mentioned in the introduction, the $U(1) \otimes U(1)$ system arises in various contexts within particle physics, and the results of this paper may be applied to domain walls or phase boundaries in those contexts. The same formalism can also be used for more general gauge groups, as in the work of Manuel and Rajagopal [55]. Quark matter provides a possible area of application, since it has a rich phase diagram, including a variety of patterns of confinement or Higgsing of various subgroups of the $SU(3)_{\text{color}} \otimes U(1)_Q$ gauge group [50].

Finally, in our analysis we only concerned ourselves with the gauge symmetries, not with any global symmetries. If massless fermionic fields are included in the theory then chiral symmetry complicates the complementarity principle [88]. It would be interesting to see how this affects the distinguishability of our $U(1) \otimes U(1)$ interfaces. One immediate question is the contradiction between Ref. [88], which predicts that chiral symmetries will not not be broken in weakly-coupled Higgsed phases, and the accepted picture of high-density quark matter, according to which CFL pairing produces Higgs breaking of the color gauge symmetry and simultaneously breaks chiral symmetry. This is crucial to the concept of quark-hadron continuity, which

identifies the CFL phase as a controlled continuation of the confined phase.

5.4   Non-zero-frequency effects

The macroscopic calculations of section 5.1 are performed under the simplifying assumption that the frequencies are very small, and therefore the time-derivative terms in the Maxwell equations are neglected. It is also assumed that the Higgsed or confined fields are quickly screened, so the field amplitudes are set to zero from the beginning. The advantage of this approach is that the spatial behavior of the screened fields and the screening currents does not have to be determined, so the solution is straightforward. However, any finite frequency effects are thrown away, and as mentioned in section 5.3.3, Higgsed/Higgsed and confined/confined interfaces have singular behavior in the $\alpha \to 0$ limit. To rectify this problem, we performed the calculation again for the Higgsed/Higgsed combination, keeping the contributions of screened fields and finite frequency.

First, we briefly review the behavior of electromagnetic fields in a superconductor. In addition to the Maxwell equations (5.5), we have the London equations (see Ref. [89], chapter 34)

$$
\begin{aligned}
\frac{d\vec{J}}{dt} &= \gamma \vec{E}, \\
\vec{\nabla} \times \vec{J} &= -\gamma \vec{B}
\end{aligned}
\tag{5.47}
$$

that describe how the supercurrents respond to applied fields. The parameter γ depends on microscopic details such as the density and charge of Cooper pairs that

make up the supercurrents, but the details are not important for this discussion. Inserting equations (5.47) into the "curl" equation for $\vec{B}$, we obtain the wave equation for the magnetic field in the superconductor,

$$\nabla^2 \vec{B} = \mu\gamma\vec{B} + \frac{1}{c^2}\frac{\partial^2 \vec{B}}{\partial t^2} \tag{5.48}$$

From dimensional considerations the definition of the screening length ξ is defined as

$$\xi \equiv \frac{1}{\sqrt{\mu\gamma}} \tag{5.49}$$

and the solutions of the wave equation have the form

$$\vec{B} = \vec{B_0}\exp\left[\vec{\kappa}\cdot\vec{x} - i\omega t\right]. \tag{5.50}$$

Plugging this solution back into the wave equation obtains the magnitude of the wavevector,

$$|\kappa| = \pm\sqrt{\frac{1}{\xi^2} - \frac{\omega^2}{c^2}}. \tag{5.51}$$

For frequencies less than c/ξ, the waves are completely damped, while for frequencies greater than c/ξ, the waves propagate without any damping. For $\omega = c/\xi$, the wave has no spatial variation and only oscillates in time. The choice of the positive or negative solution for the wavevector depends on the boundary conditions of the superconducting phase. We can obtain identical wave equations for $\vec{J}$ and $\vec{E}$; since we are still interested in the low-frequency limit, we can use the limiting value $|\kappa| = \pm\xi^{-1}$ to obtain the magnitudes of the current and the electric field as

$$|J_0| = \mp\xi\gamma|B_0|,$$

$$|E_0| = \pm i\omega\xi|B_0| \tag{5.52}$$

For the Higgsed/Higgsed phase combination, the Higgsed fields on either side of

the boundary will satisfy the equations above. Explicitly, we have

$$
\begin{aligned}
\vec{E}_i^Q &= \mathcal{E}_i^Q \vec{n}_i \exp(i(\vec{k}_i \cdot \vec{x} - \omega t)) \ , \\[1.2em]
\vec{E}_r^Q &= \mathcal{E}_r^Q \vec{n}_r \exp(i(\vec{k}_r \cdot \vec{x} - \omega t)) \ , \\[1.2em]
\vec{E}_r^{T_8} &= \mathcal{E}_r^{T_8} \vec{n}_r \exp(-\vec{\kappa}_r \cdot \vec{x} - i\omega t) \ , \\[1.2em]
\vec{E}_t^{\tilde{Q}} &= \mathcal{E}_t^{\tilde{Q}} \vec{n}_t \exp(i(\vec{k}_t \cdot \vec{x} - \omega t)), \\[1.2em]
\vec{E}_t^X &= \mathcal{E}_t^X \vec{n}_t \exp(+\vec{\kappa}_t \cdot \vec{x} - i\omega t)) \ ,
\end{aligned}
\tag{5.53}
$$

The "$\mathcal{E}$" amplitudes are the magnitudes of the electric field at the boundary itself

($z = 0$); all screening is due to the spatial terms.

Now we will rewrite the boundary condition equations keeping everything that

was thrown away previously. The "curl" equations are sufficient to solve for the field

amplitudes. We obtain

$$
E_\parallel^Q \begin{pmatrix} 1 \\ 0 \end{pmatrix} + E_\parallel^{T_8} \begin{pmatrix} 0 \\ 1 \end{pmatrix} - E_\parallel^{\tilde{Q}} \begin{pmatrix} \cos\alpha \\ \sin\alpha \end{pmatrix} - E_\parallel^X \begin{pmatrix} -\sin\alpha \\ \cos\alpha \end{pmatrix}
$$

$$
= \frac{i\omega}{\kappa_z} B_\parallel^{T_8} \begin{pmatrix} 0 \\ 1 \end{pmatrix} + \frac{i\omega}{\tilde{\kappa}_z} B_\parallel^X \begin{pmatrix} -\sin\alpha \\ \cos\alpha \end{pmatrix} \tag{5.54}
$$

$$
B_\parallel^Q \begin{pmatrix} 1 \\ 0 \end{pmatrix} + \left(1 - \frac{1}{\xi\kappa_z}\right) B_\parallel^{T_8} \begin{pmatrix} 0 \\ 1 \end{pmatrix} - B_\parallel^{\tilde{Q}} \begin{pmatrix} \cos\alpha \\ \sin\alpha \end{pmatrix}
$$

$$
- \left(1 + \frac{1}{\tilde{\xi}\tilde{\kappa}_z}\right) B_\parallel^X \begin{pmatrix} -\sin\alpha \\ \cos\alpha \end{pmatrix}
$$

$$
= -\frac{i\omega}{c^2\kappa_z} E_\parallel^{T_8} \begin{pmatrix} 0 \\ 1 \end{pmatrix} - \frac{i\omega}{\tilde{c}^2\tilde{\kappa}_z} E_\parallel^X \begin{pmatrix} -\sin\alpha \\ \cos\alpha \end{pmatrix} \tag{5.55}
$$

For polarization 1 of Figure 5.2, the solutions for the amplitudes are

$$
\frac{\mathcal{E}_r^Q}{\mathcal{E}_i^Q} = \frac{\omega\tilde{\xi}(c_i - \cos^2\alpha\frac{\tilde{n}}{n}c_t) + ic(1 + c_t)\sin^2\alpha}{\omega\tilde{\xi}(c_i + \cos^2\alpha\frac{\tilde{n}}{n}c_t) - ic(1 + c_t)\sin^2\alpha}
$$

$$
\frac{\mathcal{E}_r^{T_8}}{\mathcal{E}_i^Q} = \frac{\sin 2\alpha\,\omega\xi c_i(1 + c_t)}{\omega\tilde{\xi}(c_i + \cos^2\alpha\frac{\tilde{n}}{n}c_t) - ic(1 + c_t)\sin^2\alpha}
$$

$$
\frac{\mathcal{E}_t^{\tilde{Q}}}{\mathcal{E}_i^Q} = \frac{2\cos\alpha\,\omega\tilde{\xi}c_i}{\omega\tilde{\xi}(c_i + \cos^2\alpha\frac{\tilde{n}}{n}c_t) - ic(1 + c_t)\sin^2\alpha} \tag{5.56}
$$

$$
\frac{\mathcal{E}_t^X}{\mathcal{E}_i^Q} = \frac{2\sin\alpha\,\omega\tilde{\xi}c_i}{\omega\tilde{\xi}(c_i + \cos^2\alpha\frac{\tilde{n}}{n}c_t) - ic(1 + c_t)\sin^2\alpha}.
$$

Taking the $\omega \to 0$ limit, we recover the amplitudes of the first row of Table 5.4 presented below in section 5.5. However, more importantly, taking the $\alpha \to 0$ limit

first, we obtain

$$
\begin{aligned}
\mathcal{E}_r^Q &= \mathcal{E}_i^Q \left[\frac{c_i - \frac{\tilde{n}}{n}c_t}{c_i + \frac{\tilde{n}}{n}c_t} \right] \\
\mathcal{E}_r^{T_8} &\to 0 \\
\mathcal{E}_t^{\tilde{Q}} &= \mathcal{E}_i^Q \left[\frac{2c_i}{c_i + \frac{\tilde{n}}{n}c_t} \right] \\
\mathcal{E}_t^X &\to 0,
\end{aligned}
\tag{5.57}
$$

which are the normal reflection and refraction amplitudes from electrodynamics. Similarly, for polarization 2 of Figure 5.2, the solutions for the amplitudes are

$$
\begin{aligned}
\frac{\mathcal{E}_r^Q}{\mathcal{E}_i^Q} &= \frac{2\omega\left[\xi(1+c_i^2)(1+c_t)(\frac{\tilde{n}}{n}c_i - \cos^2\alpha c_t) - \tilde{\xi}(1+c_i)(1+c_t^2)(\cos^2\alpha\frac{\tilde{n}}{n}c_i - c_t)\right] + 2i\sin^2\alpha cc_ic_t(1+c_i)(1+c_t)}{2\omega\left[\xi(1+c_i^2)(1+c_t)(\frac{\tilde{n}}{n}c_i + \cos^2\alpha c_t) - \tilde{\xi}(1+c_i)(1+c_t^2)(\cos^2\alpha\frac{\tilde{n}}{n}c_i + c_t)\right] + 2i\sin^2\alpha cc_ic_t(1+c_i)(1+c_t)} \\[2mm]
\frac{\mathcal{E}_r^{T_8}}{\mathcal{E}_i^Q} &= \frac{-2\omega\xi\sin 2\alpha c_i^2 c_t(1+c_t)}{2\omega\left[\xi(1+c_i^2)(1+c_t)(\frac{\tilde{n}}{n}c_i + \cos^2\alpha c_t) - \tilde{\xi}(1+c_i)(1+c_t^2)(\cos^2\alpha\frac{\tilde{n}}{n}c_i + c_t)\right] + 2i\sin^2\alpha cc_ic_t(1+c_i)(1+c_t)} \\[2mm]
\frac{\mathcal{E}_t^{\tilde{Q}}}{\mathcal{E}_i^Q} &= \frac{4\omega\cos\alpha c_i\left[\xi(1+c_i^2)(1+c_t) - \tilde{\xi}(1+c_i)(1+c_t^2)\right]}{2\omega\left[\xi(1+c_i^2)(1+c_t)(\frac{\tilde{n}}{n}c_i + \cos^2\alpha c_t) - \tilde{\xi}(1+c_i)(1+c_t^2)(\cos^2\alpha\frac{\tilde{n}}{n}c_i + c_t)\right] + 2i\sin^2\alpha cc_ic_t(1+c_i)(1+c_t)} \\[2mm]
\frac{\mathcal{E}_t^X}{\mathcal{E}_i^Q} &= \frac{4\omega\tilde{\xi}\sin\alpha c_i(1+c_i)c_t^2}{2\omega\left[\xi(1+c_i^2)(1+c_t)(\frac{\tilde{n}}{n}c_i + \cos^2\alpha c_t) - \tilde{\xi}(1+c_i)(1+c_t^2)(\cos^2\alpha\frac{\tilde{n}}{n}c_i + c_t)\right] + 2i\sin^2\alpha cc_ic_t(1+c_i)(1+c_t)}.
\end{aligned}
\tag{5.58}
$$

Once again, taking the $\omega \to 0$ limit, we recover the amplitudes of the first row of Table 5.5 presented below in section 5.5. Taking the $\alpha \to 0$ limit first, we obtain

$$
\begin{aligned}
\mathcal{E}_r^Q &= \mathcal{E}_i^Q \left[\frac{\frac{\tilde{n}}{n}c_i - c_t}{\frac{\tilde{n}}{n}c_i + c_t} \right] \\
\mathcal{E}_r^{T_8} &\to 0 \\
\mathcal{E}_t^{\tilde{Q}} &= \mathcal{E}_i^Q \left[\frac{2c_i}{\frac{\tilde{n}}{n}c_i + c_t} \right] \\
\mathcal{E}_t^X &\to 0,
\end{aligned}
\tag{5.59}
$$

the normal reflection and refraction amplitudes for perpedicularly polarized light.

This shows that our "singular" limit problem is actually an order-of-limits problem. For most of the possible phase combinations, we could take the $\omega \to 0$ limit

at the beginning and not encounter any problems, but for the Higgsed/Higgsed or confined/confined phases, that is incorrect. Although the frequency drops out in the $\alpha \to 0$ limit, we need to keep a nonzero frequency value to obtain the correct expression.

5.5   Field strengths and complementarity

In tables 5.4 and 5.5 we show the reflection and transmission *amplitudes*, i.e. the ratios between electric field strengths in the incident, reflected, and transmitted beams. It is clear that the transmission amplitudes do not show invariance under the duality transformation (5.46). Does this mean that measurements of electric and magnetic fields can overcome the complementarity ambiguity and distinguish a Higgsed phase from a confined phase? In this section, we show that although electric and magnetic fields are gauge-invariant quantities, what can actually be measured is the force exerted on a charge, so that even experiments that seem to directly measure field strengths suffer from the Higgsed/confined ambiguity.

For illustrative purposes, we calculate the Lorentz force on a test charge in the inner phase due to electromagnetic waves transmitted from the outer phase. First, we will calculate the force in the case where the outer phase is confined and the inner phase is Higgsed; then we will calculate the force in the dual picture, where the outer phase is Higgsed and the inner phase is confined. We will see that although the transmission amplitudes are not invariant under the duality transformation, the

Table 5.4: Reflected and Transmitted Amplitudes for Polarization 1

Outer region (T_8)	Inner region (X)	$\mathcal{E}_r^Q/\mathcal{E}_i^Q$	$\mathcal{E}_r^{T_8}/\mathcal{E}_i^Q$	$\mathcal{E}_t^{\tilde{Q}}/\mathcal{E}_i^Q$	$\mathcal{E}_t^X/\mathcal{E}_i^Q$
Higgsed	Higgsed	-1	0	0	0
Confined	Confined	1	0	0	0
Free	Higgsed	$\dfrac{c_i \cos 2\alpha - rc_t}{c_i + rc_t}$	$\dfrac{c_i \sin 2\alpha}{c_i + rc_t}$	$\dfrac{2c_i \cos \alpha}{c_i + rc_t}$	0
Higgsed	Free	$\dfrac{c_i - rc_t}{c_i + rc_t}$	0	$\dfrac{2c_i \cos \alpha}{c_i + rc_t}$	$\dfrac{-2c_i \sin \alpha}{c_i + rc_t}$
Free	Confined	$\dfrac{c_i - rc_t \cos 2\alpha}{c_i + rc_t}$	$\dfrac{-rc_t \sin 2\alpha}{c_i + rc_t}$	$\dfrac{2c_i \cos \alpha}{c_i + rc_t}$	0
Confined	Free	$\dfrac{c_i - rc_t}{c_i + rc_t}$	0	$\dfrac{2c_i \cos \alpha}{c_i + rc_t}$	$\dfrac{-2c_i \sin \alpha}{c_i + rc_t}$
Higgsed	Confined	$\dfrac{c_i - rc_t \cos^2\alpha}{c_i + rc_t \cos^2\alpha}$	0	$\dfrac{2c_i \cos \alpha}{c_i + rc_t \cos^2\alpha}$	0
Confined	Higgsed	$\dfrac{c_i \cos^2\alpha - rc_t}{c_i \cos^2\alpha + rc_t}$	0	$\dfrac{2c_i \cos \alpha}{c_i \cos^2\alpha + rc_t}$	0

physically measureable quantity, force, is invariant.

A linearly polarized electromagnetic wave is sent from the outside, through the interface, to the inside, where its effect on a test charge is measured. On the outside, we calibrate the wave by measuring how it causes an electric Q charge to move, and from the induced motion we measure the electric field strength $\mathcal{E}_i$. On the inside, the transmitted wave causes an electric $\tilde{Q}$ charge to move, and the resulting motion allows calculation of the force. For our example, we assume the wave to be in polarization 1 of figure 5.2. As we have calculated in this paper, the transmitted $\tilde{Q}$-fields and the

Table 5.5: Reflected and Transmitted Amplitudes for Polarization 2

Outer region (T_8)	Inner region (X)	$\mathcal{E}_r^Q/\mathcal{E}_i^Q$	$\mathcal{E}_r^{T_8}/\mathcal{E}_i^Q$	$\mathcal{E}_t^{\tilde{Q}}/\mathcal{E}_i^Q$	$\mathcal{E}_t^X/\mathcal{E}_i^Q$
Higgsed	Higgsed	1	0	0	0
Confined	Confined	-1	0	0	0
Free	Higgsed	$\dfrac{rc_i - c_t\cos 2\alpha}{rc_i + c_t}$	$\dfrac{-c_t\sin 2\alpha}{rc_i + c_t}$	$\dfrac{2c_i\cos\alpha}{rc_i + c_t}$	0
Higgsed	Free	$\dfrac{rc_i - c_t}{rc_i + c_t}$	0	$\dfrac{2c_i\cos\alpha}{rc_i + c_t}$	$\dfrac{-2c_i\sin\alpha}{rc_i + c_t}$
Free	Confined	$\dfrac{rc_i\cos 2\alpha - c_t}{rc_i + c_t}$	$\dfrac{rc_i\sin 2\alpha}{rc_i + c_t}$	$\dfrac{2c_i\cos\alpha}{rc_i + c_t}$	0
Confined	Free	$\dfrac{rc_i - c_t}{rc_i + c_t}$	0	$\dfrac{2c_i\cos\alpha}{rc_i + c_t}$	$\dfrac{-2c_i\sin\alpha}{rc_i + c_t}$
Higgsed	Confined	$\dfrac{rc_i\cos^2\alpha - c_t}{rc_i\cos^2\alpha + c_t}$	0	$\dfrac{2c_i\cos\alpha}{rc_i\cos^2\alpha + c_t}$	0
Confined	Higgsed	$\dfrac{rc_i - c_t\cos^2\alpha}{rc_i + c_t\cos^2\alpha}$	0	$\dfrac{2c_i\cos\alpha}{rc_i + c_t\cos^2\alpha}$	0

force are

$$\vec{E}_t = -\hat{z}\mathcal{E}_t,$$

$$\vec{B}_t = (-c_t\hat{x} + s_t\hat{y})\frac{1}{\tilde{c}}\mathcal{E}_t,$$

$$\vec{F} = -q_e\mathcal{E}_i\left(\frac{2c_i\cos 2\alpha}{c_i + rc_t}\right)\times$$
$$\left(\hat{z}\left(1 + \frac{v_x s_t + v_y c_t}{\tilde{c}}\right) + \hat{y}\frac{v_z c_t}{\tilde{c}} + \hat{x}\frac{v_z s_t}{\tilde{c}}\right) \tag{5.60}$$

Now transform to the dual picture, where the outer phase is Higgsed and the inner phase is confined, using the transformation (5.46). Our calibration experiment now appears to have involved a magnetic charge, feeling a "Lorentz" force

$$\vec{F} = q_m(\vec{H} - \vec{v} \times \vec{D}). \tag{5.61}$$

136

The transmitted wave is in polarization state 2, with

$$\vec{H} = -\hat{z}\sqrt{\frac{\tilde{\epsilon}}{\tilde{\mu}}}\mathcal{E}'_t,$$

$$\vec{D} = (c_t\hat{x} - s_t\hat{y})\tilde{\epsilon}\mathcal{E}'_t,$$

$$\vec{F} = -q_m\mathcal{E}'_i\sqrt{\frac{\tilde{\epsilon}}{\tilde{\mu}}}\left(\frac{2c_i\cos 2\alpha}{rc_i + c_t}\right) \times$$

$$\left(\hat{z}\left(1 + \frac{v_x s_t + v_y c_t}{\tilde{c}}\right) + \hat{y}\frac{v_z c_t}{\tilde{c}} + \hat{x}\frac{v_z s_t}{\tilde{c}}\right) \tag{5.62}$$

However, $\mathcal{E}'_i$ and $\mathcal{E}_i$ are not equal; because of the switch between electric and magnetic fields, the amplitude of the waves at their source will be calibrated so that

$$\mathcal{E}'_i = \sqrt{\frac{\mu}{\epsilon}}\mathcal{E}_i. \tag{5.63}$$

Finally, we find that, in terms of the original incident amplitude $\mathcal{E}_i$, the force measured in the inner phase is

$$\vec{F} = -q_m\mathcal{E}_i r\left(\frac{2c_i\cos 2\alpha}{rc_i + c_t}\right) \times$$

$$\left(\hat{z}\left(1 + \frac{v_x s_t + v_y c_t}{\tilde{c}}\right) + \hat{y}\frac{v_z c_t}{\tilde{c}} + \hat{x}\frac{v_z s_t}{\tilde{c}}\right) \tag{5.64}$$

By taking the force calculated in the first picture (equation (5.60)), applying the duality transformation $r \to 1/r$ and then replacing q_e by q_m (which were assumed to have equal magnitudes), we end up with the expression of the force measured in the second picture (equation (5.64)). Since the two pictures are equivalent, the ambiguity remains and cannot be resolved by an attempt to measure the field amplitudes.

Bibliography

[1] M. G. Alford, Nucl. Phys. A830:385c-392c (2009)

[2] F. Weber, "Pulsars as Astrophysical Laboratories for Nuclear and Particle Physics", Chapters 1 and 3, Institute of Physics Publishing, Bristol, UK, 1999.

[3] F. Weber, R. Negreiros, P. Rosenfield, arxiv:0705.2708 (2007)

[4] J. R. Schrieffer, "Theory of Superconductivity", Perseus Books, 3rd ed., Reading, 1983.

[5] G. Baym, C. Pethick, D. Pines, Nature 224, 673 (1969).

[6] M. Alpar, S. Langer, and J. Sauls, Astrophys. J. 282, 533 (1984); for a relativistic treatment see also G. L. Comer and R. Joynt, Phys. Rev. D **68**, 023002 (2003) [arXiv:gr-qc/0212083].

[7] B. Link, Phys. Rev. Lett. **91**, 101101 (2003) [arXiv:astro-ph/0302441].

[8] P. B. Jones, Phys. Rev. Lett. **92**, 149001 (2004).

[9] A. Sedrakian, arXiv:astro-ph/0408467.

[10] K. B. W. Buckley, M. A. Metlitski and A. R. Zhitnitsky, Phys. Rev. Lett. **92**, 151102 (2004) [arXiv:astro-ph/0308148]; Phys. Rev. C **69**, 055803 (2004) [arXiv:hep-ph/0403230].

[11] A. L. Fetter and J. D. Walecka, "Quantum Theory of Many-Particle Systems", McGraw-Hill, 1971.

[12] M. Tinkham, "Introduction to Superconductivity", 2nd ed., (McGraw-Hill, 1996). Sections (3.1) and (3.4.2).

[13] Mark Alford, Gerald Good, and Sanjay Reddy, Phys. Rev. **C72** 055801 (2005), arXiv:nucl-th/0505025.

[14] Mark G. Alford and Gerald Good, Phys. Rev. **B78** 024510 (2008), arXiv:0712.1810.

[15] E. Babaev and J. M. Speight, Phys. Rev. B **72**, 180502(R) (2005) [arXiv:cond-mat/0411681].

[16] D. J. Dean and M. Hjorth-Jensen, Rev. Mod. Phys. **75**, 607 (2003) [arXiv:nucl-th/0210033].

[17] H. Muther and W. H. Dickhoff, Phys. Rev. C **72**, 054313 (2005) [arXiv:nucl-th/0508035].

[18] A. Fabrocini, S. Fantoni, A. Y. Illarionov and K. E. Schmidt, Phys. Rev. Lett. **95**, 192501 (2005) [arXiv:nucl-th/0607034].

[19] D. Page, U. Geppert and F. Weber, Nucl. Phys. A **777**, 497 (2006) [arXiv:astro-ph/0508056].

[20] E. Babaev, Phys. Rev. D **70**, 043001 (2004) [arXiv:astro-ph/0211345].

[21] R. MacKenzie, M. A. Vachon and U. F. Wichoski, Phys. Rev. D **67**, 105024 (2003) [arXiv:hep-th/0301188].

[22] A. F . Andreev and E. Bashkin, Sov. Phys. JETP **42**, 164 (1975); see also G. E. Volvic, V. P. Mineev, and I. M. Khalatnikov, Sov. Phys. JETP **42**, 342 (1975).

[23] G. A. Vardanyan, D. M. Sedrakyan, Sov. Phys. JETP **54**, 919 (1981); D. M. Sedrakyan, K. M. Shahabasyan, Sov. Phys. Usp. **34**, 555 (1991).

[24] N. Andersson, Astrophys. J. **502** (1998) 708-713, [gr-qc/9706075].

[25] L. Lindblom, astro-ph/0101136.

[26] B. J. Owen *et. al.*, Phys. Rev. **D58** (1998) 084020, [gr-qc/9804044].

[27] P. Haensel, K. P. Levenfish, and D. G. Yakovlev, Astron. Astrophys. **357** (2000) 1157-1169, [astro-ph/0004183].

[28] P. Haensel, K. P. Levenfish, and D. G. Yakovlev, Astron. Astrophys. **372** (June, 2001) 130-137, [astro-ph0103290].

[29] N. Andersson, G. L. Comer, and K. Glampedakis, Nucl. Phys. **A763** (2005), 212-229, [astro-ph/0411748].

[30] D. Chatterjee and D. Bandyopadhay, Phys. Rev. **D75** (2007) 123006, [astro-ph/0702259].

[31] M. .E. Gusakov, Phys. Rev. **D76** (2007) 083001, [arXiv:0704.1071].

[32] D. Chatterjee and D. Bandyopadhay, arXiv:0712.4347.

[33] L. Lindblom and B. J. Owen, Phys. Rev **D65** (2002) 063006, [astro-ph/0110558].

[34] P. Haensel, K. P. Levenfish, and D. G. Yakovlev, Astron. Astrophys. **381** (Jan 2002) 1080-1089, [astro-ph/0110575].

[35] D. Chatterjee and D. Bandyopadhay, Astrophys. J. **680** (June, 2008) 686-694, [arXiv:0712.3171].

[36] J. Madsen, Phys. Rev. Lett. **85** (2000) 10-13, [astro-ph/9912418].

[37] J. Madsen, Phys. Rev. **D46** (1992) 3290-3295.

[38] B. A. Sa'd, I. A. Shovkovy, and D. H. Rischke, Phys. Rev. **D75** (2007) 125004, [astro-ph/0703016].

[39] C. Manuel, A. Dobado, and F. J. Llanes-Estrada, JHEP **09** (2005) 076, [hep-ph/0406058].

[40] M. G. Alford and A. Schmitt, J. Phys **G34** (2007) 67-102, [nucl-th/0608019].

[41] B. A. Sa'd, I. A. Shovkovy, and D. H. Rischke, Phys. Rev. **D75** (2007) 065016, [astro-ph/0607643].

[42] C. Manuel and F. J. Llanes-Estrada, JCAP **0708** (2007) 001, [arXiv:0705.3909].

[43] H. Dong, N. Su, and Q. Wang, J. Phys. **G34** (2007) S643-6476, [astro-ph/0702181].

[44] M. G. Alford, M. Braby, S. Reddy, and T. Schafer, Phys. Rev. **C75** (2007) 055209, [nucl-th/0701067].

[45] Mark Alford and Gerald Good, [arXiv:1003.1093].

[46] S. Gandolfi, A. Y. Illarionov, F. Pederiva, K. E. Schmidt, and S. Fantoni, Phys. Rev. **C80** (2009) 045802, [arXiv:0907.1588].

[47] Mark Alford and Gerald Good, Phys. Rev. **D70** 036008 (2004) , arXiv:hep-ph/0404214.

[48] B. C. Barrois, Nucl. Phys. B **129**, 390 (1977); "Nonperturbative Effects In Dense Quark Matter," Cal Tech PhD thesis, UMI 79-04847-mc (1979); S. C. Frautschi, "Asymptotic Freedom And Color Superconductivity In Dense Quark Matter," CALT-68-701, Presented at Workshop on Hadronic Matter at Extreme Energy Density, Erice, Italy, Oct 13-21, 1978; D. Bailin and A. Love, Phys. Rept. **107**, 325 (1984).

[49] M. Alford, K. Rajagopal and F. Wilczek, Phys. Lett. **B422**, 247 (1998) [hep-ph/9711395]. R. Rapp, T. Schäfer, E. V. Shuryak and M. Velkovsky, Phys. Rev. Lett. **81**, 53 (1998) [hep-ph/9711396].

[50] K. Rajagopal and F. Wilczek, [hep-ph/0011333], to appear as Chapter 35 in the Festschrift in honor of B.L. Ioffe, 'At the Frontier of Particle Physics / Handbook of QCD', M. Shifman, ed., (World Scientific). M. G. Alford, Ann. Rev. Nucl. Part. Sci. **51** (2001) 131 [hep-ph/0102047]. T. Schaefer, hep-ph/0304281. D. H. Rischke, nucl-th/0305030. D. K. Hong, Acta Phys. Polon. B **32** (2001) 1253 [hep-ph/0101025].

[51] M. G. Alford, K. Rajagopal and F. Wilczek, Nucl. Phys. B **537**, 443 (1999) [hep-ph/9804403].

[52] For a review, see J. L. Hewett and T. G. Rizzo, Phys. Rept. **183**, 193 (1989).

[53] K. S. Babu, C. F. Kolda and J. March-Russell, Phys. Rev. D **57**, 6788 (1998) [hep-ph/9710441].

[54] M. G. Alford, J. Berges and K. Rajagopal, Nucl. Phys. B **571**, 269 (2000) [hep-ph/9910254].

[55] C. Manuel and K. Rajagopal, Phys. Rev. Lett. **88**, 042003 (2002) [hep-ph/0107211].

[56] M. Stone, "The Physics of Quantum Fields", Springer, New York, 2000.

[57] A. Sedrakian and U. Lombardo, Phys. Rev. Lett. **84**, 602 (2000) [arXiv:nucl-th/9907076]. U. Lombardo, P. Nozieres, P. Schuck, H. J. Schulze and A. Sedrakian, Phys. Rev. C **64**, 064314 (2001) [arXiv:nucl-th/0109024]. M. Baldo, U. Lombardo, H. J. Schulze and Z. Wei, Phys. Rev. C **66**, 054304 (2002).

D. J. Dean and M. Hjorth-Jensen, Rev. Mod. Phys. **75**, 607 (2003) [arXiv:nucl-th/0210033].

[58] M. Juneau, R. MacKenzie, M. A. Vachon and J. M. Cline, Phys. Rev. B **65**, 140512 (2002) [arXiv:cond-mat/0106172].

[59] F. Mohamed, I. Luk'yanchuk, M. Troyer, G. Blatter, Phys. Rev. B65, 224504 (2002) [arXiv:cond-mat/0201499].

[60] N. Glendenning, "Compact Stars", 2nd edition, Springer-Verlag, New York (2000). See Fig 5.27.

[61] A. Akmal, V.R. Pandharipande, D.G. Ravenhall, Phys. Rev. C **58**, 1804 (1998) [arXiv:nucl-th/9804027], Fig. 7.

[62] N. Chamel and P. Haensel, Phys. Rev. C **73**, 045802 (2006) [arXiv:nucl-th/0603018].

[63] N. Andersson, G. L. Comer and D. Langlois, Phys. Rev. D **66**, 104002 (2002) [arXiv:gr-qc/0203039].

[64] L. Lindblom and G. Mendell, Phys. Rev. D **61**, 104003 (2000) [arXiv:gr-qc/9909084].

[65] C. Kittel, *Introduction to Solid State Physics*, 7th Edition, Wiley, 1996, pp. 360 and 661-2.

[66] E. B. Bogomolnyi, Yad. Fiz. **24**, 861 (1976) [Sov. J. Nucl. Phys. **24**, 449 (1976)];
E. B. Bogomolnyi and A. I. Vainstein, Yad. Fiz. **23**, 1111 (1976) [Sov. J. Nucl.
Phys. **23**, 588 (1976)]

[67] H. J. de Vega and F. A. Schaposnik, Phys. Rev. D **14**, 1100 (1976).

[68] I. Luk'yanchuk, Phys. Rev. B **63**, 174504 (2001) [arXiv:cond-mat/0009030].

[69] L. Jacobs and C. Rebbi, Phys. Rev. B**19**, 4486 (1979).

[70] J. M. Speight, Phys. Rev. D **55**, 3830 (1997) [arXiv:hep-th/9603155].

[71] L. M. A. Bettencourt and R. J. Rivers, Phys. Rev. D **51**, 1842 (1995) [arXiv:hep-ph/9405222].

[72] J. Hove, S. Mo, A. Sudbo, Phys. Rev. B **66**, 064524 (2002).

[73] M. Gleiser and J. Thorarinson, Phys. Rev. D **76**, 041701(R) (2007) [arXiv:hep-th/0701294].

[74] M. Srednicki, "Quantum Field Theory", Cambridge University Press, 2007.

[75] P. Jaikumar, C. Gale, and D. Page, Phys. Rev. **D72** (2005) 123004, [hep-ph/0508245].

[76] A. D. Kaminker and P. Haensel, Acta. Phys. Pol. **B30** (1999) 1125, [astro-ph/9908249].

[77] V. D. Barger and R. J. N. Phillips, "Collider Physics (Updated Edition)",
Addison-Wesley, 1996.

[78] H. Heiselberg, G. Baym, C. J. Pethick, and J. Popp, Nucl. Phys. **A544** (1992), 569c-572c.

[79] H. Heiselberg and C. J. Pethick, Phys. Rev. **D48** (1993) 2916-2928.

[80] P. S. Shternin and D. G. Yakovlev, Phys. Rev. **D78** (2008) 063006, [arXiv:0808.2018].

[81] P. S. Shternin and D. G. Yakovlev, Phys. Rev. **D75** (2007) 103004, [arXiv:0705.1963].

[82] R. Mertig, M. Böhm, and A. Denner, Comput. Phys. Commun. **64** (1991) 345-359.

[83] M. E. Gusakov and N. Andersson, Mon. Not. Roy. Astron. Soc. **372** (2006) 1776-1790, [astro-ph/0602282].

[84] P. Haensel, K. P. Levenfish, and D. G. Yakovlev, Astron. Astrophys. **394** (2002) 213-218, [astro-ph/0208078].

[85] G. 't Hooft, in "High Energy Physics", ed. A. Zichichi (Editrice Compositori, Bologna, 1976); S. Mandelstam, Phys. Rept. **23**, 245 (1976).

[86] J. D. Jackson, "Classical Electrodynamics", second edition, John Wiley and Sons, New York, 1975.

[87] K. Osterwalder and E. Seiler, Annals Phys. **110**, 440 (1978). E. H. Fradkin and S. H. Shenker, Phys. Rev. D **19**, 3682 (1979). S. Dimopoulos, S. Raby and

L. Susskind, Nucl. Phys. B **173**, 208 (1980). T. Banks and E. Rabinovici, Nucl. Phys. B **160**, 349 (1979).

[88] I. H. Lee and R. E. Shrock, Phys. Rev. Lett. **59**, 14 (1987). S. D. H. Hsu, Phys. Rev. D **48**, 4458 (1993) [hep-ph/9302235].

[89] N. W. Ashcroft and N. D. Mermin, "Solid State Physics", Brooks/Cole, 1976.